

**Electronic Supplementary Information (ESI)**

**Alkyl vs Aryl Modifications: A Comparative Study on  
Modular Modifications of Triphenylphosphonium  
Mitochondrial Vectors**

How Chee Ong,<sup>a</sup> João T. S. Coimbra,<sup>b</sup> Germain Kwek,<sup>a</sup> Maria J. Ramos,<sup>b</sup> Bengang Xing,<sup>a</sup> Pedro A. Fernandes<sup>b\*</sup>  
and Felipe García<sup>a\*</sup>

<sup>a</sup> School of Physical and Mathematical Sciences, Division of Chemistry and Biological Chemistry,  
Nanyang Technological University, 21 Nanyang Link, 637371, Singapore

<sup>b</sup> LAQV, REQUIMTE, Departamento de Química e Bioquímica, Faculdade de Ciências, Universidade  
do Porto, Rua do Campo Alegre s/n, 4169-007, Portugal.

---

**Content:**

1. Chemicals .....	1
2. Instrumentation .....	1
3. Single crystal X-ray diffraction (SCXRD) study .....	1
4. Synthesis of delocalized lipophilic cations .....	2
5. Measurement of lipophilicity .....	7
6. Cells culture and in vitro biological studies.....	8
7. 7. Confocal microscopy and flow cytometry.....	11
8. Excitation/Emission spectra.....	13
9. Theoretical methods.....	14
10. NMR Spectra.....	22
11. High Resolution Mass Spectra.....	55
12. Single crystal X-ray data.....	66
References	68

---

## Experimental

### 1. Chemicals

Triphenylphosphine, tris(3,5-dimethylphenyl)phosphine, 1-bromopentane and 1-bromooctane were purchased from Sigma Aldrich, and all other chemicals (tri-(p-tolyl)phosphine and bromoethane) were purchased from TCI Chemicals. The starting materials were used without further purification. Solvents used were dried and stored under 4 Å molecular sieves. Reactions were carried out using standard Schlenk techniques and performed under argon. Human epithelial carcinoma cell line (HeLa) was purchased from ATCC® (ATCC no. CCL-2).

### 2. Instrumentation

<sup>1</sup>H, <sup>13</sup>C, <sup>31</sup>P{<sup>1</sup>H} NMR spectra were collected using Bruker Avance III, 400 MHz and 500 MHz spectrometers with the <sup>1</sup>H, <sup>13</sup>C NMR chemical shifts internally referenced to the relevant residual solvent peaks. All NMR spectroscopic analysis were performed at room temperature (300 K). High-resolution mass spectra were obtained from Water Q-ToF Premier, with ESI mode. Reverse-phase HPLC analysis was performed on a Shimadzu Prominence-I LC-2030 using a C-8/C-18 analytical column at a flow rate of 1.0 mL/min for analysis. UV absorption spectra and fluorescence emission spectra were recorded in a 10 mm path quartz cell on an Agilent Cary 300 UV-Vis spectrometer and an Agilent Cary Eclipse fluorescence spectrophotometer. Resazurin Reduction Assays were measured by Tecan's Infinite M200 microplate reader. Confocal imaging was carried out on a Carl Zeiss LSM 800 confocal laser microscope.

### 3. Single crystal X-ray diffraction (SCXRD) studies

Diffraction-quality crystals were obtained by crystallization from acetonitrile/diethyl ether at room temperature. The crystals were mounted onto quartz fibers, and the X-ray diffraction intensity data were measured at 100 K with a Bruker Kappa diffractometer equipped with a CCD detector, employing Mo K<sub>α</sub> radiation ( $\lambda = 0.71073 \text{ \AA}$ ), with the SMART suite of programs.<sup>1</sup> All data were processed and corrected for Lorentz and polarization effects with SAINT and for absorption effects with SADABS.<sup>2</sup> Structural solution and refinement were carried out with the SHELXTL suite of programs.<sup>3</sup> The structures were solved by direct methods or Patterson maps to locate the heavy atoms, followed by difference maps for the light, non-hydrogen atoms. All non-hydrogen atoms were refined with anisotropic thermal parameters. CCDC 2078443 - 2078444 contains the supplementary crystallographic data for this paper. These data can be obtained free of charge from The Cambridge Crystallographic Data Centre via [www.ccdc.cam.ac.uk/structures](http://www.ccdc.cam.ac.uk/structures)

---

#### 4. Synthesis of delocalized lipophilic cations

The synthesis for compound **1a** – **1c** and fluorescein methyl ester (methyl 2-(6-hydroxy-3-oxo-3H-xanthen-9-yl)benzoate) are achieved by following procedures in the literature<sup>4,5</sup> and hence they are not described here.

##### 4.1. Synthesis of pentyltriphenylphosphonium bromide

Triphenylphosphine (0.262 g, 1 mmol) was heated under reflux with 1-bromopentane (0.302 g, 2 mmol) in acetonitrile (5 mL) overnight. The mixture was cooled to room temperature and the product was precipitated with the addition of diethyl ether. The white precipitate was filtered and was crystallized in acetonitrile and diethyl ether to obtain a white crystalline solid. Single crystals used for SCXRD were grown from acetonitrile/diethyl ether. Yield: 85 %, 0.353 g. <sup>1</sup>H NMR (400 MHz, CDCl<sub>3</sub>) δ 7.67 – 7.52 (m, 15H), 3.52 – 3.45 (m, 2H), 1.49 – 1.38 (m, 4H), 1.15 – 1.07 (m, 2H), 0.62 (t, *J* = 7.3 Hz, 3H). <sup>31</sup>P{<sup>1</sup>H} NMR (162 MHz, CDCl<sub>3</sub>) δ 24.05. <sup>13</sup>C{<sup>1</sup>H} NMR (101 MHz, CDCl<sub>3</sub>) δ 134.80 (d, *J* = 2.9 Hz), 133.27 (d, *J* = 10.0 Hz), 130.25 (d, *J* = 12.5 Hz), 117.92 (d, *J* = 86.0 Hz), 32.04 (d, *J* = 15.5 Hz), 22.51 (d, *J* = 49.7 Hz), 21.93 (d, *J* = 4.4 Hz), 21.78, 13.27. TOF-MS-ES+ for [M-Br]<sup>+</sup>: Calcd. *m/z* 333.1772; Found 333.1771.

##### 4.2. Synthesis of octyltriphenylphosphonium bromide

Triphenylphosphine (0.341 g, 1.3 mmol) was heated under reflux with 1-bromopentane (0.193 g, 1 mmol) in toluene (1 mL) overnight. Two liquid phases were observed, and the product solidified upon cooling to room temperature. The waxy solid was washed with toluene followed by diethyl ether. The residue was dried in vacuo to obtain a white waxy solid. Yield: 75 %, 0.342 g. <sup>1</sup>H NMR (400 MHz, CDCl<sub>3</sub>) δ 7.76 – 7.61 (m, 15H), 3.62 – 3.55 (m, 2H), 1.54 – 1.52 (m, 4H), 1.17 – 1.08 (m, 8H), 0.73 (t, *J* = 6.7 Hz, 3H). <sup>31</sup>P{<sup>1</sup>H} NMR (162 MHz, CDCl<sub>3</sub>) δ 24.15. <sup>13</sup>C{<sup>1</sup>H} NMR (101 MHz, CDCl<sub>3</sub>) δ 135.02 (d, *J* = 3.1 Hz), 133.57 (d, *J* = 10.0 Hz), 130.49 (d, *J* = 12.4 Hz), 118.27 (d, *J* = 85.8 Hz), 31.54, 30.32 (d, *J* = 15.2 Hz), 28.97, 28.70, 22.86 (d, *J* = 50.2 Hz), 22.55 (d, *J* = 4.6 Hz), 22.41, 13.90. TOF-MS-ES+ for [M-Br]<sup>+</sup>: Calcd. *m/z* 375.2242; Found 375.2245.

##### 4.3. Synthesis of pentyltri(*p*-tolyl)phosphonium bromide

Tri(*p*-tolyl)phosphine (0.396 g, 1.3 mmol) was heated under reflux with 1-bromopentane (0.302 g, 2 mmol) in toluene (1 mL) overnight. The mixture was allowed to cool to room temperature. The solution was decanted, and the solids were washed with diethyl ether. The residue was dried in vacuo to obtain a white solid. Single crystals used for SCXRD were grown from acetonitrile/diethyl ether. Yield: 75 %, 0.340 g. <sup>1</sup>H NMR (400 MHz, CDCl<sub>3</sub>) δ 7.64 (dd, *J* = 12.4, 8.0 Hz, 6H), 7.46 (dd, *J* = 8.2, 3.1 Hz, 6H), 3.56 – 3.49 (m, 2H), 2.45 (s, 9H), 1.60 – 1.55 (m, 4H), 1.31 – 1.26 (m, 2H), 0.81 (t, *J* = 7.3 Hz, 3H). <sup>31</sup>P{<sup>1</sup>H} NMR (162 MHz, CDCl<sub>3</sub>) δ 23.19. <sup>13</sup>C{<sup>1</sup>H} NMR (101 MHz, CDCl<sub>3</sub>) δ 146.29 (d, *J* = 3.0 Hz),

---

133.63 (d,  $J = 10.2$  Hz), 131.26 (d,  $J = 12.9$  Hz), 115.39 (d,  $J = 88.6$  Hz), 32.54 (d,  $J = 15.3$  Hz), 23.23 (d,  $J = 51.3$  Hz), 22.40 (d,  $J = 4.5$  Hz), 22.31, 21.92, 13.72. TOF-MS-ES+ for  $[M-Br]^+$ : Calcd.  $m/z$  375.2242; Found 375.2245.

#### 4.4. Synthesis of octyltri(p-tolyl)phosphonium bromide

Tri(p-tolyl)phosphine (0.609 g, 2 mmol) was heated under reflux with 1-bromooctane (0.773 g, 4 mmol) in acetonitrile (8 mL) overnight. The mixture was cooled to room temperature, concentrated in vacuo and the product was precipitated with the addition of diethyl ether. The mixture was decanted, and the residue was washed 3 times with diethyl ether. The residue was dried in vacuo to obtain a white solid. Yield: 92 %, 0.920 g.  $^1H$  NMR (400 MHz,  $CDCl_3$ )  $\delta$  7.57 (dd,  $J = 12.4, 8.1$  Hz, 6H), 7.43 (dd,  $J = 8.2, 3.2$  Hz, 6H), 3.42 – 3.36 (m, 2H), 2.41 (s, 9H), 1.54 – 1.52 (m, 4H), 1.20 – 1.07 (m, 8H), 0.77 (t,  $J = 6.8$  Hz, 3H).  $^{31}P\{^1H\}$  NMR (162 MHz,  $CDCl_3$ )  $\delta$  22.98.  $^{13}C\{^1H\}$  NMR (101 MHz,  $CDCl_3$ )  $\delta$  146.27 (d,  $J = 3.0$  Hz), 133.46 (d,  $J = 10.2$  Hz), 131.20 (d,  $J = 12.8$  Hz), 115.18 (d,  $J = 88.6$  Hz), 31.63, 30.44 (d,  $J = 15.3$  Hz), 29.04, 28.79, 23.20 (d,  $J = 51.3$  Hz), 22.58 (d,  $J = 4.5$  Hz), 22.50, 21.81, 13.97. TOF-MS-ES+ for  $[M-Br]^+$ : Calcd.  $m/z$  417.2711; Found 417.2709.

#### 4.5. Synthesis of pentyltris(3,5-dimethylphenyl)phosphonium bromide

Tris(3,5-dimethylphenyl)phosphine (0.173 g, 0.5 mmol) was heated under reflux with 1-bromopentane (0.151 g, 1 mmol) in acetonitrile (5 mL) overnight. The mixture was cooled to room temperature and the product was precipitated with the addition of diethyl ether. The precipitate was filtered and washed with diethyl ether. The residue was dried in vacuo to obtain a white solid. Single crystals used for SCXRD were grown from acetonitrile/diethyl ether. Yield: 99 %, 0.246 g.  $^1H$  NMR (400 MHz,  $CDCl_3$ )  $\delta$  7.35 (s, 6H), 7.31 (s, 3H), 3.55 – 3.48 (m, 2H), 2.40 (s, 18H), 1.60 – 1.56 (m, 4H), 1.33 – 1.28 (m, 2H), 0.81 (t,  $J = 7.3$  Hz, 3H).  $^{31}P\{^1H\}$  NMR (162 MHz,  $CDCl_3$ )  $\delta$  23.67.  $^{13}C\{^1H\}$  NMR (101 MHz,  $CDCl_3$ )  $\delta$  140.60 (d,  $J = 13.1$  Hz), 136.77 (d,  $J = 3.1$  Hz), 130.96 (d,  $J = 9.9$  Hz), 118.71 (d,  $J = 84.4$  Hz), 32.42 (d,  $J = 15.0$  Hz), 23.09 (d,  $J = 50.2$  Hz), 22.38 (d,  $J = 4.4$  Hz), 22.19, 21.55, 13.67. TOF-MS-ES+ for  $[M-Br]^+$ : Calcd.  $m/z$  417.2711; Found 417.2714.

#### 4.6. Synthesis of octyltris(3,5-dimethylphenyl)phosphonium bromide

Tris(3,5-dimethylphenyl)phosphine (0.173 g, 0.5 mmol) was heated under reflux with 1-bromooctane (0.193 g, 1 mmol) in acetonitrile (5 mL) overnight. The mixture was cooled to room temperature and the product was precipitated with the addition of diethyl ether. The precipitate was filtered and washed with diethyl ether. The residue was dried in vacuo to obtain a white solid. Single crystals used for SCXRD were grown from acetonitrile/diethyl ether. Yield: 85 %, 0.229 g.  $^1H$  NMR (400 MHz,  $CDCl_3$ )  $\delta$  7.36 (s, 6H), 7.33 (s, 3H), 3.59 – 3.52 (m, 2H), 2.41 (s, 18H), 1.60 – 1.57 (m, 4H), 1.25 – 1.17 (m, 8H), 0.83 (t,  $J = 6.8$  Hz, 3H).  $^{31}P\{^1H\}$  NMR (162 MHz,  $CDCl_3$ )  $\delta$  23.38.  $^{13}C\{^1H\}$  NMR

---

(101 MHz, CDCl<sub>3</sub>) δ 140.50 (d, *J* = 13.1 Hz), 136.72 (d, *J* = 3.2 Hz), 130.74 (d, *J* = 9.7 Hz), 118.44 (d, *J* = 84.6 Hz), 31.61, 30.26 (d, *J* = 14.9 Hz), 28.93, 28.74, 22.99 (d, *J* = 50.7 Hz), 22.55, 22.50, 21.41, 13.93. TOF-MS-ES+ for [M-Br]<sup>+</sup>: Calcd. *m/z* 459.3181; Found 459.3181.

#### **4.7. Synthesis of (5-((9-(2-(methoxycarbonyl)phenyl)-3-oxo-3H-xanthen-6-yl)oxy)pentyl)triphenylphosphonium bromide**

Triphenylphosphine (0.655 g, 2.5 mmol) was dissolved in 1,5-dibromopentane (2.87 g, 12.5 mmol) and heated at 90°C for 1.5 hours. The mixture was allowed to cool to room temperature and was purified by flash column chromatography (40 : 1, DCM : MeOH) to obtain a white waxy solid. (0.750 g, 1.52 mmol, 61 %) Fluorescein methyl ester (0.580 g, 1.68 mmol, 1.1 equiv) and potassium carbonate (0.632 g, 4.57 mmol, 3 equiv) was added to the phosphonium salt. The mixture was suspended in DMF (10 mL) and heated at 90 degrees for 2 hours. The mixture was allowed to cool to room temperature, and 50 mL of water was added to the mixture. The suspension was extracted with 5 x 25 mL of dichloromethane and dried with anhydrous magnesium sulfate. The product was further purified by flash column chromatography (20 : 1, DCM : MeOH). The product was washed with ether and dried in vacuo to obtain an orange solid. (0.990 g, 1.31 mmol, 86 %) <sup>1</sup>H NMR (400 MHz, CDCl<sub>3</sub>) δ 8.23 (dd, *J* = 7.9, 1.4 Hz, 1H), 7.89 – 7.64 (m, 17H), 7.30 (d, *J* = 7.3 Hz, 1H), 6.86 – 6.81 (m, 3H), 6.70 (dd, *J* = 8.9, 2.4 Hz, 1H), 6.52 (dd, *J* = 9.7, 2.0 Hz, 1H), 6.44 (d, *J* = 1.9 Hz, 1H), 4.09 – 4.01 (m, 2H), 3.99 – 3.87 (m, 2H), 3.63 (s, 3H), 1.96 – 1.82 (m, 4H). 1.78 – 1.72 (m, 2H). <sup>31</sup>P{<sup>1</sup>H} NMR (162 MHz, CDCl<sub>3</sub>) δ 24.52. TOF-MS-ES+ for [M-Br]<sup>+</sup>: Calcd. *m/z* 677.2457; Found 677.2457.

#### **4.8. Synthesis of (8-((9-(2-(methoxycarbonyl)phenyl)-3-oxo-3H-xanthen-6-yl)oxy)octyl)triphenylphosphonium bromide**

Triphenylphosphine (0.655 g, 2.5 mmol) was dissolved in 1,8-dibromooctane (3.40 g, 12.5 mmol) and heated at 90°C for 3 hours. The mixture was allowed to cool to room temperature and was purified by flash column chromatography (20 : 1, DCM : MeOH) to obtain a white waxy solid. (1.03 g, 1.93 mmol, 77 %) Fluorescein methyl ester (0.736 g, 2.12 mmol, 1.1 equiv) and potassium carbonate (0.801 g, 5.79 mmol, 3 equiv) was added to the phosphonium salt. The mixture was suspended in DMF (10 mL) and heated at 90 degrees for 2 hours. The mixture was allowed to cool to room temperature, and 50 mL of water was added to the mixture. The suspension was extracted with 5 x 25 mL of dichloromethane and dried with anhydrous magnesium sulfate. The product was further purified by flash column chromatography (20 : 1, DCM : MeOH). The product was washed with ether and dried in vacuo to obtain an orange solid. (1.40 g, 1.74 mmol, 90 %) <sup>1</sup>H NMR (400 MHz, CDCl<sub>3</sub>) δ 8.23 (dd, *J* = 7.9, 1.4 Hz, 1H), 7.86 – 7.63 (m, 17H), 7.29 (dd, *J* = 7.6, 1.4 Hz, 1H), 6.90 (d, *J* = 2.4 Hz, 1H), 6.84 (dd, *J* = 10.7, 9.3 Hz, 2H), 6.71 (dd, *J* = 8.9, 2.4 Hz, 1H), 6.51 (dd, *J* = 9.7, 2.0 Hz, 1H), 6.42 (d, *J* = 2.0 Hz, 1H), 4.02 (t, *J* = 6.5 Hz, 2H), 3.78 – 3.66 (m, 2H), 3.62 (s, 3H), 1.78 – 1.73 (m, 2H), 1.65 – 1.59 (m, 4H), 1.43 – 1.41 (m, 2H), 1.32 – 1.30 (m,

---

4H).  $^{31}\text{P}\{^1\text{H}\}$  NMR (162 MHz,  $\text{CDCl}_3$ )  $\delta$  24.43. TOF-MS-ES+ for  $[\text{M-Br}]^+$  : Calcd.  $m/z$  719.2926; Found 719.2928.

#### 4.9. Synthesis of (11-((9-(2-(methoxycarbonyl)phenyl)-3-oxo-3H-xanthen-6-yl)oxy)undecyl)triphenylphosphonium bromide

Triphenylphosphine (0.262 g, 1 mmol) was dissolved in 1,11-dibromoundecane (1.57 g, 5 mmol) and heated at  $90^\circ\text{C}$  overnight. The mixture was allowed to cool to room temperature and was purified by flash column chromatography (20 : 1, DCM : MeOH) to obtain a white waxy solid. (0.328 g, 0.569 mmol, 57 %) Fluorescein methyl ester (0.217 g, 0.626 mmol, 1.1 equiv) and potassium carbonate (0.236 g, 1.71 mmol, 3 equiv) was added to the phosphonium salt. The mixture was suspended in DMF (10 mL) and heated at 90 degrees for 1.5 hours. The mixture was allowed to cool to room temperature, and 50 mL of water was added to the mixture. The suspension was extracted with 5 x 25 mL of dichloromethane and dried with anhydrous magnesium sulfate. The product was further purified by flash column chromatography (20 : 1, DCM : MeOH). The product was washed with ether and dried in vacuo to obtain an orange solid. (0.150 g, 0.178 mmol, 31 %)  $^1\text{H}$  NMR (400 MHz,  $\text{CDCl}_3$ )  $\delta$  8.23 (dd,  $J$  = 8.0, 1.4 Hz, 1H), 7.84 – 7.64 (m, 17H), 7.31 (d,  $J$  = 7.8 Hz, 1H), 6.93 (d,  $J$  = 2.4 Hz, 1H), 6.85 (dd,  $J$  = 11.5, 9.3 Hz, 2H), 6.72 (dd,  $J$  = 8.9, 2.4 Hz, 1H), 6.52 (dd,  $J$  = 9.7, 1.9 Hz, 1H), 6.43 (d,  $J$  = 2.0 Hz, 1H), 4.04 (t,  $J$  = 6.6 Hz, 2H), 3.63 (s, 3H), 1.83 – 1.76 (m, 2H), 1.65 – 1.61 (m, 4H), 1.45 – 1.39 (m, 2H), 1.30 – 1.19 (m, 12H).  $^{31}\text{P}\{^1\text{H}\}$  NMR (162 MHz,  $\text{CDCl}_3$ )  $\delta$  24.41. TOF-MS-ES+ for  $[\text{M-Br}]^+$  : Calcd.  $m/z$  761.3396; Found 761.3398.

#### 4.10. Synthesis of (5-((9-(2-(methoxycarbonyl)phenyl)-3-oxo-3H-xanthen-6-yl)oxy)pentyl)tri-p-tolylphosphonium bromide

Tri(p-tolyl)phosphine (0.761 g, 2.5 mmol) was dissolved in 1,5-dibromopentane (2.87 g, 12.5 mmol) and heated at  $90^\circ\text{C}$  for 1.5 hours. The mixture was allowed to cool to room temperature and was purified by flash column chromatography (20 : 1, DCM : MeOH) to obtain a white waxy solid. (1.27 g, 2.37 mmol, 94 %) (5-bromopentyl)tri-p-tolylphosphonium bromide (0.267 g, 0.500 mmol), fluorescein methyl ester (0.190 g, 0.550 mmol, 1.1 equiv) and potassium carbonate (0.207 g, 1.50 mmol, 3 equiv) were suspended in DMF (6 mL), and heated at 90 degrees for 1.5 hours. The mixture was allowed to cool to room temperature, and 50 mL of water was added to the mixture. The suspension was extracted with 5 x 25 mL of dichloromethane and dried with anhydrous magnesium sulfate. The product was further purified by flash column chromatography (20 : 1, DCM : MeOH). The product was washed with ether and dried in vacuo to obtain an orange solid. (0.294 g, 0.368 mmol, 74 %)  $^1\text{H}$  NMR (500 MHz,  $\text{CDCl}_3$ )  $\delta$  8.22 (dd,  $J$  = 7.8, 1.4 Hz, 1H), 7.74 – 7.64 (m, 8H), 7.45 (dd,  $J$  = 8.3, 3.1 Hz, 6H), 7.27 (d,  $J$  = 7.7 Hz, 1H), 6.85 – 6.81 (m, 3H), 6.69 (dd,  $J$  = 9.0, 2.4 Hz, 1H), 6.51 (dd,  $J$  = 9.7, 1.9 Hz, 1H), 6.41 (d,  $J$  = 1.9 Hz, 1H), 4.04

---

(s, 2H), 3.66 – 3.59 (m, 5H), 2.45 (s, 9H), 1.87 – 1.85 (m, 4H), 1.69 – 1.67 (m, 2H).  $^{31}\text{P}\{^1\text{H}\}$  NMR (202 MHz,  $\text{CDCl}_3$ )  $\delta$  23.24. TOF-MS-ES+ for  $[\text{M-Br}]^+$ : Calcd.  $m/z$  719.2926; Found 719.2931.

#### 4.11. Synthesis of tris(3,5-dimethylphenyl)(5-((9-(2-(methoxycarbonyl)phenyl)-3-oxo-3H-xanthen-6-yl)oxy)pentyl)phosphonium bromide

Tris(3,5-dimethylphenyl)phosphine (0.346 g, 1 mmol) was dissolved in 1,5-dibromopentane (1.15 g, 5 mmol) and heated at 90°C for 1.5 hours. The mixture was allowed to cool to room temperature and was purified by flash column chromatography (40 : 1, DCM : MeOH) to obtain a white waxy solid. (0.486 g, 0.843 mmol, 84 %) Fluorescein methyl ester (0.321 g, 0.927 mmol, 1.1 equiv) and potassium carbonate (0.350 g, 2.53 mmol, 3 equiv) was added to the phosphonium salt. The mixture was suspended in DMF (6 mL) and heated at 90 degrees for 1.5 hours. The mixture was allowed to cool to room temperature, and 50 mL of water was added to the mixture. The suspension was extracted with 5 x 25 mL of dichloromethane and dried with anhydrous magnesium sulfate. The product was further purified by flash column chromatography (20 : 1, DCM : MeOH). The product was washed with ether and dried in vacuo to obtain an orange solid. (0.290 g, 0.344 mmol, 41 %)  $^1\text{H}$  NMR (400 MHz,  $\text{CDCl}_3$ )  $\delta$  8.23 (dd,  $J = 7.8, 1.5$  Hz, 1H), 7.69 (dtd,  $J = 28.0, 7.6, 1.4$  Hz, 2H), 7.39 (s, 3H), 7.35 (s, 6H), 7.29 (d,  $J = 8.7$  Hz, 1H), 6.86 – 6.81 (m, 3H), 6.70 (dd,  $J = 8.9, 2.3$  Hz, 1H), 6.51 (dd,  $J = 9.8, 1.9$  Hz, 1H), 6.43 (d,  $J = 1.9$  Hz, 1H), 4.07 – 4.04 (s, 2H), 3.67 – 3.60 (m, 3H), 2.40 (s, 18H), 1.93 – 1.86 (m, 2H), 1.71 – 1.60 (m, 3H).  $^{31}\text{P}\{^1\text{H}\}$  NMR (162 MHz,  $\text{CDCl}_3$ )  $\delta$  23.72. TOF-MS-ES+ for  $[\text{M-Br}]^+$ : Calcd.  $m/z$  761.3396; Found 761.3389.

## 5. Measurement of lipophilicity

Lipophilicity was determined by measuring octanol–water partition coefficient using HPLC measurements as described in the literature.<sup>6</sup> Calibration curves were obtained from standard solutions prepared (20 – 100  $\mu\text{M}$ ). A 100  $\mu\text{M}$  sample of phosphonium salt in octanol-saturated water was stirred vigorously with water-saturated octanol in a 1.5 mL microtube and allowed to sit for 10 minutes. The two phases were separated by centrifugation, and the concentration of the phosphonium salt in the aqueous layer was quantified by HPLC using a UV detector (220 nm). The peak area in the water layer was used to calculate the partition coefficient ( $\log P$ ):

$$\log P = \log \left[ \left( \frac{A_{std}}{A_w} - 1 \right) \left( \frac{V_w}{V_o} \right) \right]$$

where  $A_{std}$  and  $A_w$  represents the peak area for a 100  $\mu\text{M}$  standard and the aqueous layer, respectively.  $V_w$  and  $V_o$  represents the volume of water and octanol used in the mixture. The measurement for each compound was repeated 3 times and the results and solvent ratios used are shown below in **Table S1**.

**Table S1.** Results for lipophilicity measurements

<i>Compound</i>	$V_w/V_o$	$\log P$	<i>St. Dev.</i>
<i>1a</i>	0.0667	-1.36341	0.091698
<i>1b</i>	0.5	-0.84374	0.005435
<i>1c</i>	2	0.215889	0.023109
<i>2a</i>	0.5	-0.49856	0.046148
<i>2b</i>	2	0.261133	0.021482
<i>2c</i>	10	1.566637	0.01828
<i>3a</i>	1	0.083515	0.016644
<i>3b</i>	10	0.903388	0.012088
<i>3c</i>	100	2.246523	0.050932
<i>4a</i>	10	0.417092	0.039929
<i>4b</i>	10	1.249934	0.046903
<i>4c</i>	100	2.722392	0.074858
<i>4d</i>	10	1.425906	0.011654
<i>4e</i>	100	2.365476	0.01271

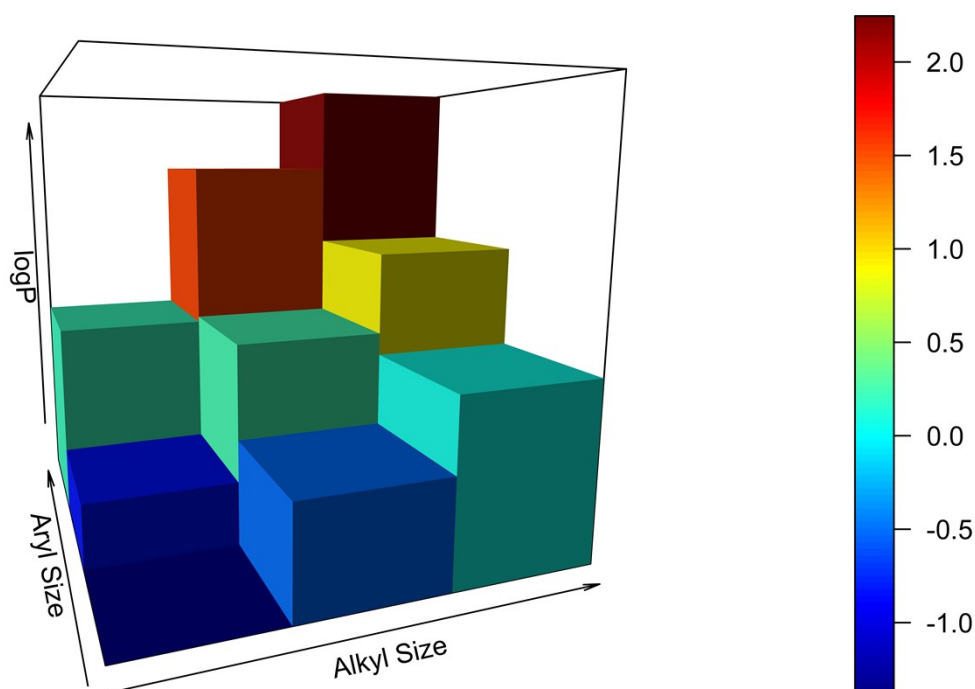


**Figure S1.** Water/1-Octanol logP values for **1a – 3c**.

## 6. Cells culture and in vitro biological studies

HeLa cells were cultured in Dulbecco's modified Eagle's medium (DMEM) solution with 10% fetal bovine serum (FBS) and 1% Penicillin/Streptomycin under humidified atmosphere of 5% CO<sub>2</sub> at 37 °C. Resazurin sodium salt was dissolved in PBS (0.2 mg/mL) to make a stock solution, which was diluted in DMEM w/o phenol red to 0.02 mg/mL before use. Stock solutions (10 μM) for **1a – 3c** was prepared by dissolving the salts in DMSO. 1 mM JC-1 solution was prepared in DMSO, and diluted using water to 2 μM before use.

### Determination of IC<sub>50</sub>

The HeLa cells were seeded on a 96-wells containing 10000 cells per well in 100 μL DMEM media and incubated overnight before the addition of **1a – 3c**. Upon incubation at 37 °C for an additional 72 h, the media was removed, and the cells were washed with PBS. Resazurin solution (100μL) was added to each well before incubation for 2 h at 37 °C. The samples were excited using a 560 nm light and the fluorescence was recorded on a Tecan's Infinite M200 microplate reader using a 590 nm emission filter. Different concentrations of **1a – 3c** were used and for each concentration and was performed in triplicate. The experiment was repeated three times and the IC<sub>50</sub> was determined from the plot of viability against concentration of samples.

### Measurement of mitochondrial membrane potential

$3 \times 10^4$  HeLa cells were seeded in a 96 well plate and allowed to attach overnight. The cells were treated with an addition of 11  $\mu\text{L}$  of 10x stock solutions of **1a** – **3c** (25  $\mu\text{M}$ ) and FCCP (1 mM). Untreated controls and background samples were included. The plate was allowed to incubate at 37°C in 5%  $\text{CO}_2$  for 4 hours. 100  $\mu\text{L}$  of JC-1 or resazurin solution were layered on top of the cells, to a final working concentration of 1  $\mu\text{M}$  and 0.02  $\text{mg mL}^{-1}$ , respectively. The plate was allowed to incubate for an additional 1 hour. The cells treated with JC-1 was washed twice with phosphate-buffered saline, and the fluorescence signals were measured using a microplate reader. The following excitation/emission wavelengths were used : JC-1 aggregate = 535 nm/590 nm, JC-1 monomer = 475 nm/530 nm, resazurin/resorufin = 560 nm/590 nm.

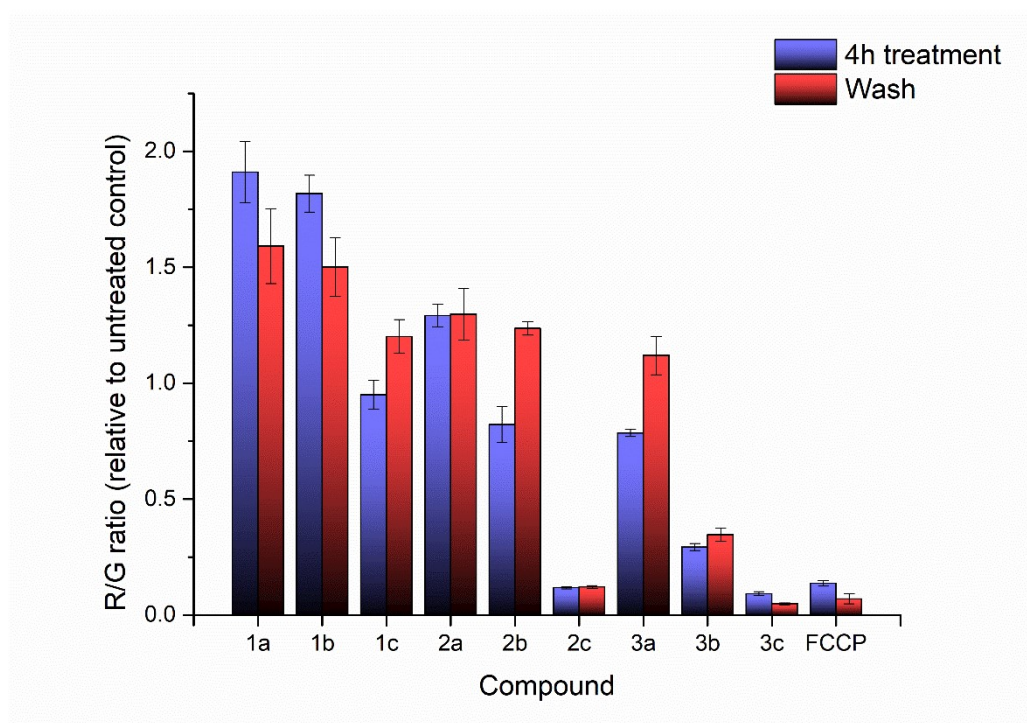


**Figure S2.** R/G ratio after treatment with compounds 1a – 3c and FCCP, before washing (blue) and after washing (red). Error bars refer to the standard deviations.

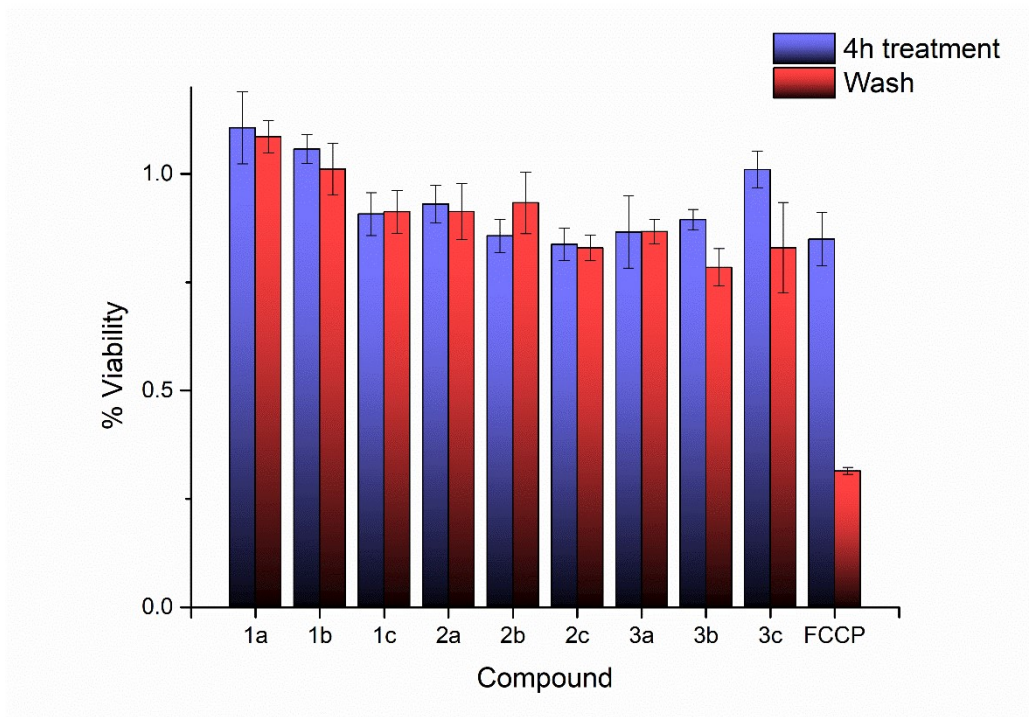


**Figure S3.** Cell viability after treatment with compounds 1a – 3c and FCCP, before washing (blue) and after washing (red). Error bars refer to the standard deviations.

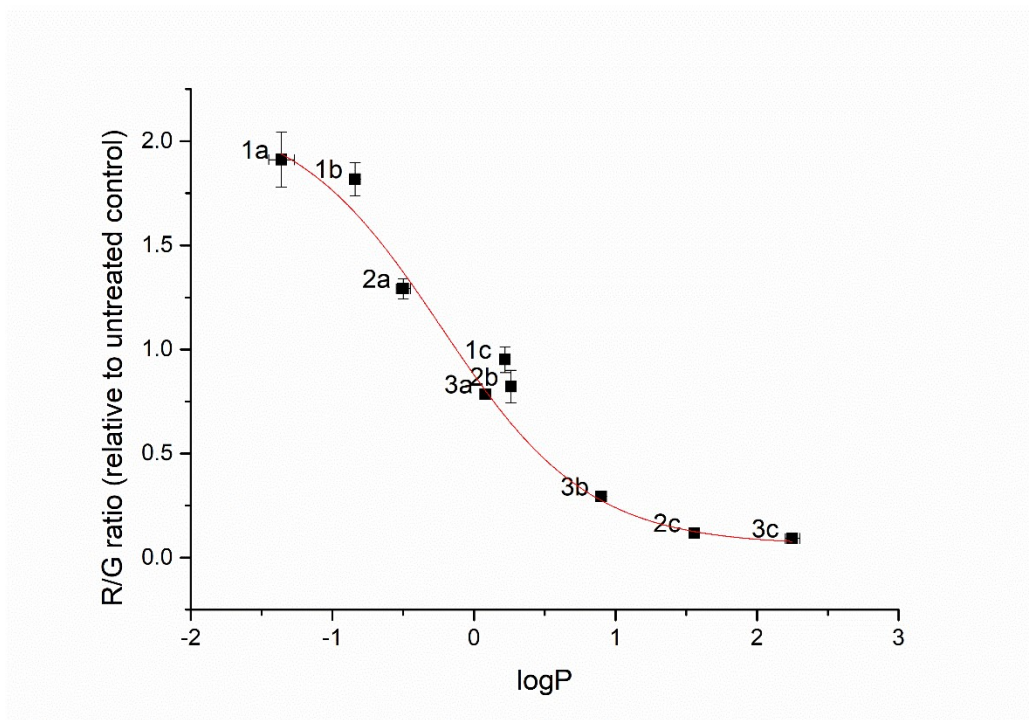


**Figure S4.** Correlation between R/G ratio and logP. Error bars refer to the standard deviations.

## 7. Confocal microscopy and flow cytometry

Confocal microscopy : HeLa cells were cultured in Dulbecco's modified Eagle's medium (DMEM) solution with 10% fetal bovine serum (FBS) and 1% Penicillin/Streptomycin under humidified atmosphere of 5% CO<sub>2</sub> at 37 °C. 25 x 10<sup>4</sup> HeLa cells were seeded on a microscope slide (Ibidi #80827) overnight in 200 µL of DMEM, and was subsequently treated with compounds **4a** – **4e** (100 nM, λ<sub>ex</sub> = 488 nm) and Mitotracker DeepRed FM (50 nM, λ<sub>ex</sub> = 640 nm) at 37 °C for 1 hour. The cells were washed 3 x 200 µL of PBS, and the chambers were filled with DMEM for imaging.

Flow cytometry : 2 x 10<sup>6</sup> HeLa cells in 2 mL of DMEM w/o phenol red supplemented with 10% FBS were harvested and incubated in 100 nM of 4c and 4e at 37°C for 1 hour. Cells were washed with phosphate-buffered saline, and were subsequently lysed via needle homogenization (20 strokes, 30G). The mitochondria isolation was done using a mitochondria isolation kit (Miltenyi Biotec, 130-094-532), and the isolated mitochondria was kept under ice. Isolated mitochondria samples were analysed using a BD LSRFortessa X-20 flow cytometer.

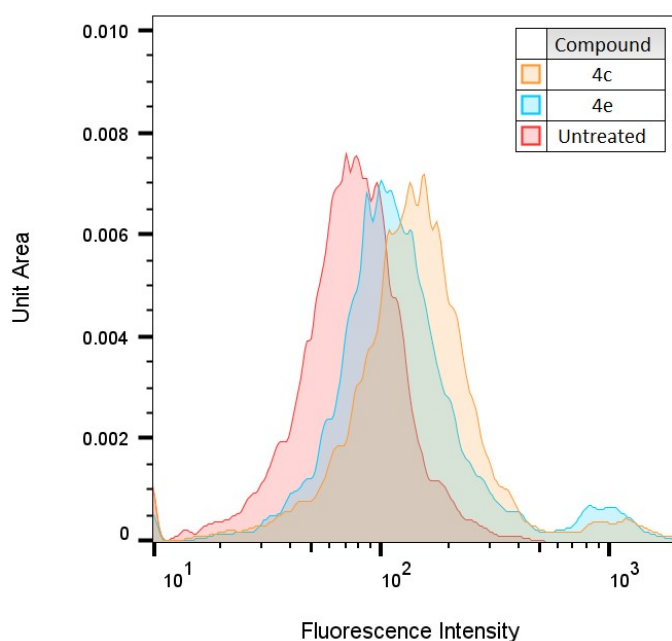
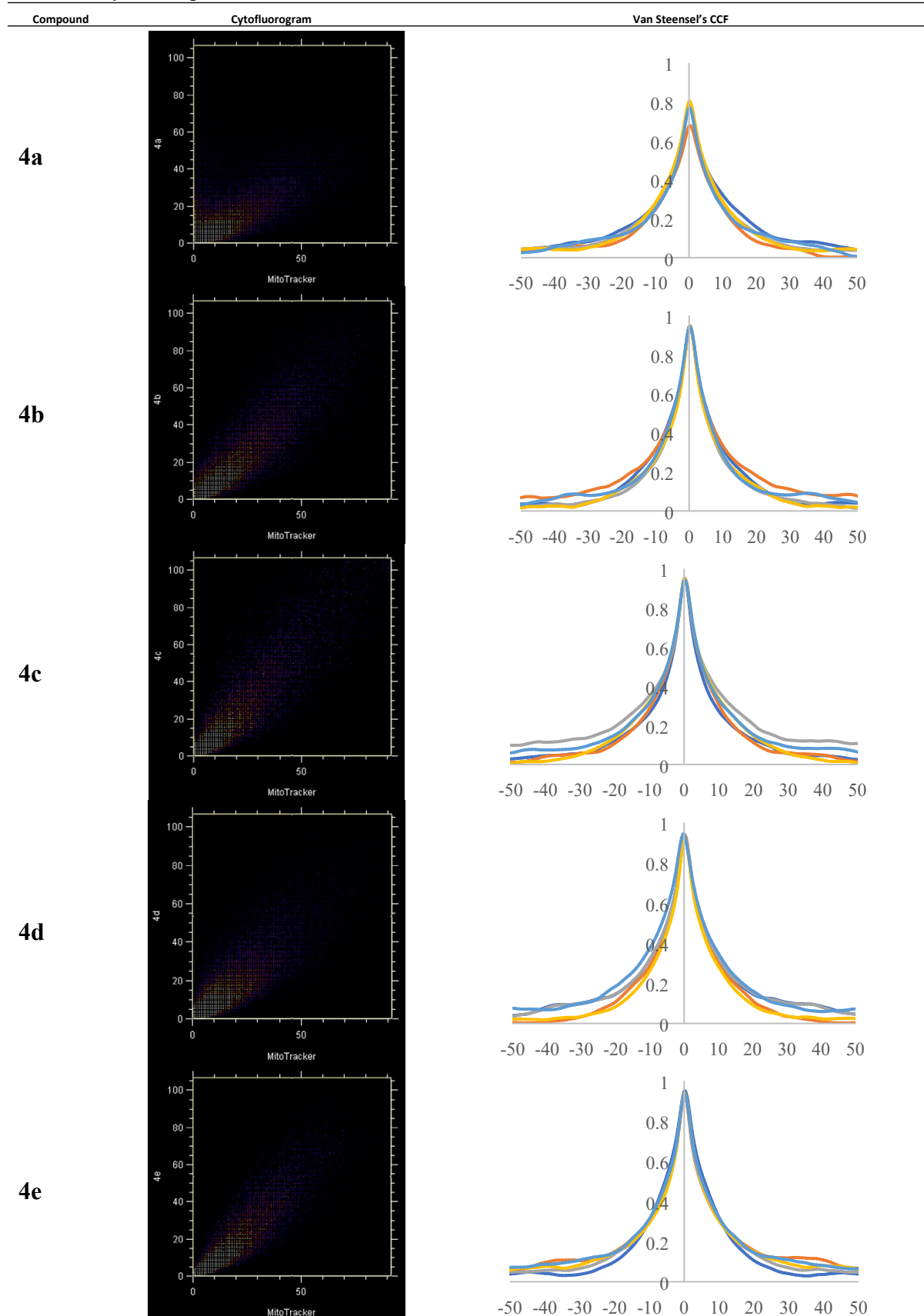


**Figure S5.** Histogram of fluorescence intensity for compound **4c**, **4e** and the control.

**Table S2.** Cytofluorogram and Van Steensel's cross-correlation function for **4a – 4e**



## 8. Excitation/Emission spectra

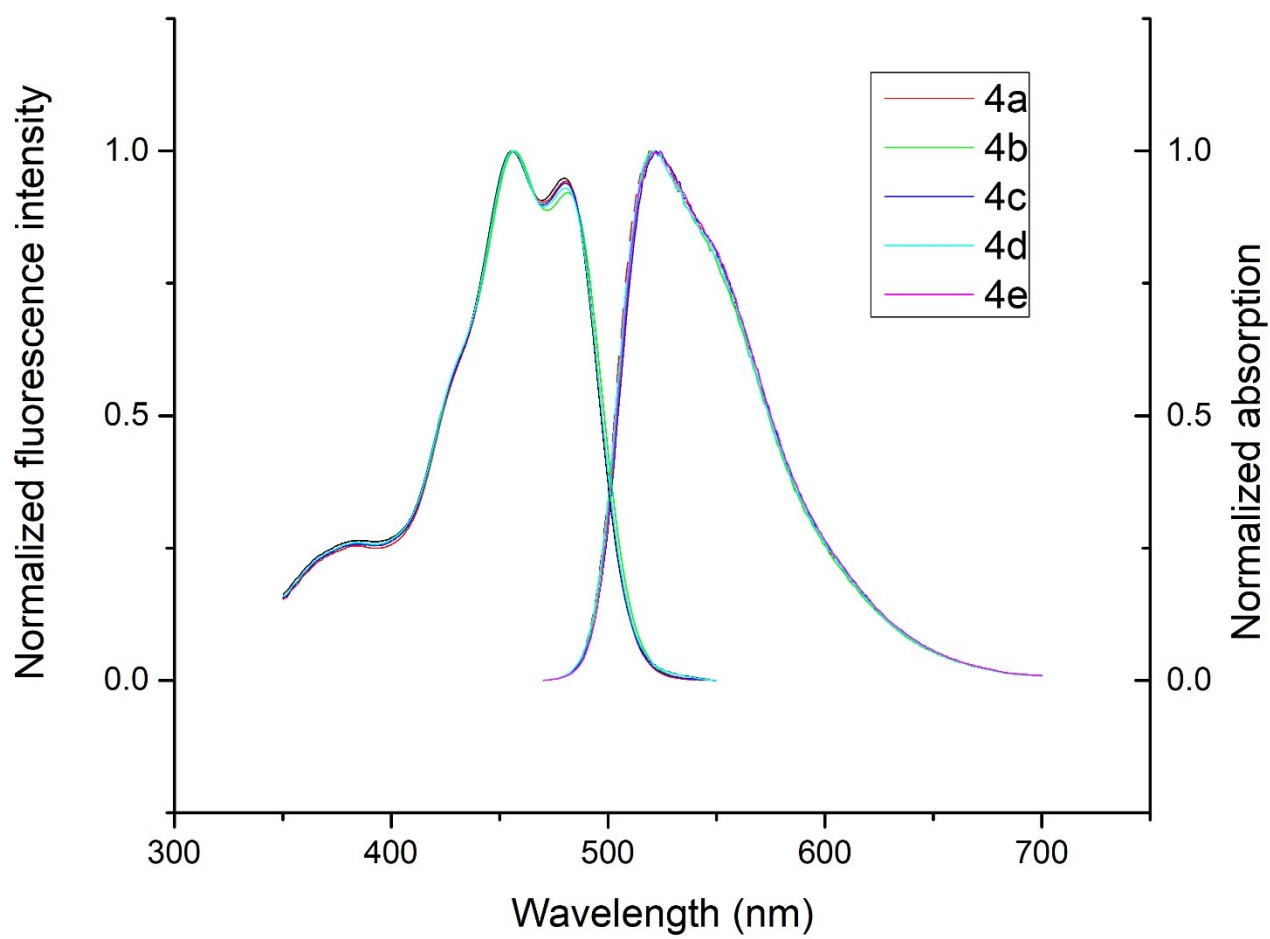


**Figure S6.** Fluorescence excitation and emission spectra for compounds **4a** – **4e**.

---

## 9. Theoretical methods

### 9.1. Molecular dynamics simulations and free energy calculations

Molecular dynamics (MD) simulations of the studied compounds were performed with the GROMACS 2018 software.<sup>7-9</sup>

The molecules were parameterized with the Antechamber program,<sup>10</sup> following a standard protocol: i) molecular mechanics parameters for bonded and van der Waals terms were extracted from the second-generation general amber force field (GAFF2); and ii) restrained electrostatic potential (RESP) charges<sup>11</sup> were derived at the HF/6-31G(d)//B3LYP/6-31G(d) level of theory. The conversion from amber-generated files to GROMACS-compatible ones was achieved with parmed.<sup>12</sup> We have confirmed that our optimized structures were true stationary points by performing a frequency calculation. All quantum mechanics calculations were performed with the Gaussian 09 software.<sup>13</sup>

Water molecules were described with the TIP3P model,<sup>14</sup> and 1-octanol molecules were parameterized using the previously described protocol. The amber99sb-ildn ion parameters,<sup>15</sup> already present in GROMACS, were used to describe the chlorine counter-ions used in the simulations.

The solvated systems were assembled using either GROMACS, in the case of the hydrated systems; or packmol,<sup>16</sup> in the case of the 1-octanol solvated systems. For the water solvated systems, we have used a cubic box of 1.5 nm, defined as the distance between any atom of the solute and the edges of the simulation box. For the 1-octanol solvated solutes, 300 1-octanol molecules were packed in a cubic box with sides of *ca.* 4.6 nm.

The solvated systems were then simulated using a 4-step protocol, that included: i) an optimization of the system using a steepest descent algorithm for energy minimization, until the maximum force was smaller than 100 kJ mol<sup>-1</sup> nm<sup>-1</sup>; ii) a 100 ps stage with the canonical (NVT) ensemble; iii) a 100 ps density equilibration using the isothermal-isobaric (NPT) ensemble; and iv) a 10 ns production run for data acquisition and for further equilibration of the systems.

---

A non-bonded cut-off of 1.2 nm was employed for Particle Mesh Ewald (PME)<sup>16</sup> electrostatics and plain cut-off van der Waals interactions, both with a potential-shift-Verlet modifier at 0.0 nm. Long-range dispersion corrections were applied for energy and pressure. For neighbor searching we have used the Verlet scheme. Periodic boundary conditions were employed in all three directions.

The MD simulations were performed with a leap-frog stochastic integrator (2 fs time step for integration). Constraints were applied to all bonds involving hydrogen atoms, with the LINCS constraint algorithm.<sup>17</sup> The same integrator was used as a thermostat, using a 2 ps time constant for temperature coupling of the system. The reference temperature was set to 298.15 K. For isotropic pressure coupling at 1 atm, we used the Berendsen barostat<sup>18</sup> for the density equilibration stage, using a 2 ps time constant for pressure coupling. Then, for the production stage we have switched to the Parrinello-Rahman barostat,<sup>19, 20</sup> with the same time constant for pressure coupling.

The solvent accessible surface area (SASA) and the volume of the compounds were assessed with the gmx sasa tool also integrated in GROMACS, using a probe radius of 1.4 nm. In this analysis, we used the last 5 ns of the 10 ns production stage of the conventional MD simulations.

The alchemical solvation considering the van der Waals interactions was broken into 16 lambda states. Specifically, the Lennard-Jones interactions were scaled using  $\lambda = [0.00, 0.05, 0.10, 0.20, 0.30, 0.40, 0.50, 0.60, 0.65, 0.70, 0.75, 0.80, 0.85, 0.90, 0.95, 1.00]$ . For these calculations, the charges on the solutes were set to zero. Although electrostatic interactions are necessary for obtaining the solvation/hydration free energy of the compounds, these were not considered for two reasons: i) previous studies have shown that this component showed little correlation with the experimental partition results for similar compounds;<sup>21</sup> and ii) known issues have been described for compounds carrying a net charge (in particular for the solute's charging free energy).<sup>22</sup> The latter effect arises from finite-size effects due to the discrepancy between the actual simulations and the ideal bulk conditions, which results in inaccuracies on the determination of the electrostatic component of the solvation/hydration free energy for these compounds.

Each  $\lambda$  state was minimized using GROMACS' steepest descent minimization algorithm and equilibrated for a total of 150 ps. The equilibration stage included a 50 ps constant volume stage, and 100 ps constant pressure stage with the Berendsen barostat. These were followed by a 5 ns production phase at each  $\lambda$ , using the Parrinello-Rahman barostat. The overall simulation conditions were adapted from the work by Bannan CC *et al.* from 2016.<sup>23</sup>

The contribution of the van der Waals interactions for the hydration/solvation free energy was assessed using the Multistate Bennett Acceptance Ratio (MBAR)<sup>24</sup> through the Alchemical Analysis tool.<sup>25</sup> For this analysis we discarded the initial 100 ps of the production stage.

The results for the vdW component of the free energy of transfer are shown as:

$$\Delta G_{aq \rightarrow oct}^{vdw} = \Delta G_{solvation}^{vdw} - \Delta G_{hydration}^{vdw} \quad [1]$$

The correlation plots between the experimental partition results and the SASA, Volume and  $\Delta G_{aq \rightarrow oct}^{vdw}$  are shown in Figure S7.

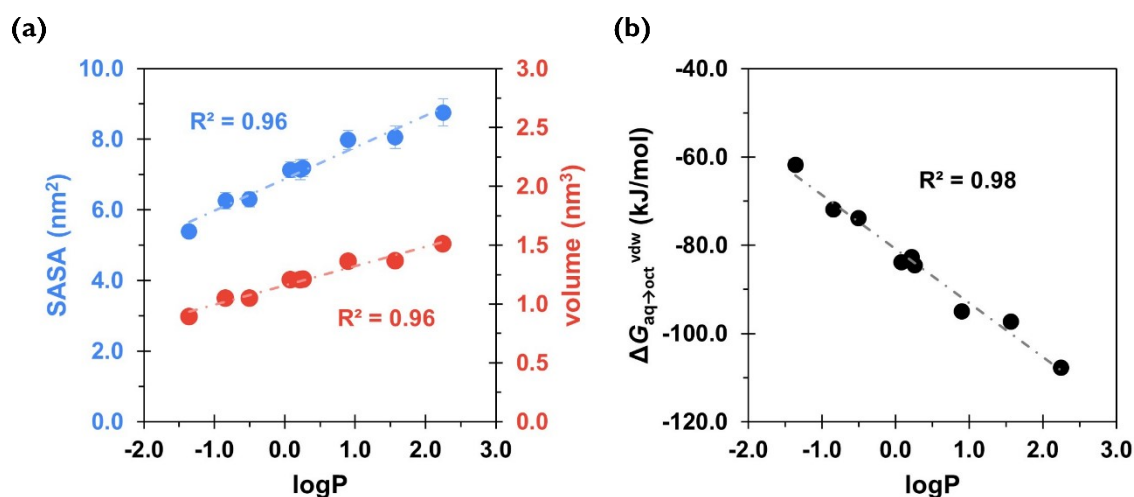


**Figure S7.** Correlation plots between (a) SASA and volume against the experimental  $\log P$ ; and (b)  $\Delta G_{aq \rightarrow oct}^{vdw}$  against the experimental  $\log P$ . Error bars correspond to the standard deviation and the  $R^2$  values for the linear fits are provided.

---

## 9.2 Umbrella sampling simulations

*System modeling.* Our all-atom hydrated bilayer model system was composed of 72 1-palmitoyl-2-oleoyl-glycero-3-phosphocholine (POPC) lipids (36 lipids per leaflet), a hydration level of 60 water molecules per lipid, and an ionic concentration of *ca.* 0.15 M NaCl. It was assembled using the CHARMM-GUI interface using the AMBER force field.<sup>26-29</sup> After an initial minimization and equilibration of the system, we have inserted two replicas of the studied compounds at different bilayer depths in the simulation box: one of the replicas was inserted in the water phase, and the other at the center of the lipid bilayer (see next sections for details). The cations were parameterized as described in the previous section.

*Molecular dynamics simulations parameters.* The all-atom simulations were performed with the GROMACS 2018 software, with the Verlet cut-off scheme. A non-bonded cut-off value of 1.0 nm was employed. The LINCS constraint algorithm was applied to all bonds involving hydrogen atoms, and for the production stage to all bonds. We have also employed a hydrogen mass repartition protocol for the production stage,<sup>30</sup> which allowed for an integration time step of 4 fs. Temperature was set to 298.15 K with the v-rescale thermostat (0.5 ps time constant for coupling for the production stage and 1 ps for the equilibration stages),<sup>31</sup> and a semi-isotropic pressure scaling to 1 atm was maintained with the Parrinello–Rahman barostat (5 ps time constant for coupling). During the NPT equilibration, the Berendsen barostat was employed. Dispersion corrections were applied to energy and pressure terms. Periodic boundary conditions were considered, and long-range electrostatic interactions were treated by a Particle Mesh Ewald (PME) scheme. The center of mass motion was removed in a linear fashion and individually for the upper and lower leaflets and the rest of the system (including the solvent, ions and the two solute molecules).

*Umbrella sampling simulations and analysis.* The hydrated bilayers coming from CHARMM-GUI were minimized and equilibrated in the NVT and NPT ensembles. Subsequently, an NPT conventional MD simulation of 300 ns was run. From the density profiles and as in previous works,<sup>32-34</sup> we have defined a four-region model to aid in the analysis of the PMFs. Region I contained only the hydrophobic lipid

tails. Region II contained both hydrophobic tails and the initial portion of the polar headgroup density, ending where the lipid tail density intercepted the choline density. Region III contained most of the charged phosphate and choline density. Finally, region IV was composed primarily of bulk water, and a small portion of the lipid's headgroup density.

Two replicas of each compound were inserted at different bilayer depths using the last structure of the previous run – one in the water phase and the other near the bilayer's center. The interactions with the hydrated bilayer system were then gradually switched on during 7.5 ns, with the compounds harmonically restrained to the initial positions relative to the bilayer's COM (with a harmonic force constant of 2000 kJ·mol<sup>-1</sup>·nm<sup>-2</sup>). Afterwards, a constant pulling simulation of 50 ns was performed to sample the desired translocation coordinate (pulling rate of -0.000074 nm·ps<sup>-1</sup>). The translocation coordinate in this case was defined by the COM distance between the solute and the lipid bilayer and was discretized into 38 sampling windows spaced by 0.1 nm. This comprised the COM distances of [-3.5; 0.2] nm and [-0.2; 3.5] nm, depending on whether the compound started in the water phase or near the center of the bilayer. Then production runs were performed for 160 ns (with a harmonic force constant of 1500 kJ·mol<sup>-1</sup>·nm<sup>-2</sup>). The binding free energy,  $\Delta G_{bind}^{\circ}$ , was then derived from the energy profile using equation [2]:<sup>35, 36</sup>

$$\Delta G_{bind}^{\circ} = -k_B T \ln \left( \frac{1}{2z_b} \int_{-z_b}^{z_b} e^{-\beta w(z)} dz \right) \quad [2]$$

where  $z_b = 3.4 \text{ nm}$  represents the distance at which the potential of mean force (PMF),  $w(z)$ , is zero and  $\beta = 1/k_B T$ , where  $T$  is adjusted to the temperature in which the profiles were generated, and  $k_B$  represents the Boltzmann constant. The partition coefficient,  $P$  can then be derived using equation [3]:<sup>37</sup>

$$P = e^{-\beta \Delta G_{bind}^{\circ}} \quad [3]$$

---

For the calculation of the binding free energies, we have considered the energy profiles produced from the last 100 ns of each window of the production runs. These were assessed with the weighted histogram analysis method (WHAM) tool<sup>38,39</sup> available in GROMACS 2018. A bootstrapping analysis (200 bootstraps) was also performed to assess for the error of the energy profile.

In Table S3, we provide additional parameters of the free energy diagrams for the cations' translocation through the hydrated bilayer system.

**Table S3.** Additional parameters of the energy profile diagrams. We show the maximum at region III,  $\Delta G_{\max}$ ; the minimum of the profile after the membrane entry and located in region II,  $\Delta G_{\min}$ ; and the barrier at the centre of the bilayer that is in region I,  $\Delta G_{\text{B}}$ .  $\Delta G_{\text{B}}$  was determined from the difference between maximum and minimum values of the energy profiles, but we also show in parenthesis the maximum value of the profiles relative to water (defined at 0.0 kcal·mol<sup>-1</sup>).

compound	$\Delta G_{\max}$ / kcal·mol <sup>-1</sup>	$\Delta G_{\min}$ / kcal·mol <sup>-1</sup>	$\Delta G_{\text{B}}$ / kcal·mol <sup>-1</sup>
<b>1a</b>	3.17	2.14 <sup>a</sup>	13.34 (13.33)
<b>1b</b>	2.58	-0.05	9.86 (9.80)
<b>1c</b>	1.71	-1.71	10.32 (8.61)
<b>2a</b>	2.78	0.13 <sup>a</sup>	9.85 (9.85)
<b>2b</b>	3.02	-0.19	8.17 (7.98)
<b>2c</b>	1.88	-3.42	8.05 (4.63)
<b>3a</b>	2.97	-0.61	7.89 (7.28)
<b>3b</b>	2.05	-2.57	6.56 (3.99)
<b>3c</b>	1.73	-4.15	6.40 (2.25)

<sup>a</sup> The energy profile in region II did not drop below zero, but we have presented the value of the energy profile at the first minimum after the membrane entry.

We have also compared the experimental and simulated logP results. This analysis is depicted in Figure S8.

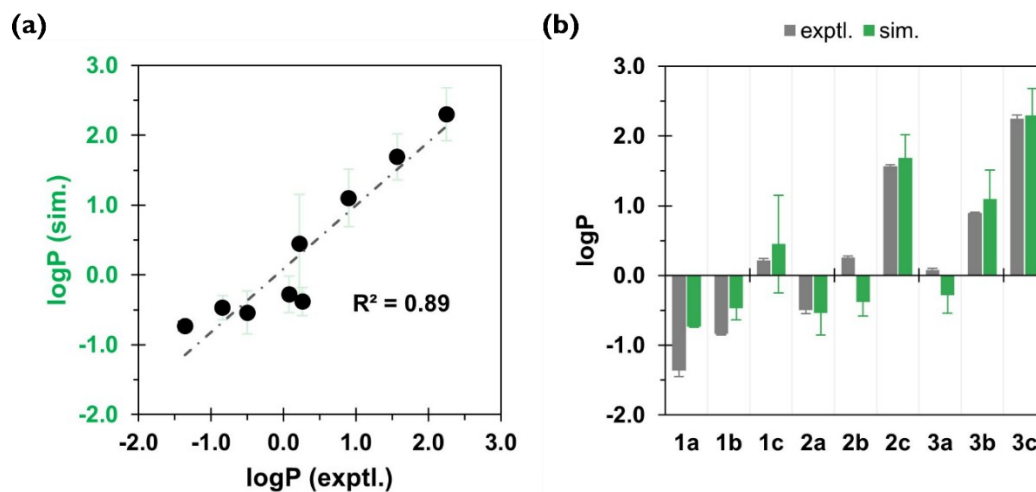


**Figure S8.** Correlation between logP (sim.) against logP (exptl.) (a) and comparison between experimental and simulated logP results (b). The  $R^2$  value for the linear fit is provided. Error bars correspond to the standard deviation. For the logP simulation errors, we have defined the standard deviation between the partition results for the two replicate molecules in the system and they do not represent the errors from the free energy profile curves. Experimental logP results have been determined using water and 1-octanol, and simulated logP results have been measured in a hydrated bilayer system composed of POPC glycerophospholipids.

For assessing the influence of the ion pair to the translocation of **1a**, we have defined two additional coordinates, representing the distance between two distinct Cl<sup>-</sup> counter-ions and the center of mass of each of the two **1a** cations in the system. Using again an umbrella potential, this distance was restrained with a force constant of 1500 kJ·mol<sup>-1</sup>·nm<sup>-2</sup> at 0.55 nm, for the entire translocated distance. This distance was defined from the X-ray distances between the cations and the bromide ions present in the crystals. In Figure S9 we compare the free energy profiles of **1a** and of **1a** when we restrained the distance between the cation and one Cl<sup>-</sup> counter-ion (which we defined as **1a ion-pair**). Figure S9 also shows the average number of contacts with Cl<sup>-</sup> ions for both situations.

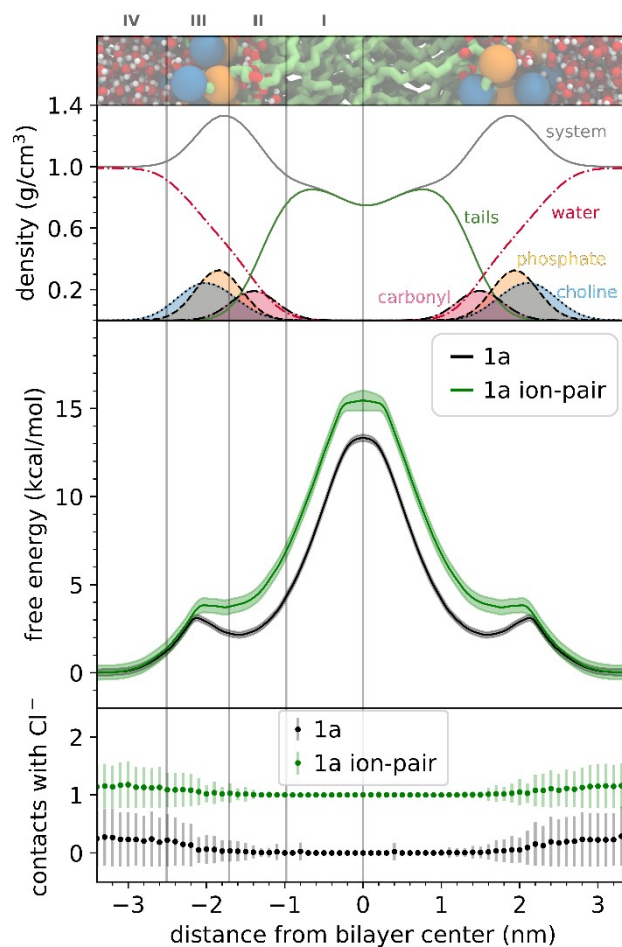


**Figure S9.** Free energy profiles of the translocation of **1a** and of **1a** with a harmonic potential restraint for the distance between the cation and a  $\text{Cl}^-$  counter-ion (defined as **1a ion-pair**), and average number of contacts with  $\text{Cl}^-$  ions in a POPC hydrated bilayer model system. The top two panels show a representation of the hydrated bilayer model system and the partial density profiles for the different functional groups or molecules in the system. The third panel shows the free energy profiles for the translocation of **1a** and of **1a ion-pair** (black and green, respectively). The bottom panel shows the average number of contacts with  $\text{Cl}^-$  counter-ions in the simulation cell for both situations (considering a distance threshold of 0.6 nm). Vertical lines define the four-membrane regions as described in the main text.

Visual inspection of the simulations was attained with the VMD 1.9.3 software.<sup>40</sup>

## 10. NMR Spectra

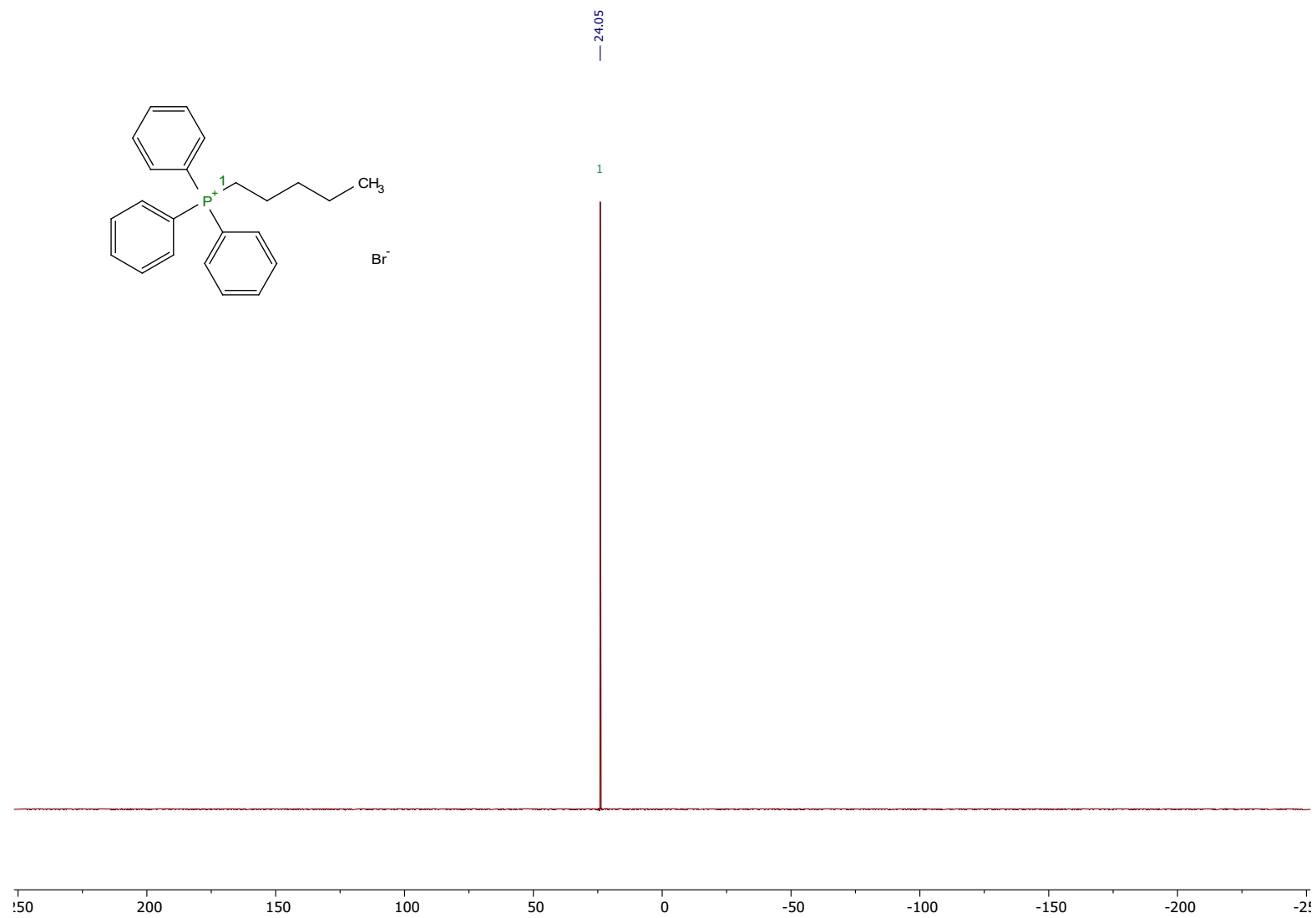


Figure S10.  $^{31}\text{P}\{^1\text{H}\}$  NMR spectrum for **1b**.

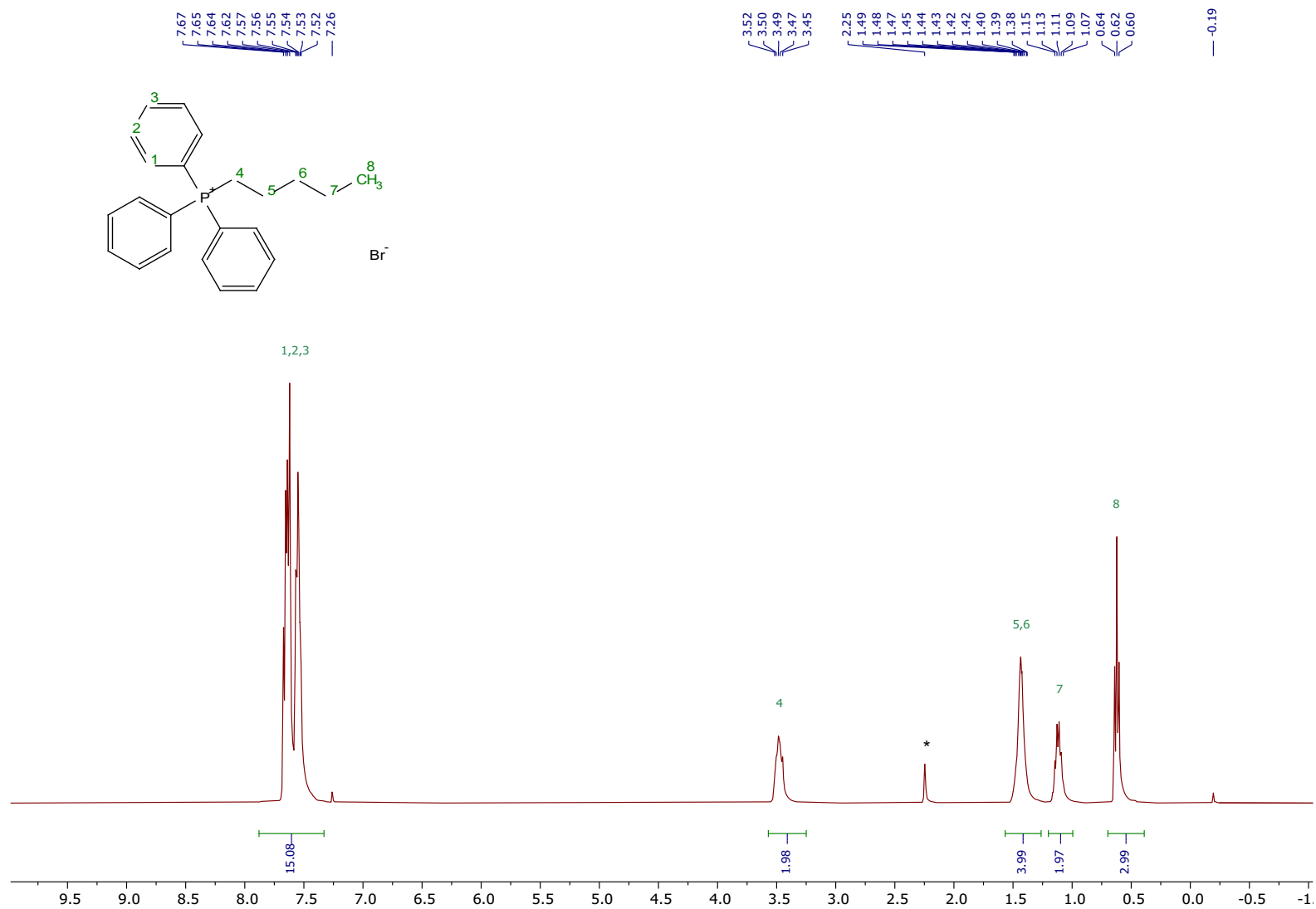


Figure S11.  $^1\text{H}$  NMR spectrum for **1b**.

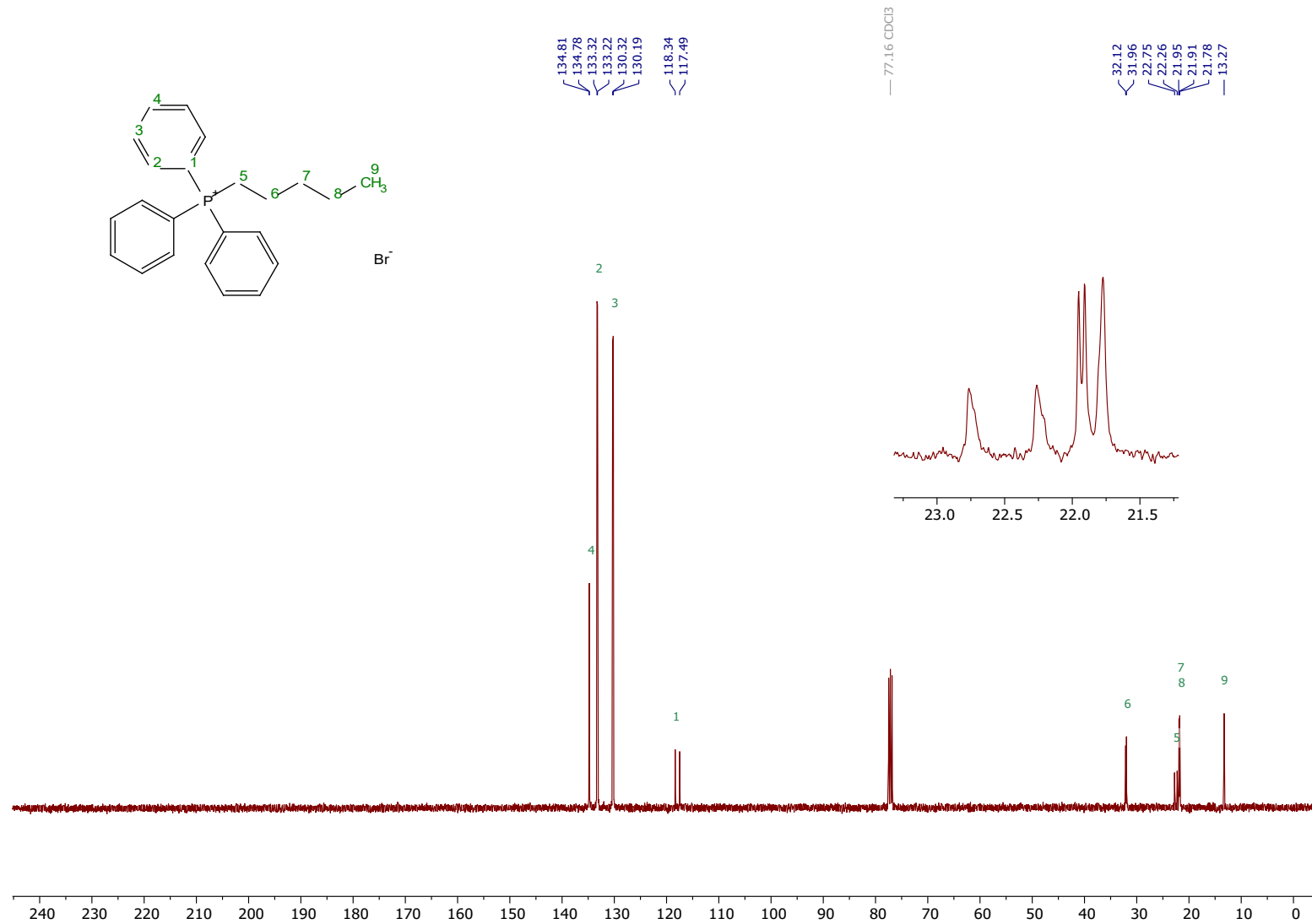


Figure S12.  $^{13}\text{C}\{^1\text{H}\}$  NMR spectrum for **1b**.

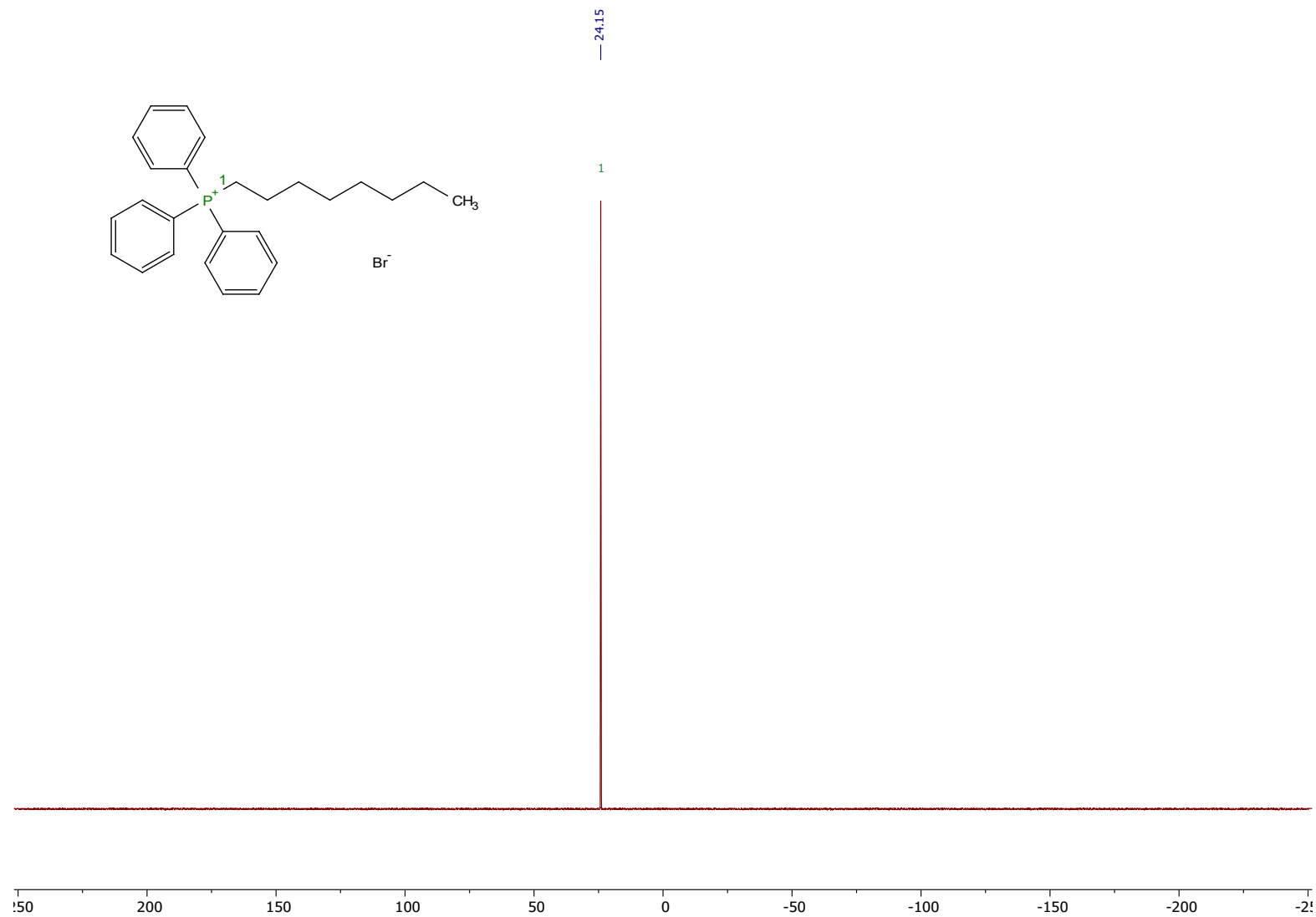


Figure S13.  $^{31}\text{P}\{^1\text{H}\}$  NMR spectrum for **1c**.

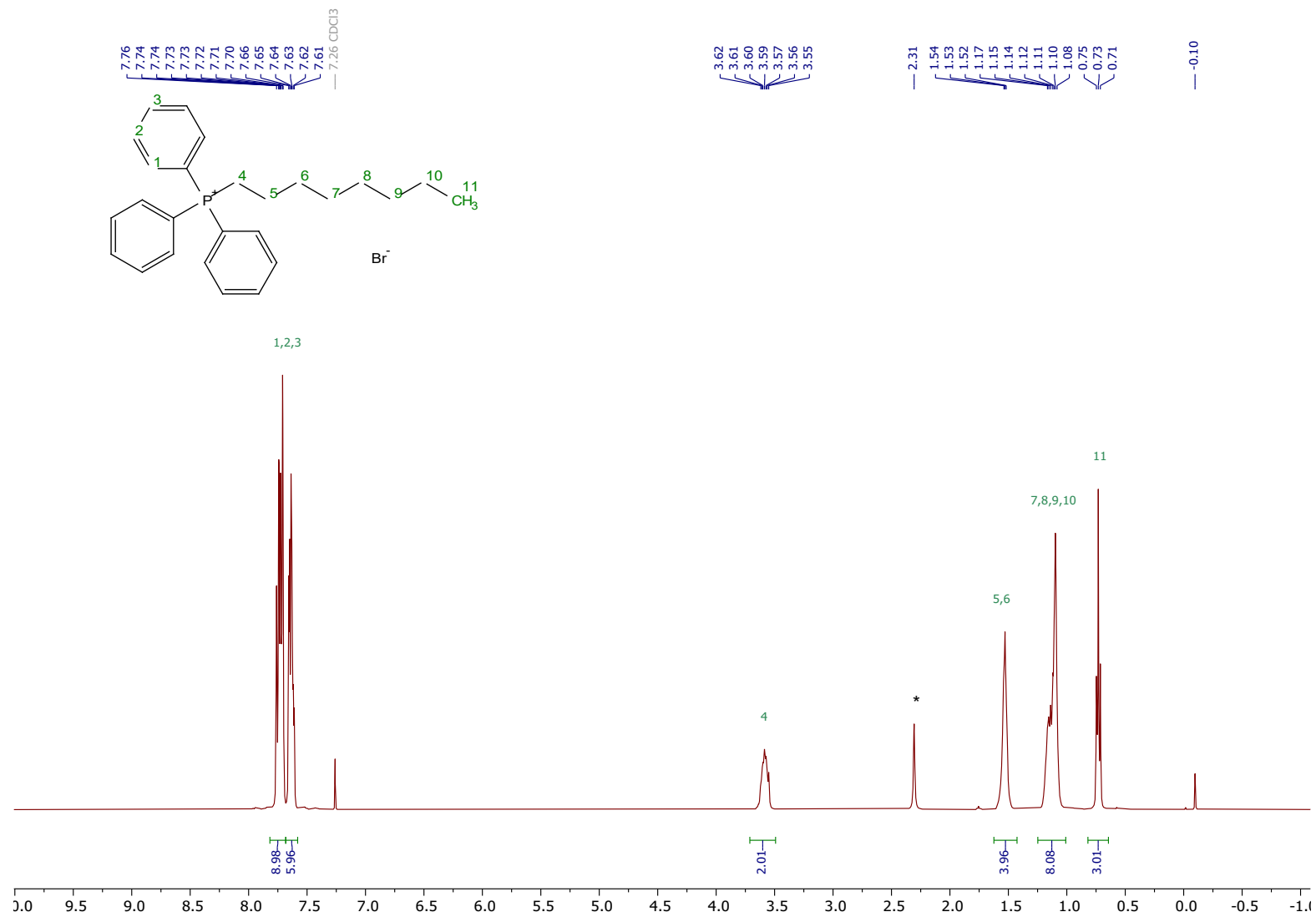


Figure S14.  $^1\text{H}$  NMR spectrum for **1c**.

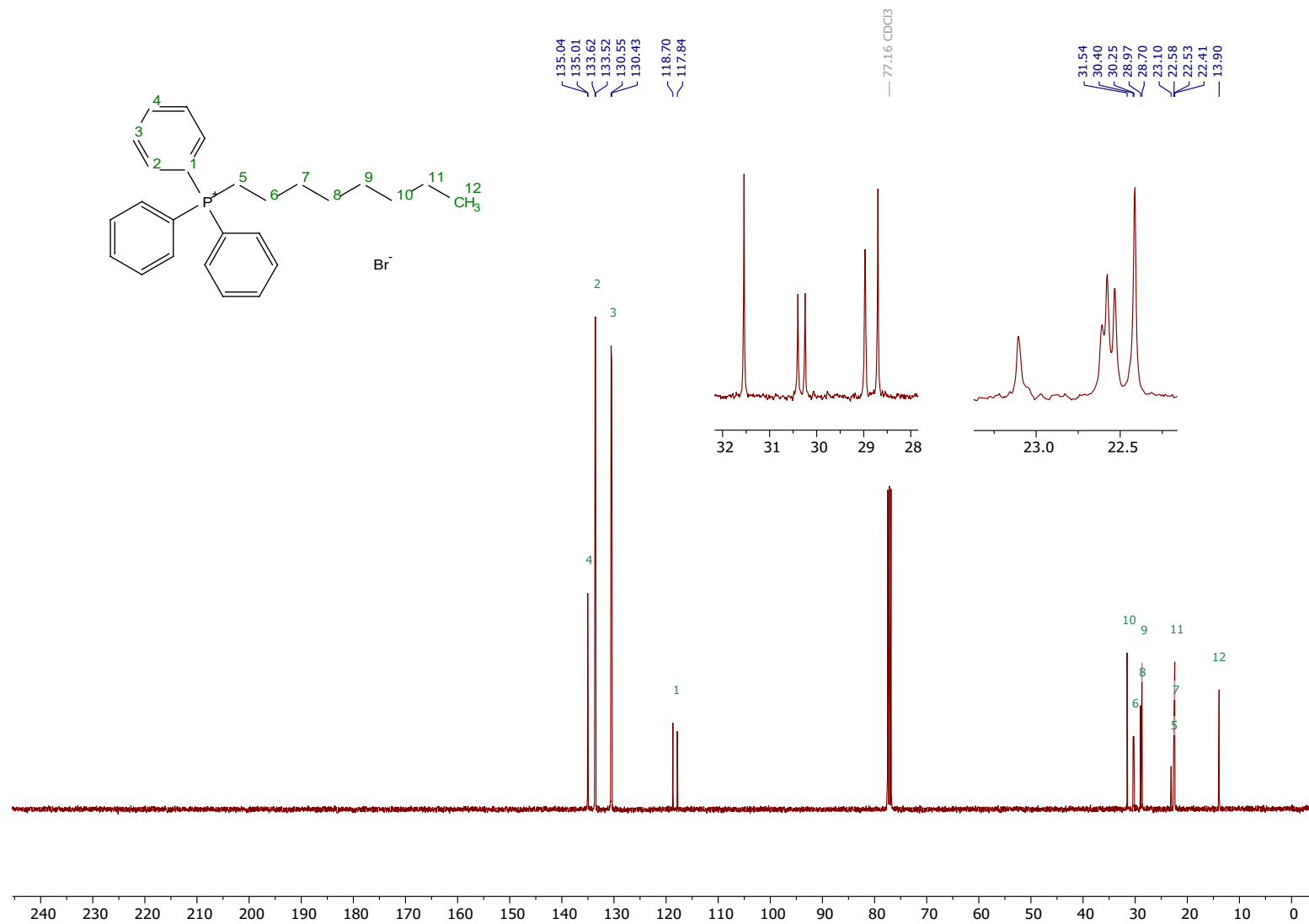


Figure S15.  $^{13}\text{C}\{^1\text{H}\}$  NMR spectrum for **1c**.

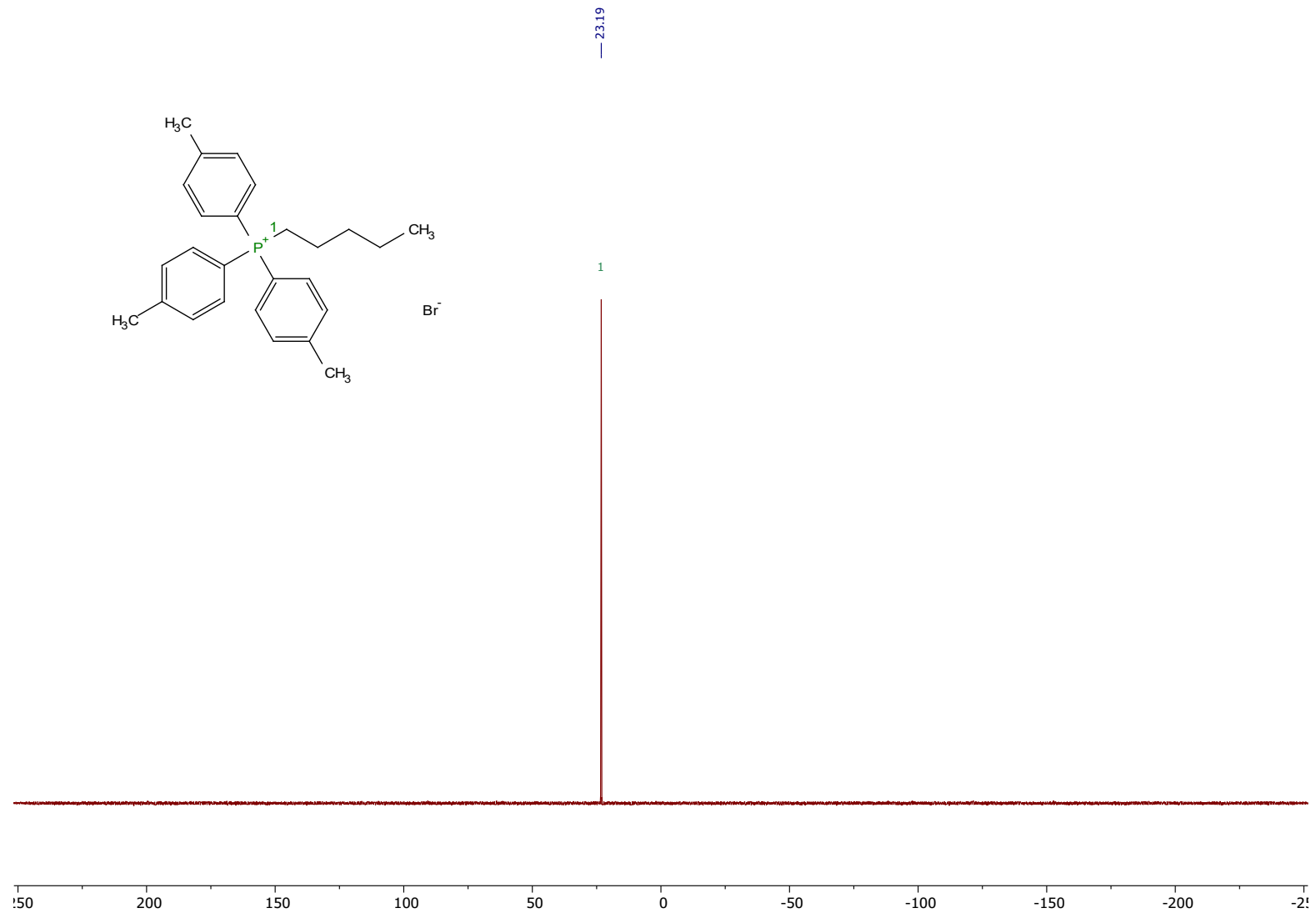
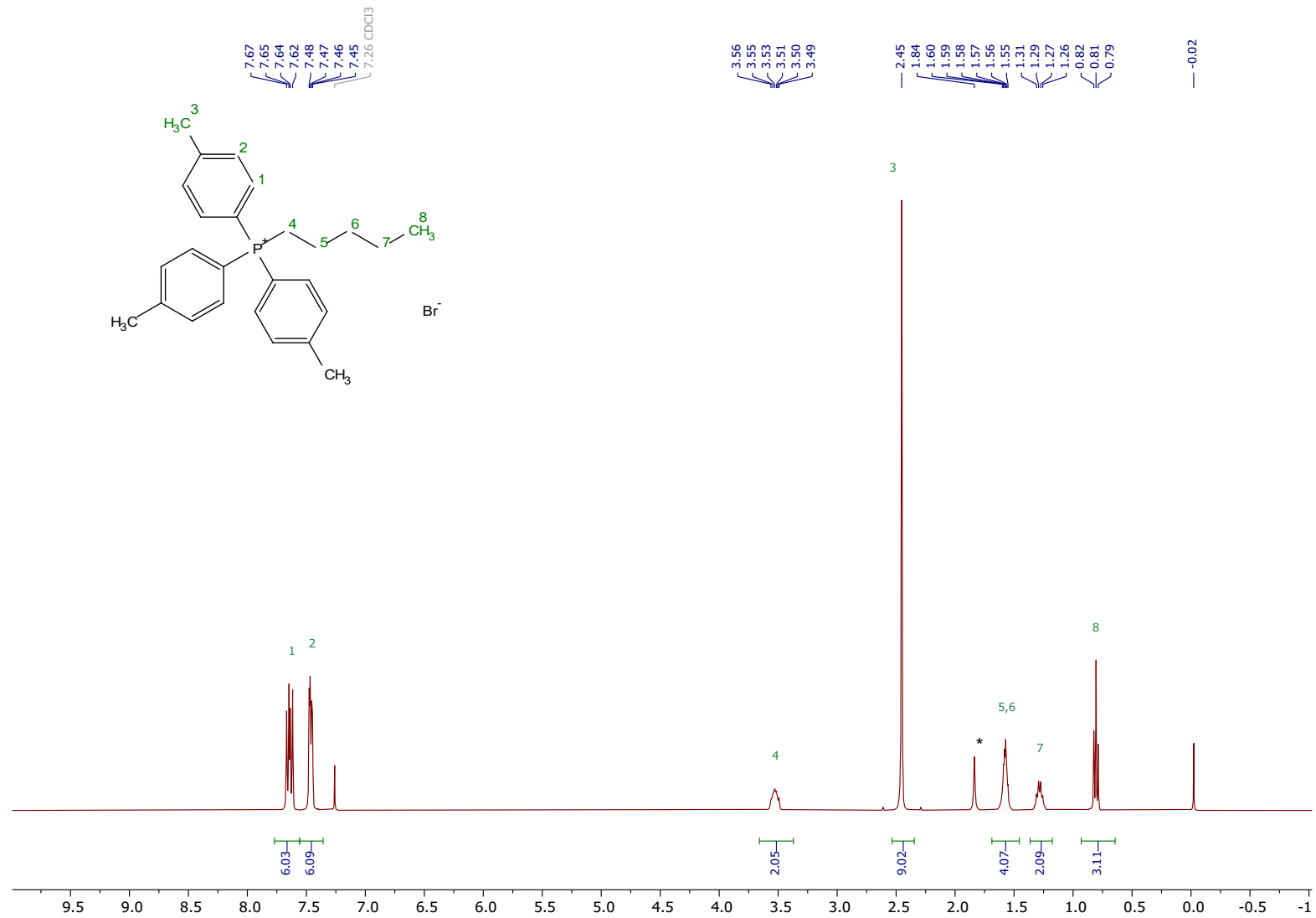


Figure S16.  $^{31}P\{^1H\}$  NMR spectrum for **2b**.



**Figure S17.**  $^1\text{H}$  NMR spectrum for **2b**.

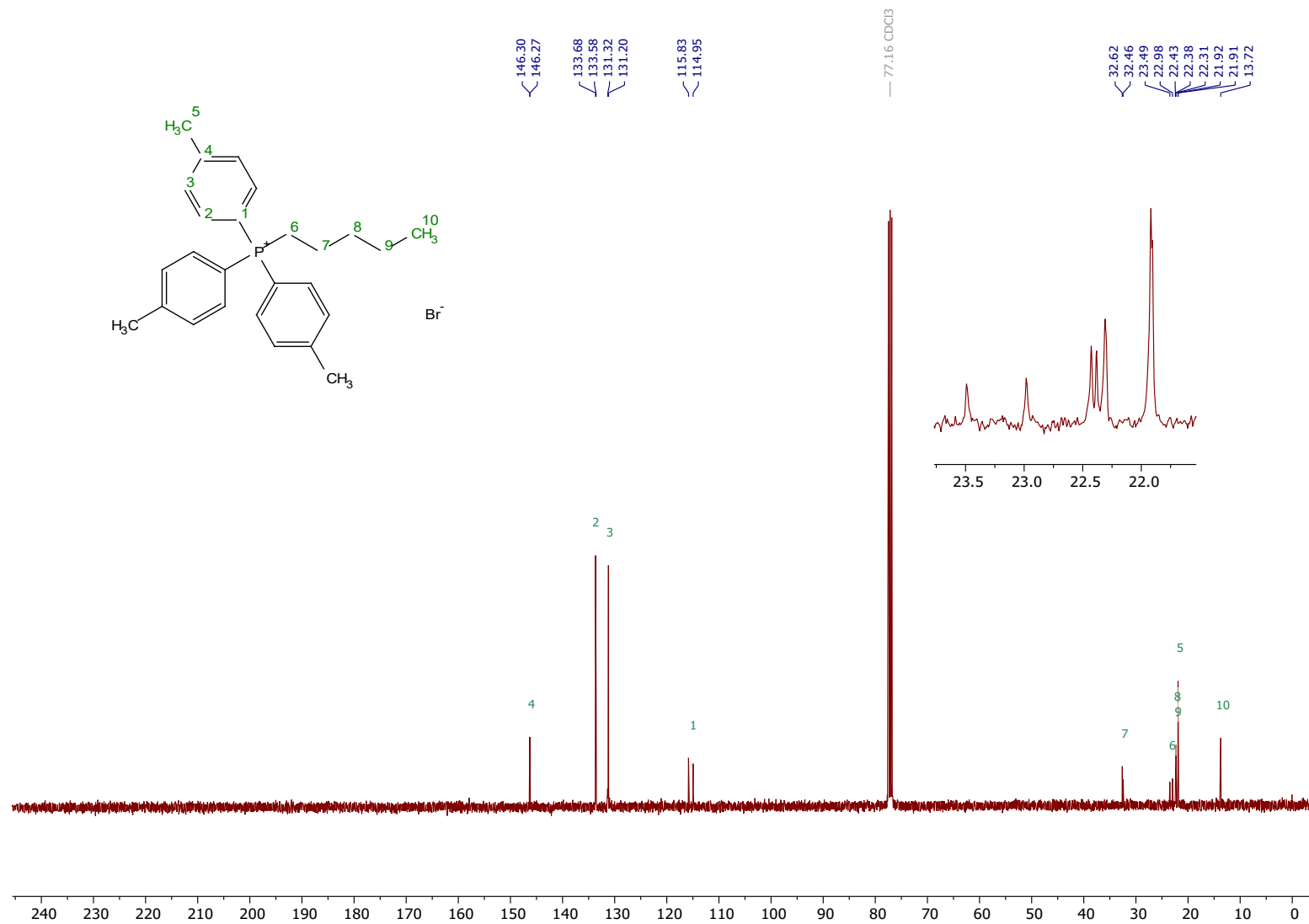


Figure S18.  $^{13}\text{C}\{^1\text{H}\}$  NMR spectrum for **2b**.

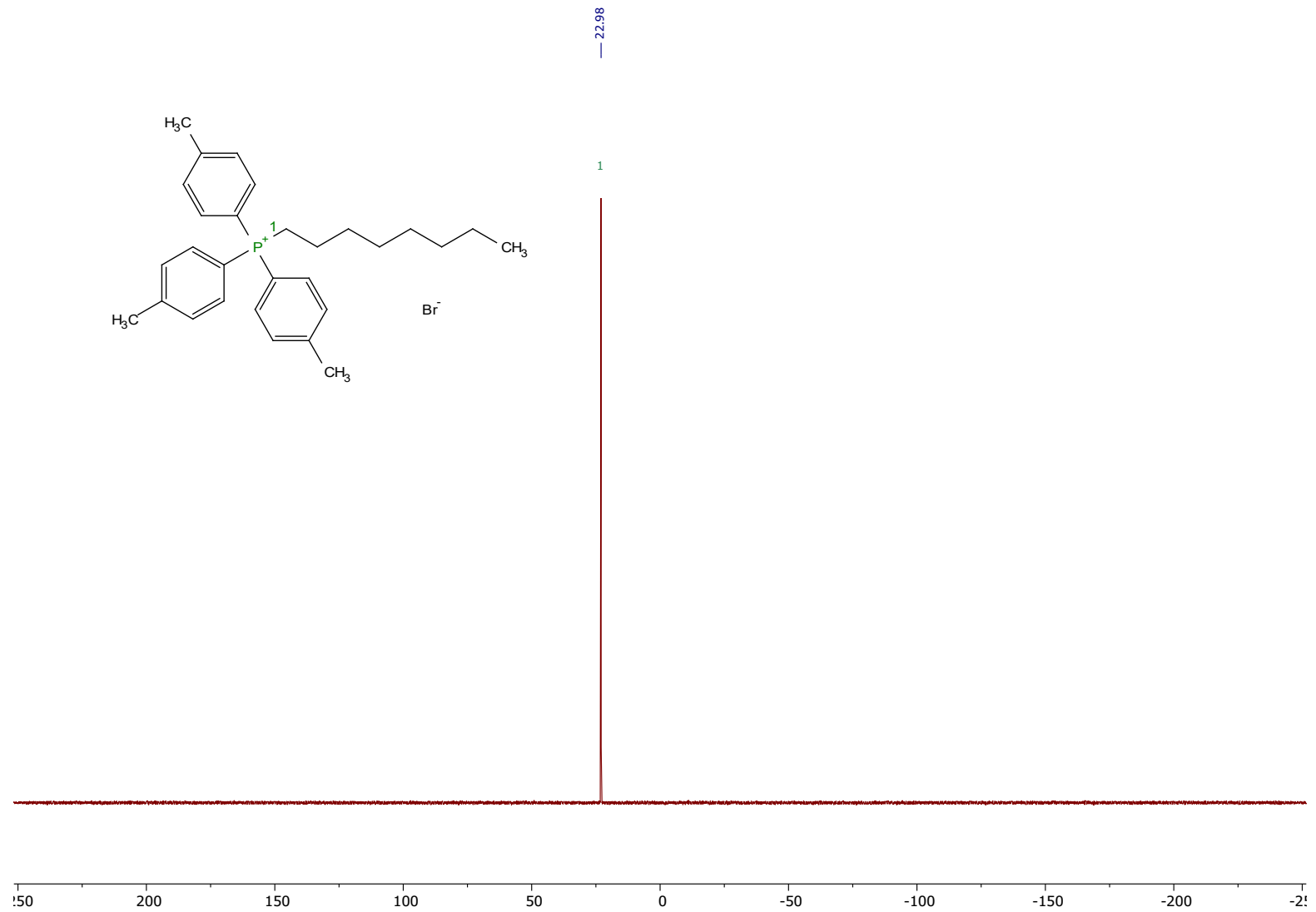


Figure S19.  $^{31}\text{P}\{^1\text{H}\}$  NMR spectrum for **2c**.

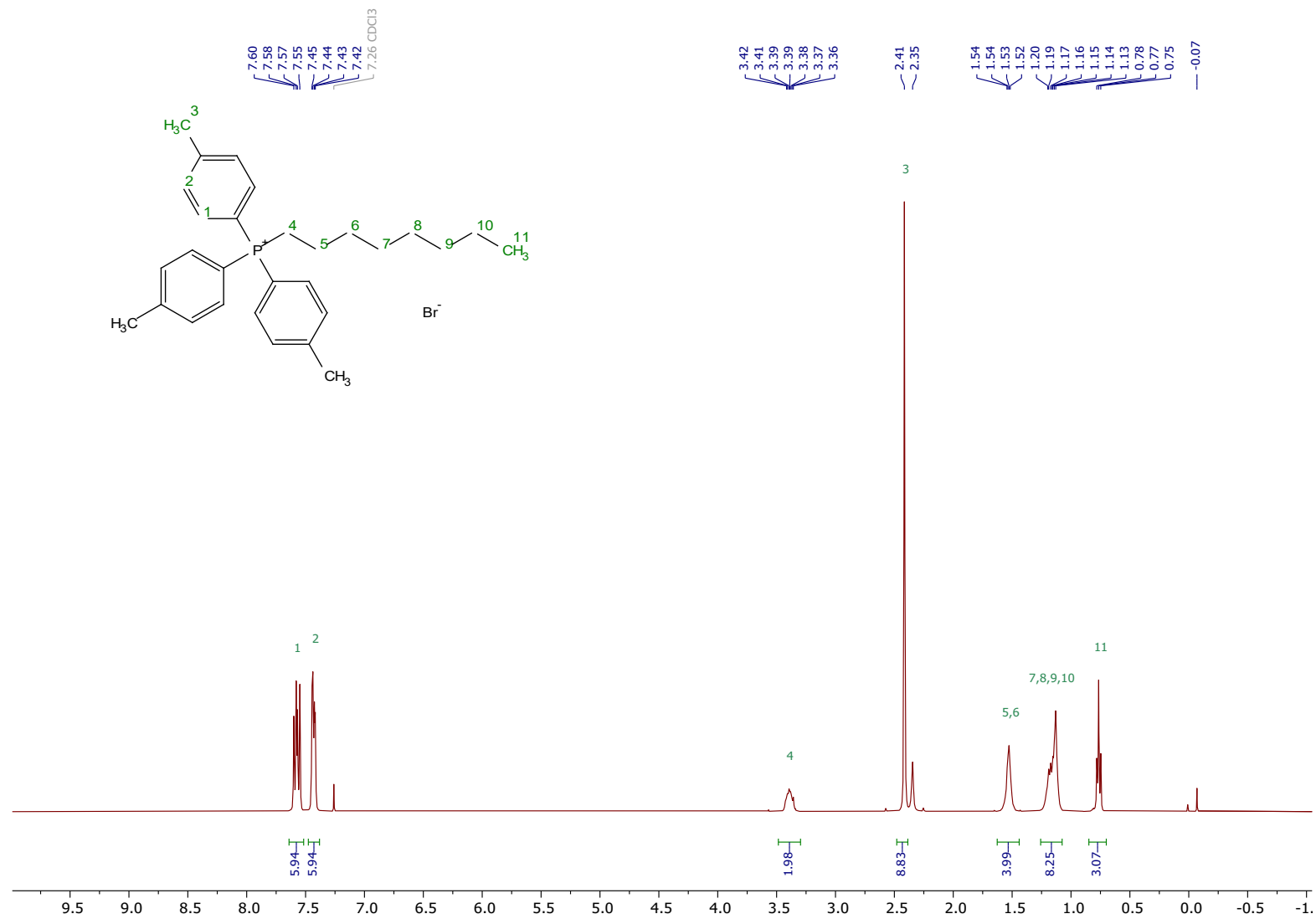


Figure S20. <sup>1</sup>H NMR spectrum for 2c.

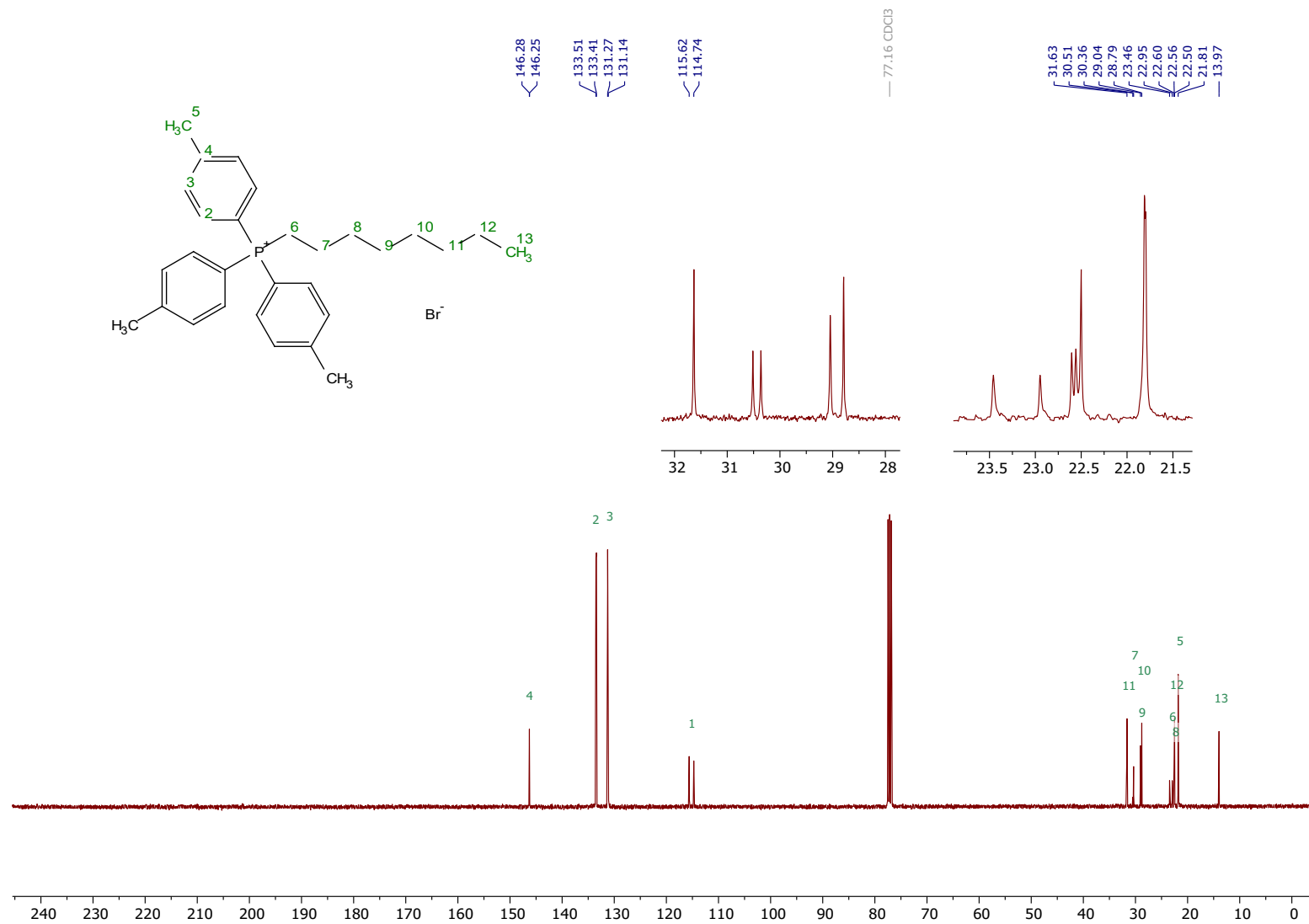


Figure S21.  $^{13}\text{C}\{^1\text{H}\}$  NMR spectrum for **2c**.

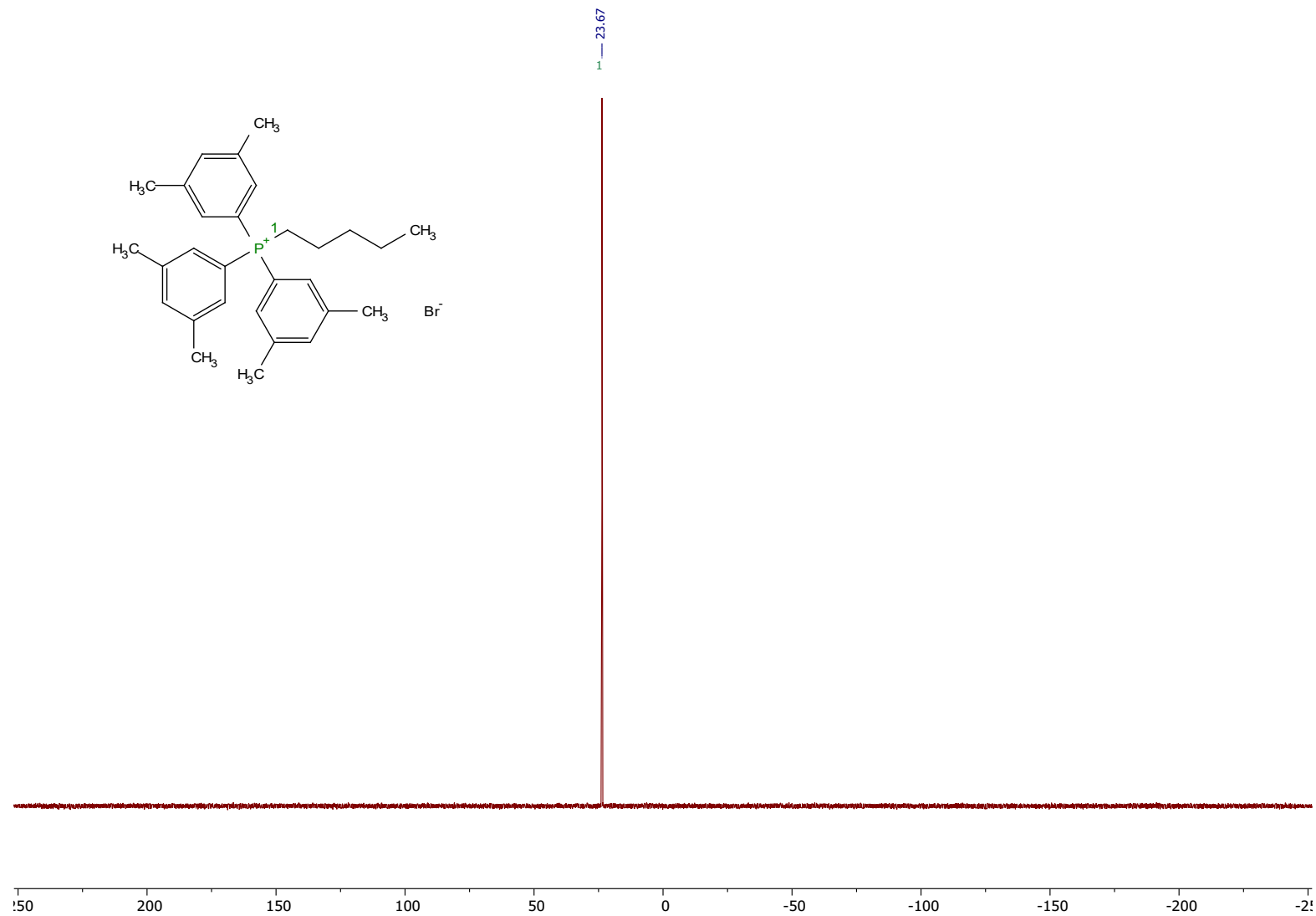
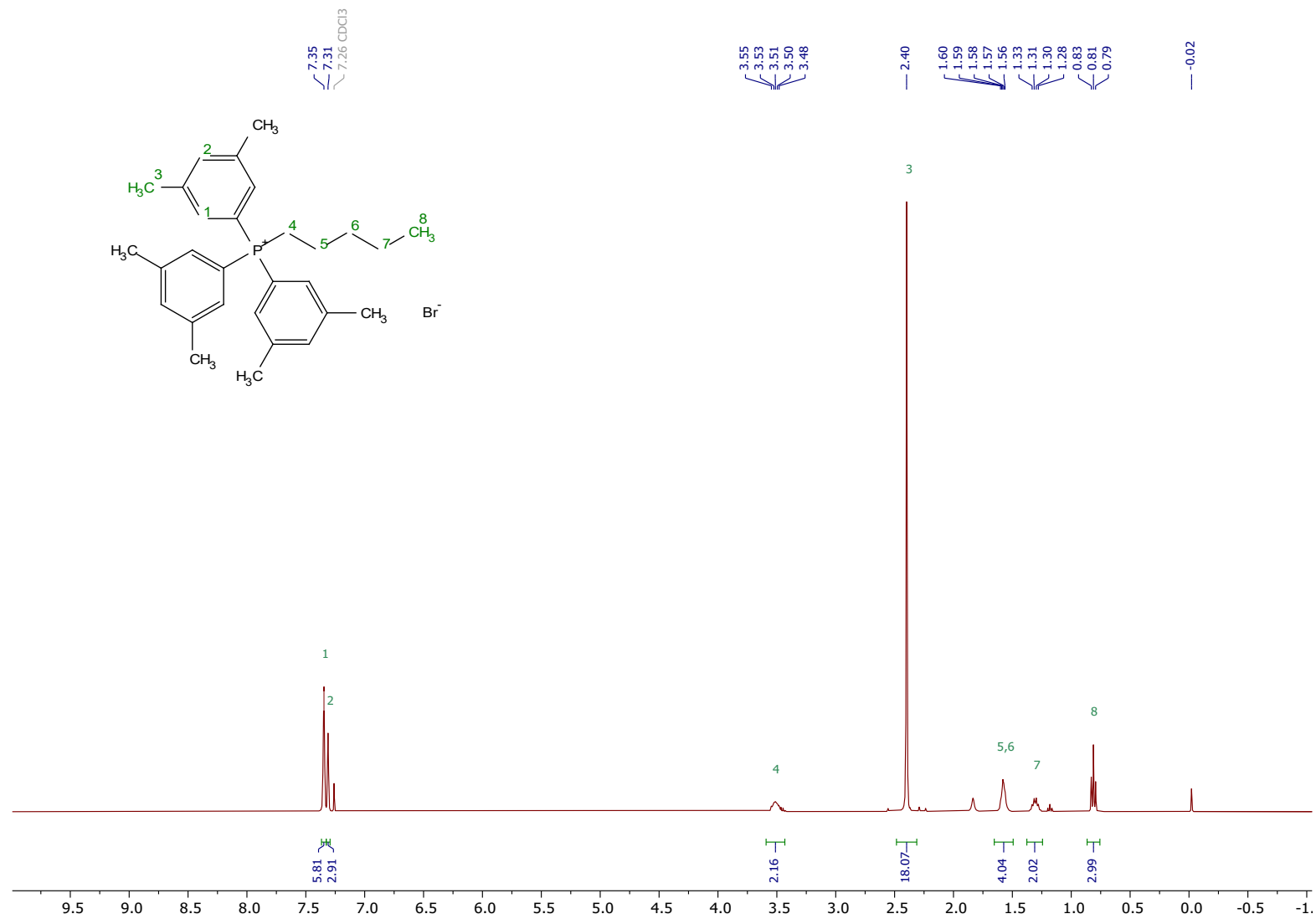


Figure S22.  $^{31}\text{P}\{^1\text{H}\}$  NMR spectrum for **3b**.



**Figure S23.** <sup>1</sup>H NMR spectrum for **3b**.

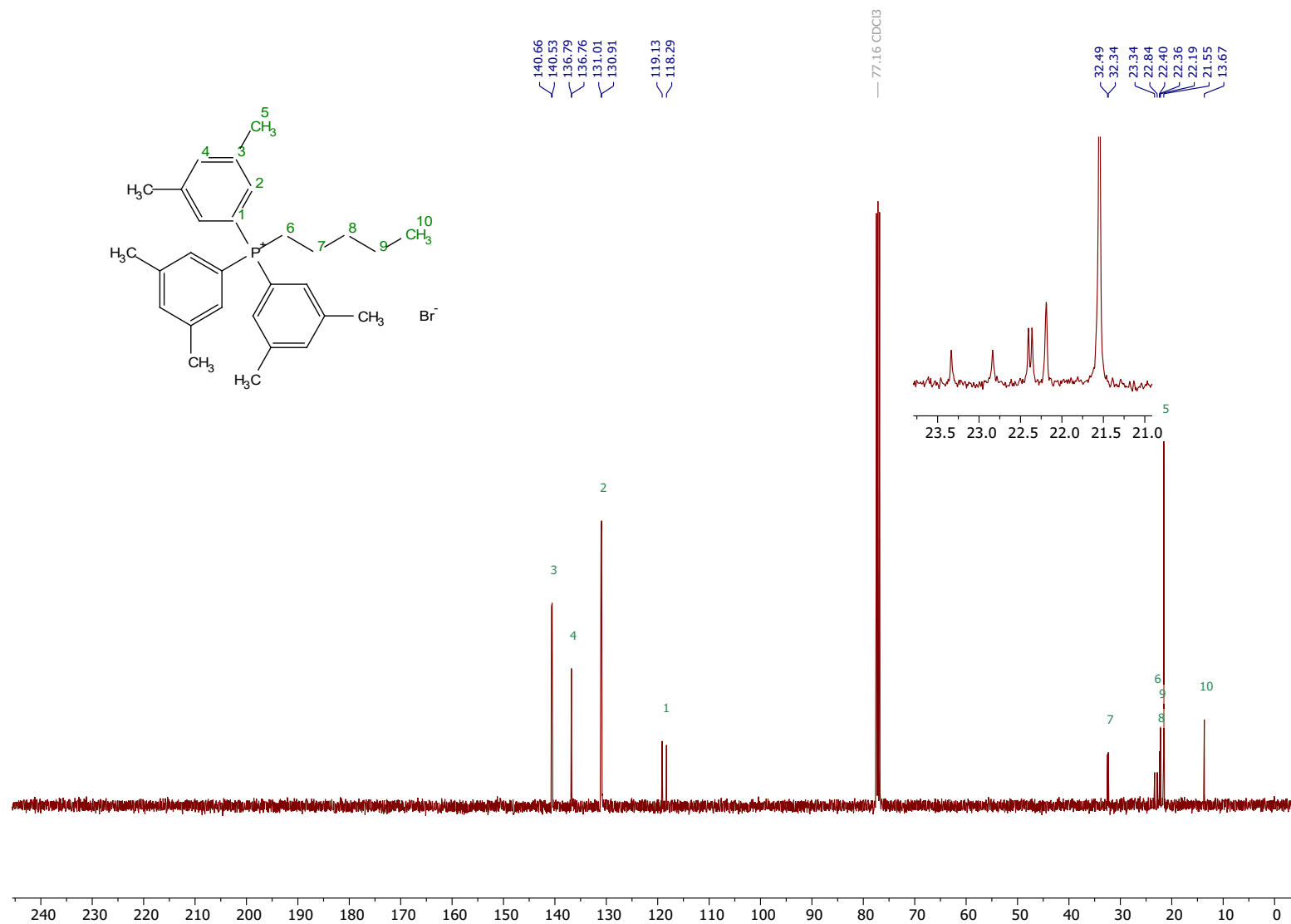


Figure S24.  $^{13}\text{C}\{^1\text{H}\}$  NMR spectrum for **3b**.

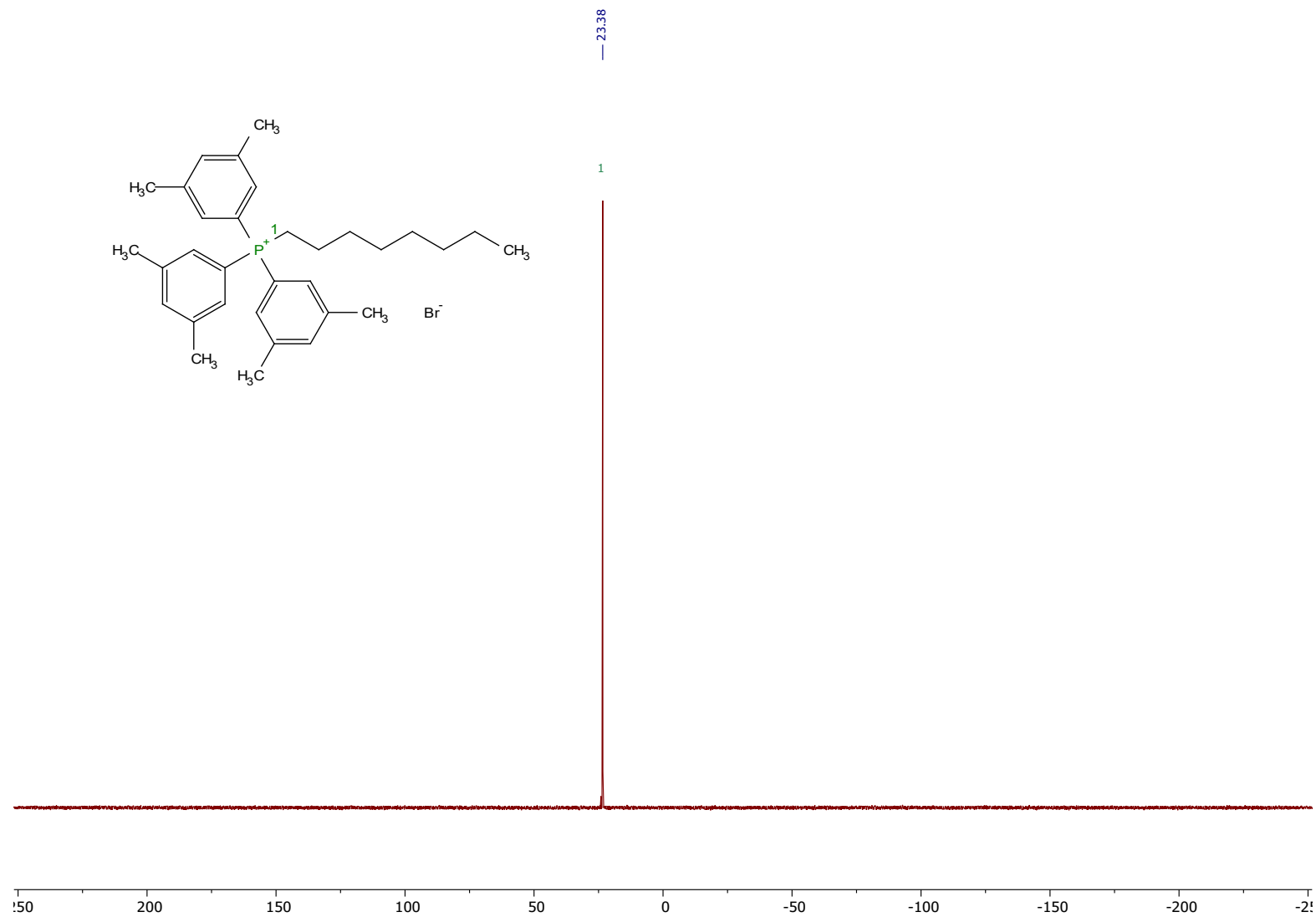


Figure S25.  $^{31}\text{P}\{^1\text{H}\}$  NMR spectrum for **3c**.

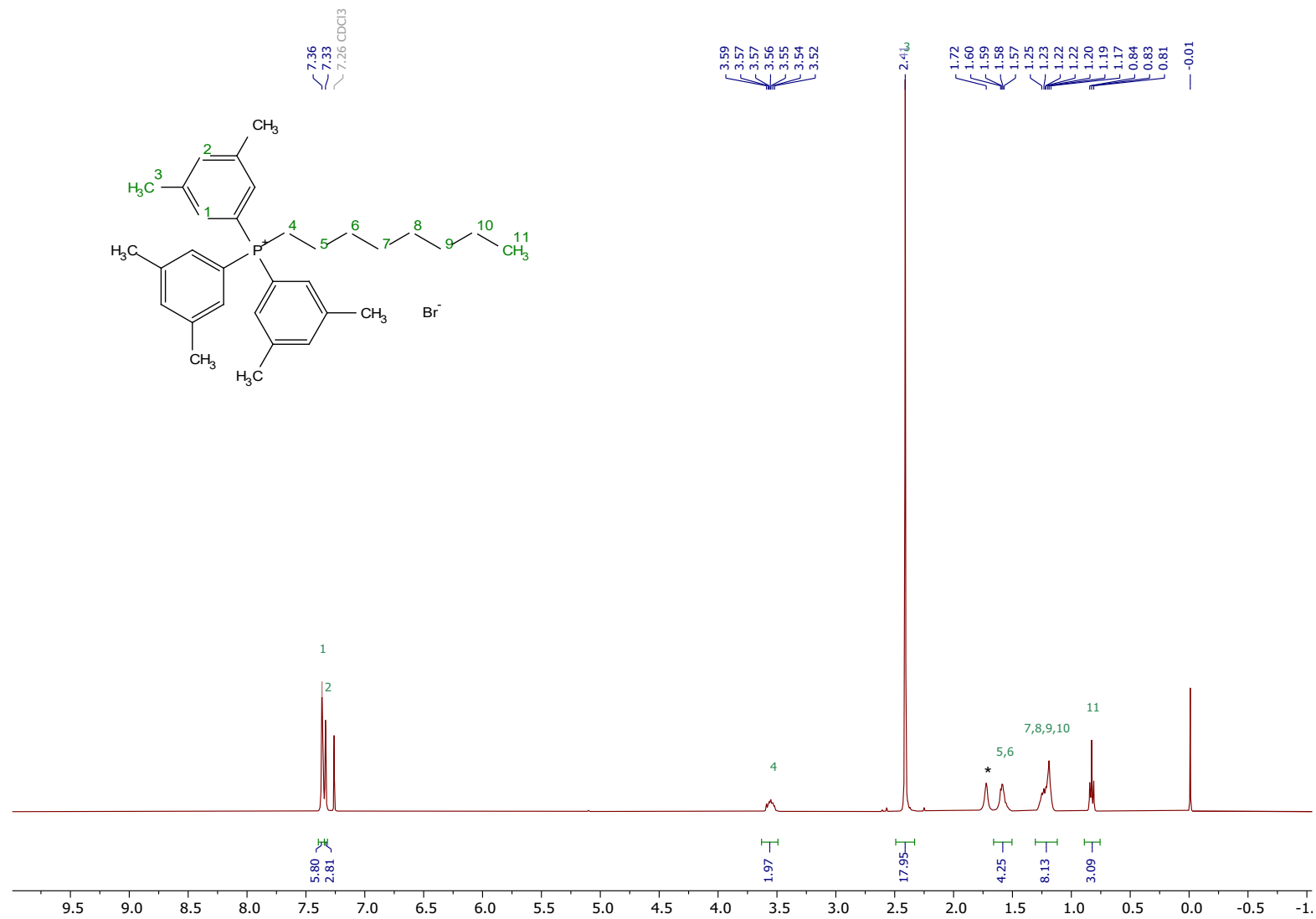


Figure S26. <sup>1</sup>H NMR spectrum for 3c.

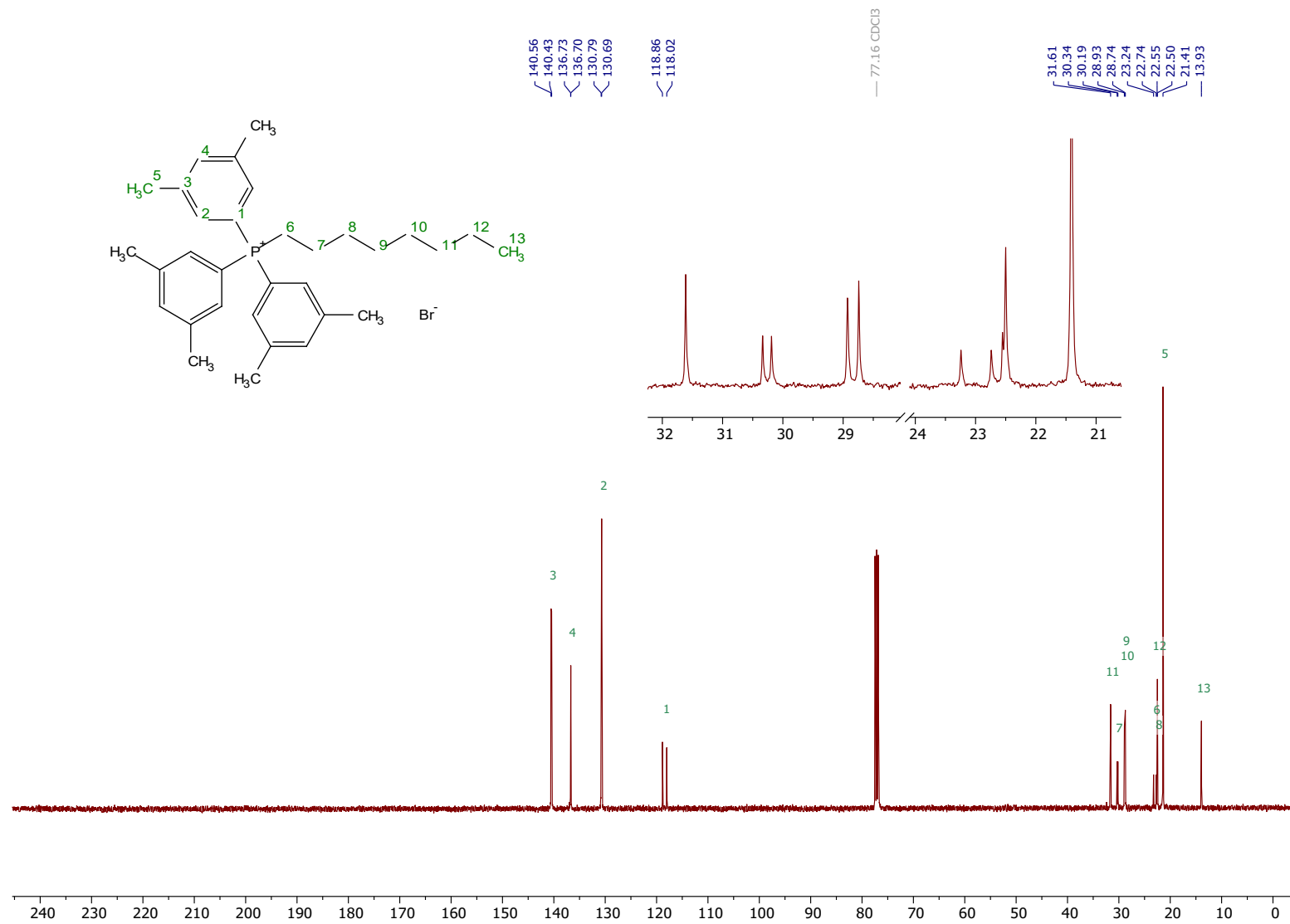


Figure S27. <sup>13</sup>C{<sup>1</sup>H} NMR spectrum for **3c**.

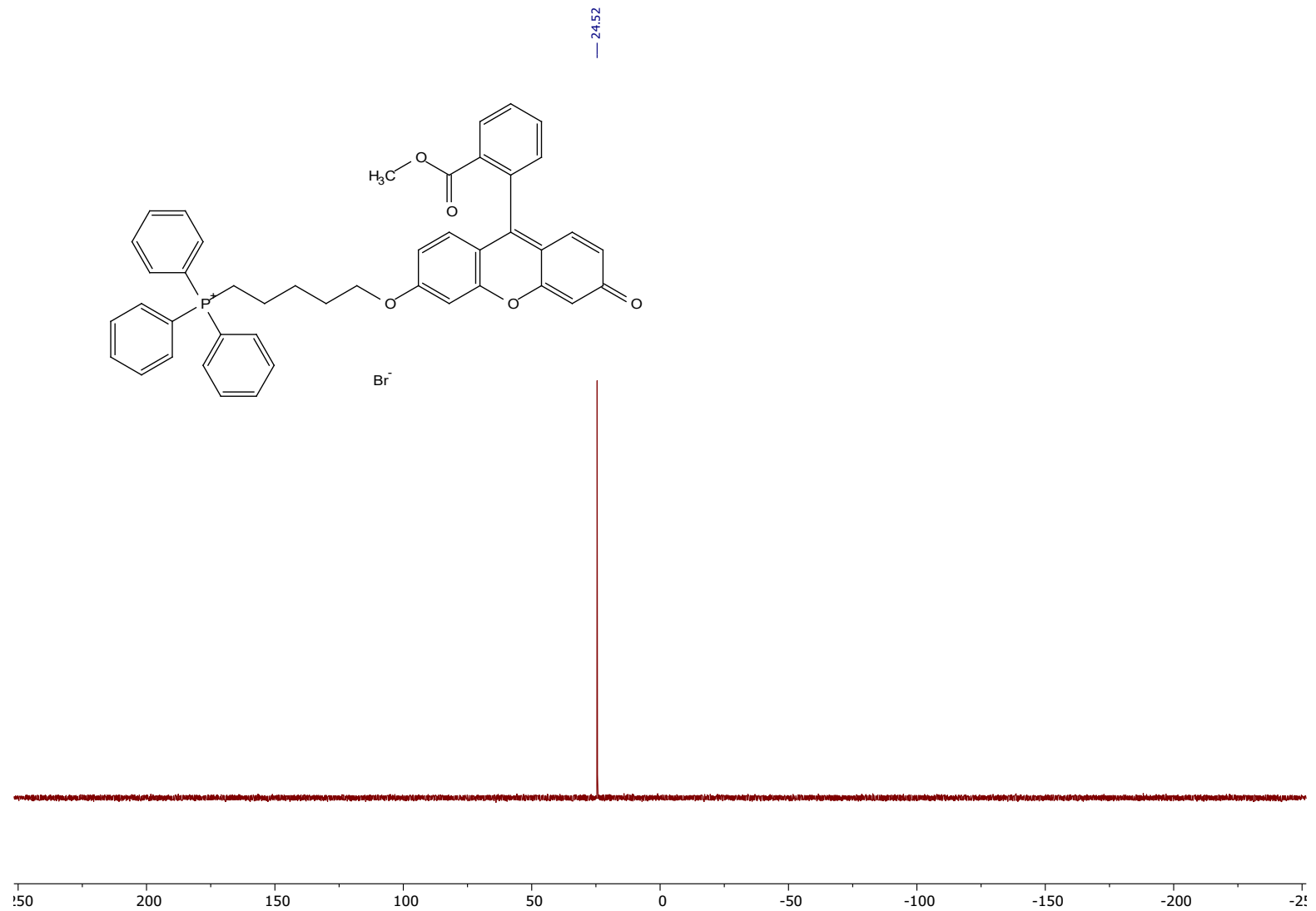


Figure S28. <sup>31</sup>P{<sup>1</sup>H} NMR spectrum for 4a.

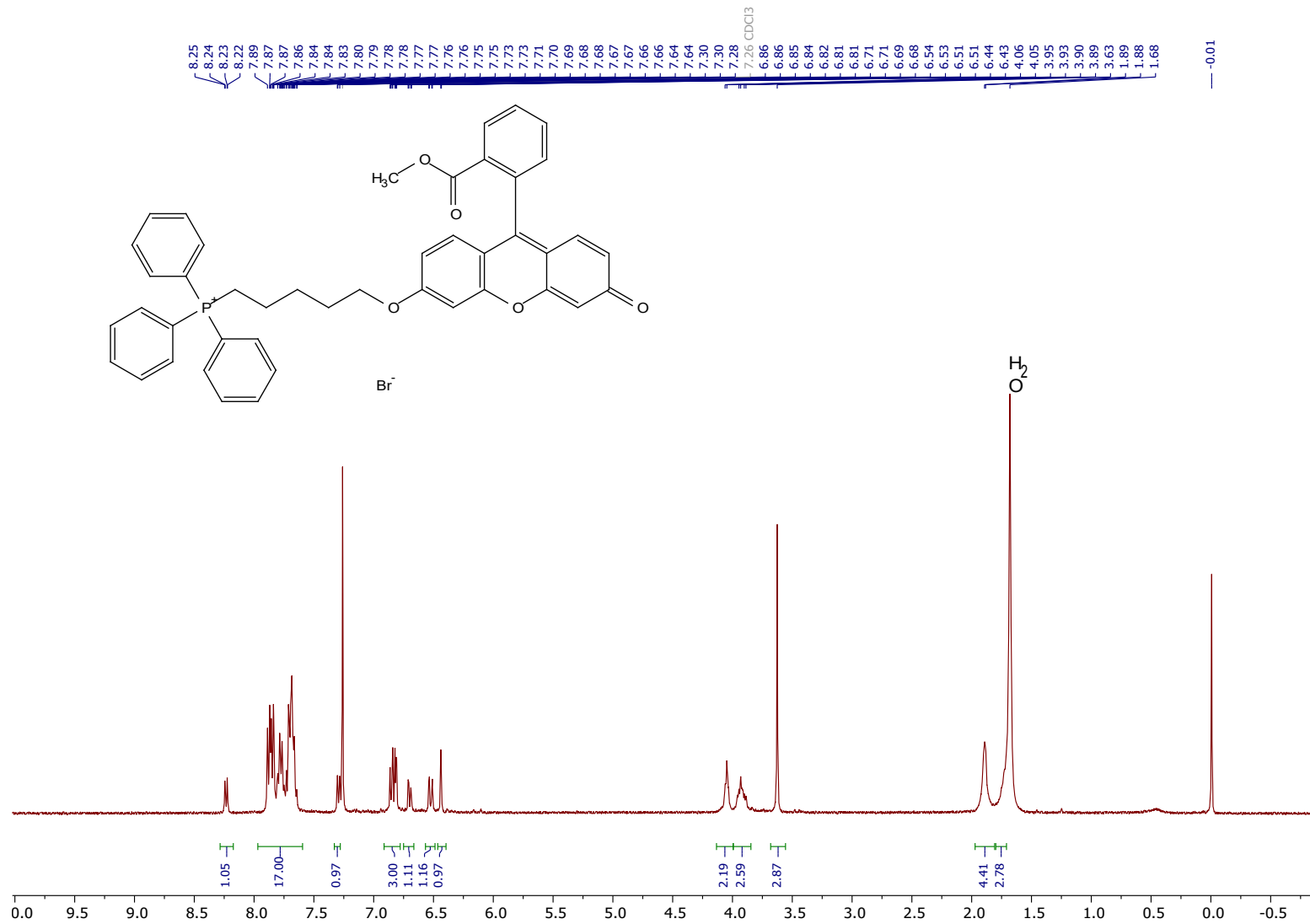


Figure S29.  $^1\text{H}$  NMR spectrum for 4a.

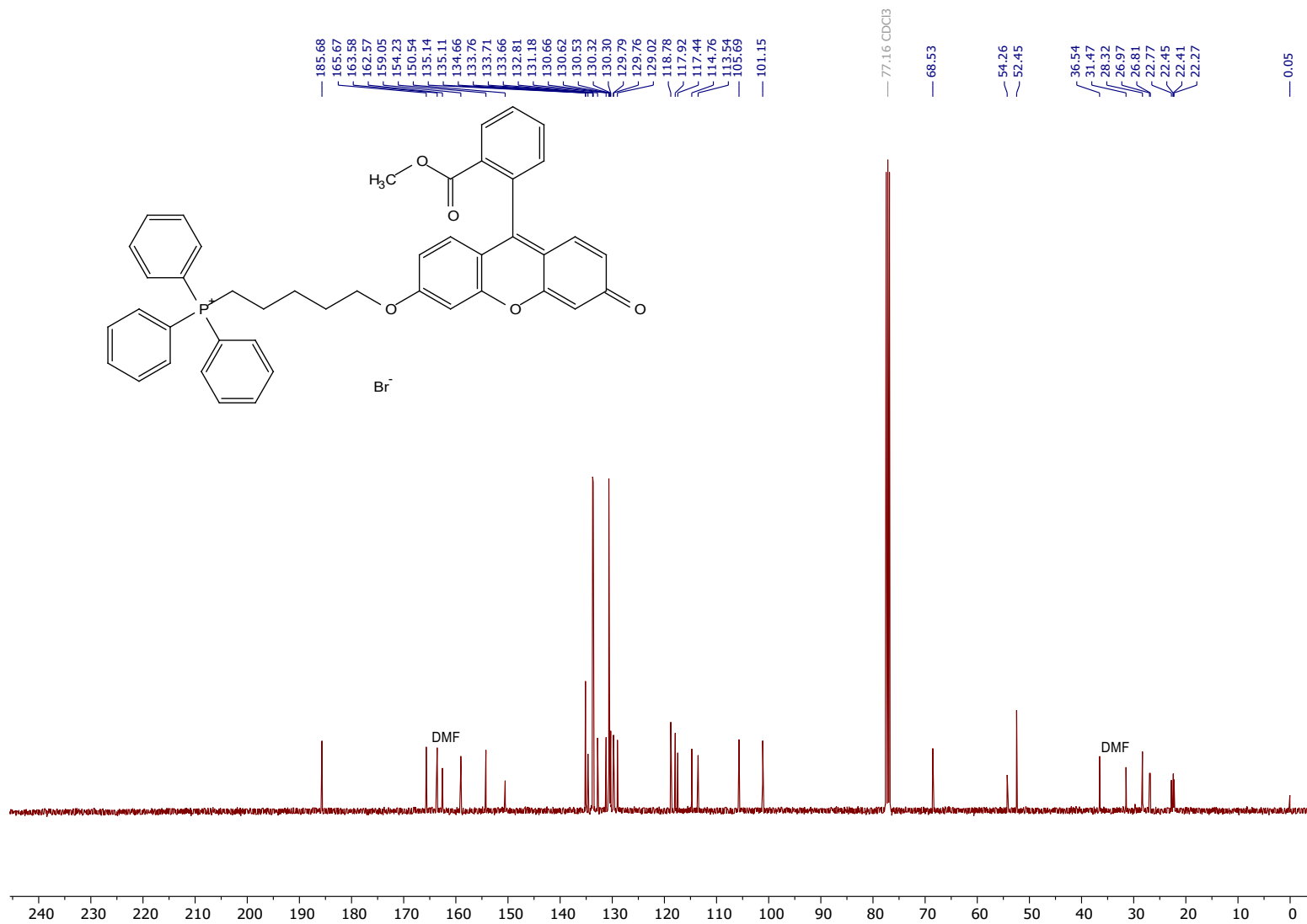
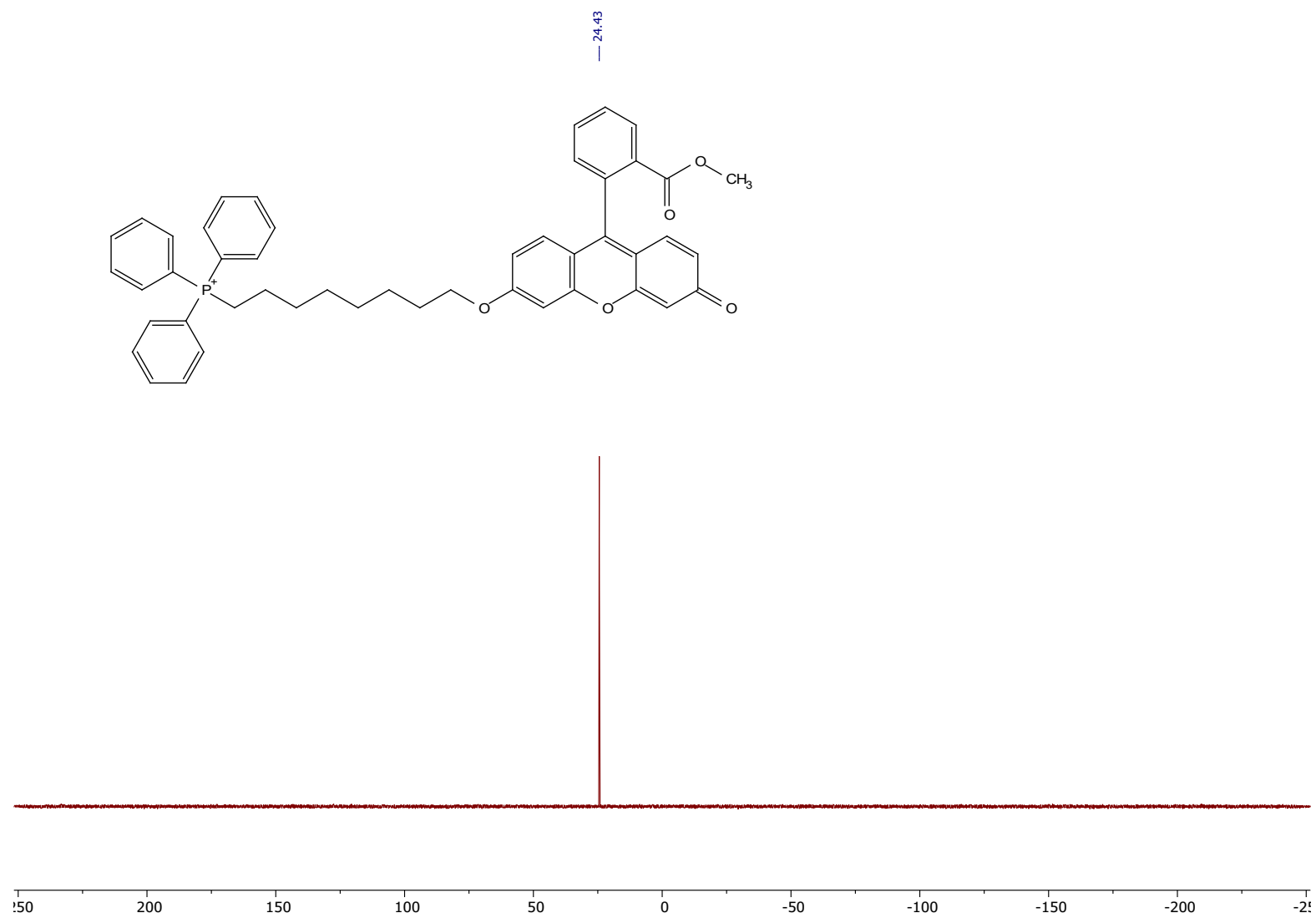


Figure S30.  $^{13}\text{C}\{^1\text{H}\}$  NMR spectrum for 4a.



**Figure S31.**  $^{31}P\{^1H\}$  NMR spectrum for **4b**.



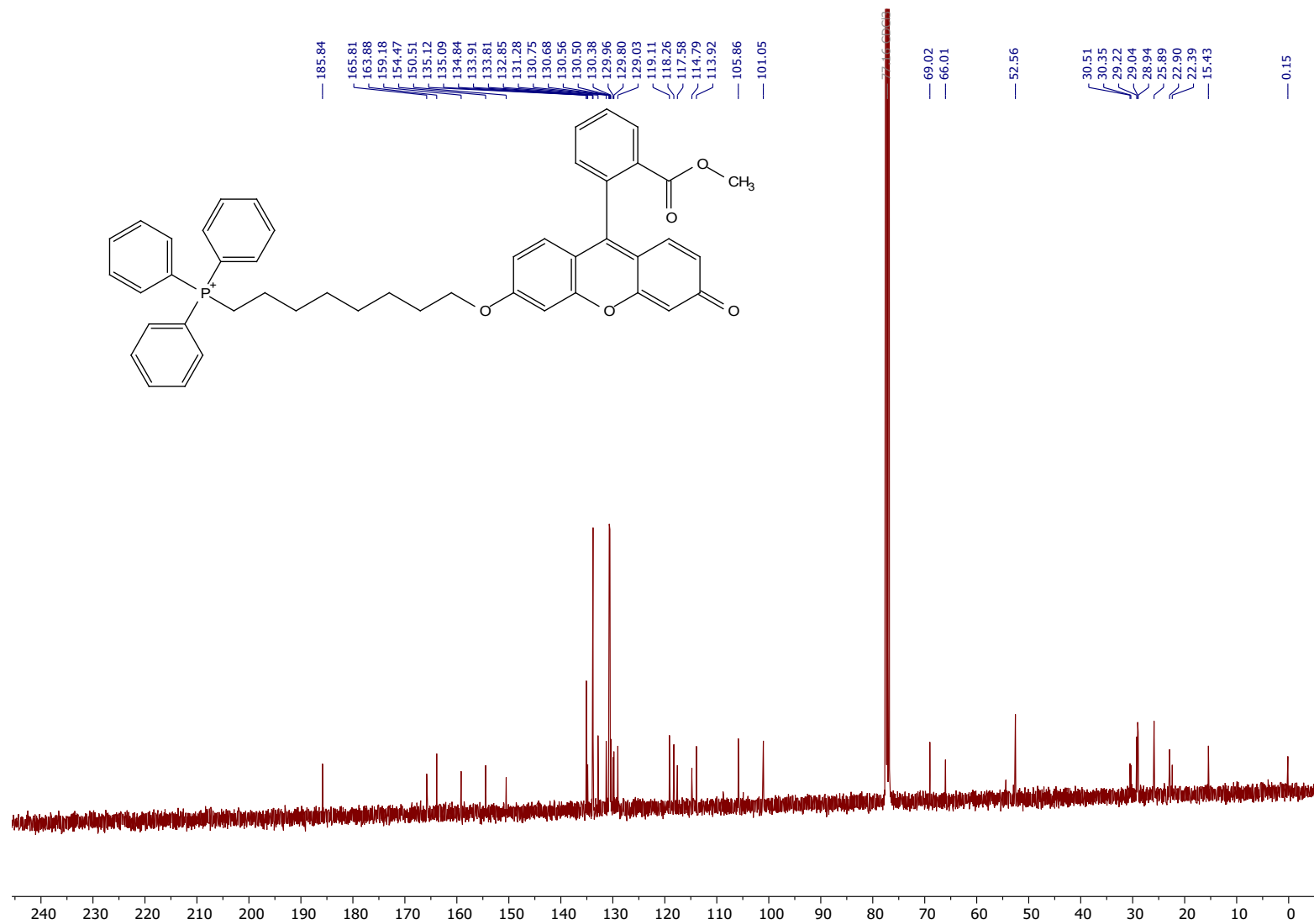


Figure S33.  $^{13}\text{C}\{^1\text{H}\}$  NMR spectrum for **4b**.

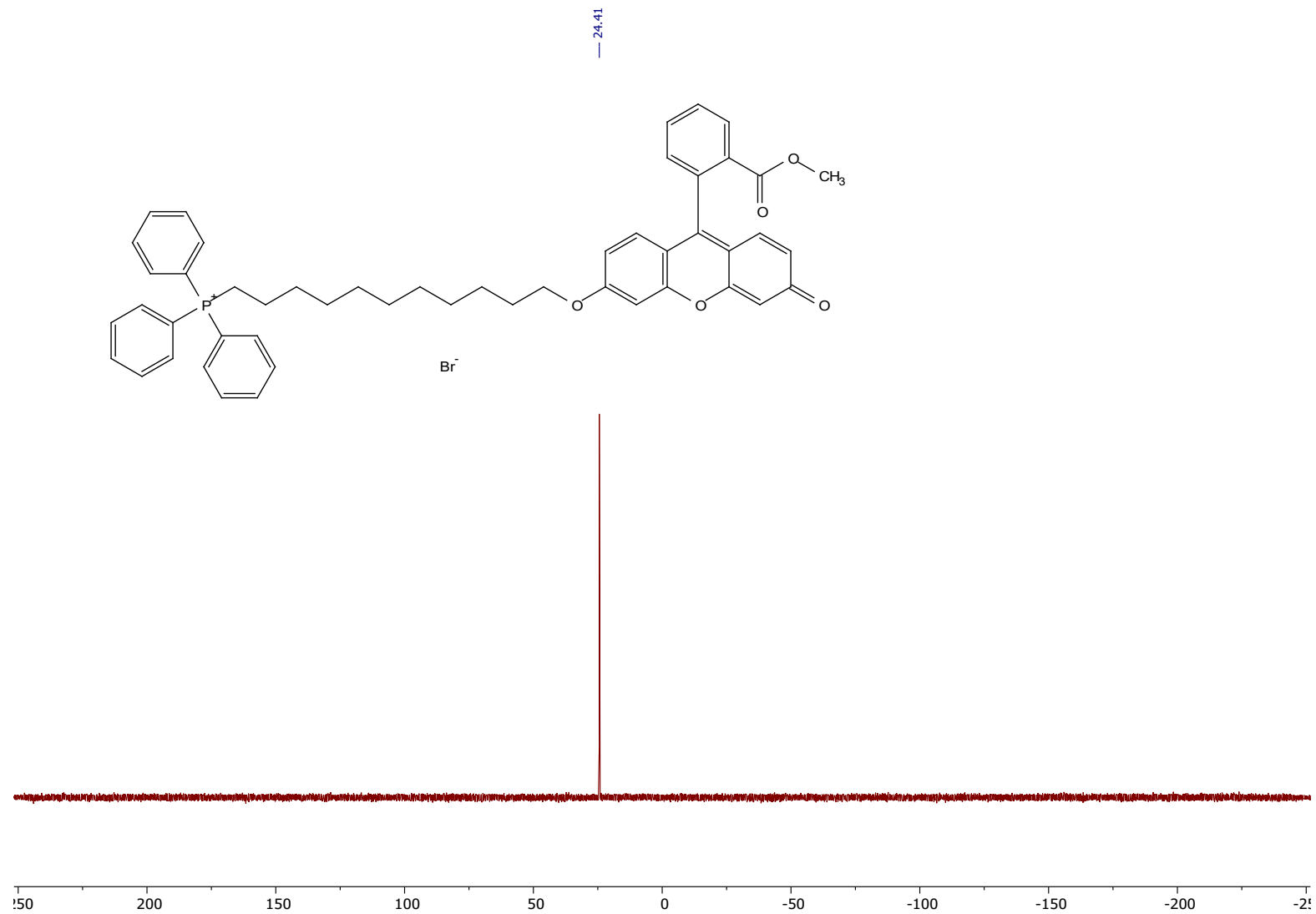


Figure S34.  $^{31}\text{P}\{^1\text{H}\}$  NMR spectrum for **4c**.

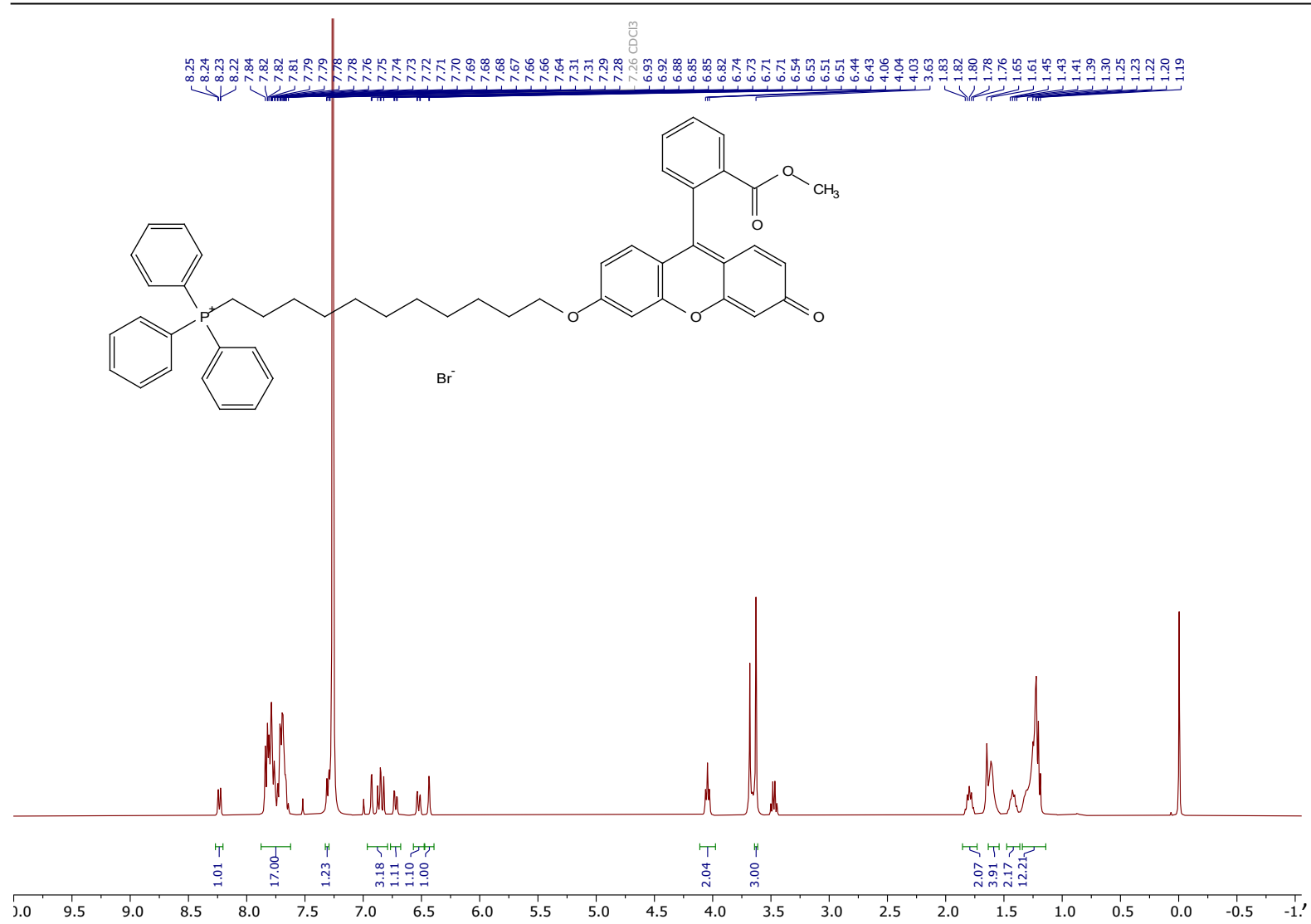


Figure S35. <sup>1</sup>H NMR spectrum for 4c.

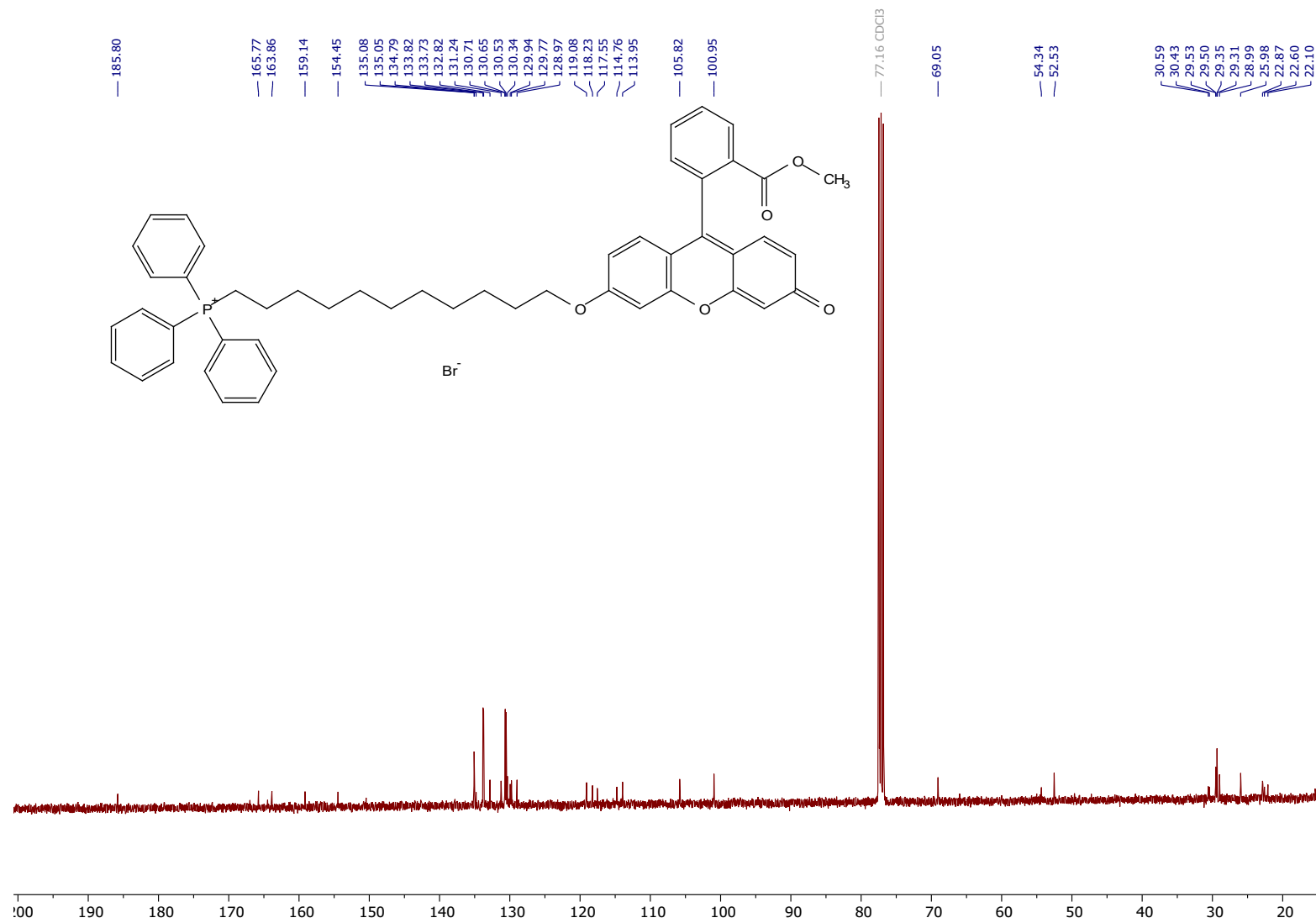


Figure S36. <sup>13</sup>C{<sup>1</sup>H} NMR spectrum for 4c.

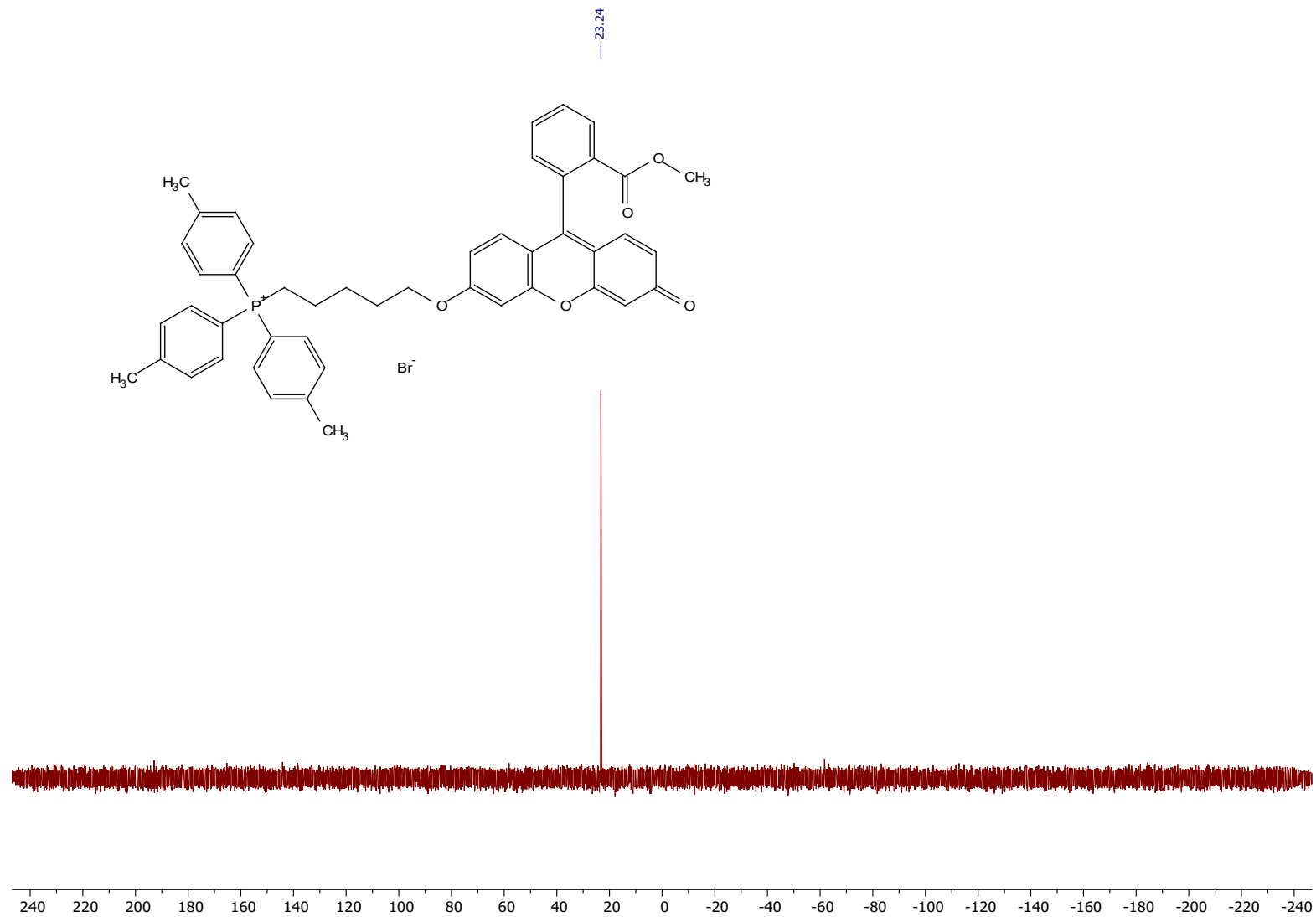


Figure S37.  $^{31}\text{P}\{^1\text{H}\}$  NMR spectrum for **4d**.

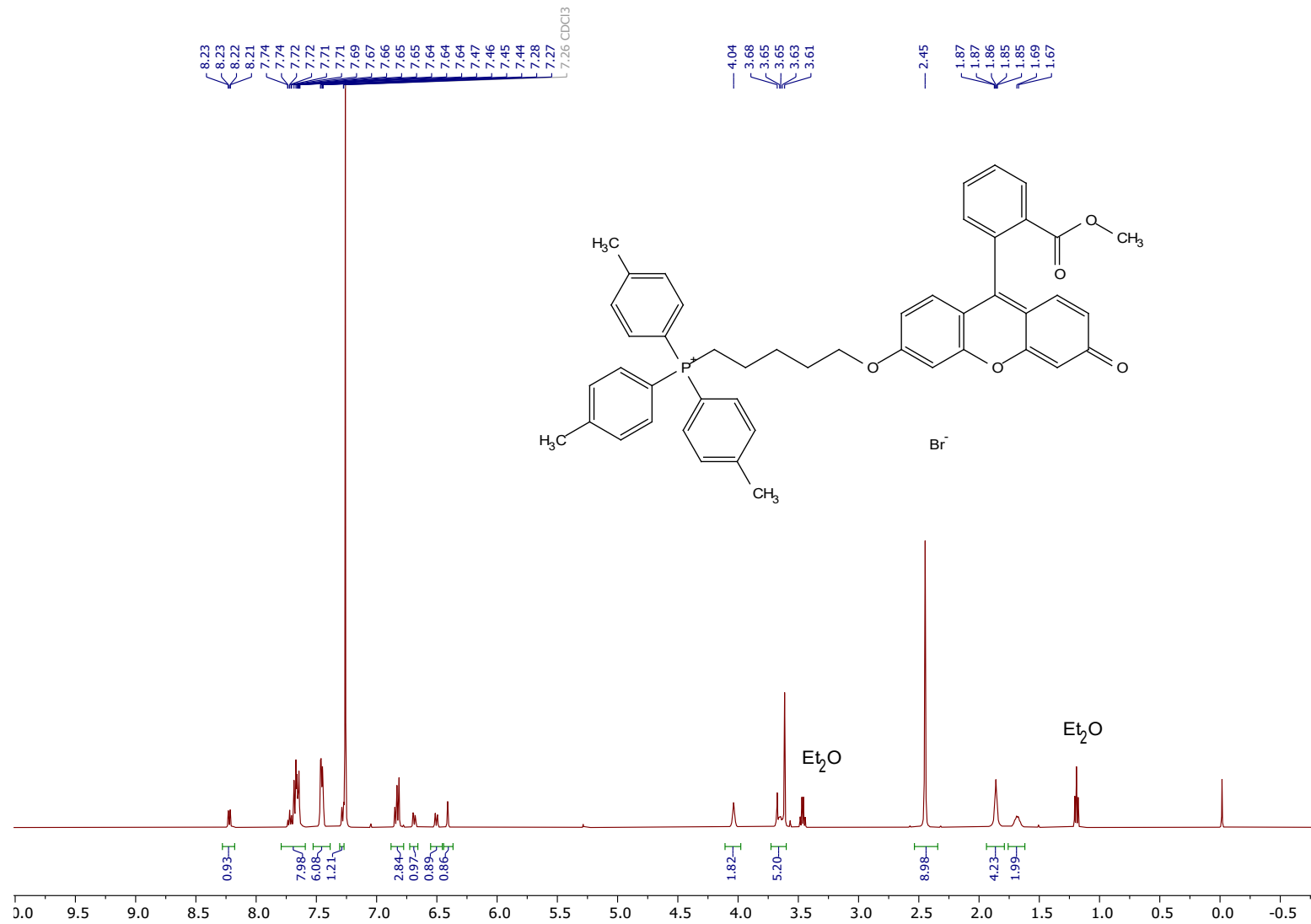


Figure S38. <sup>1</sup>H NMR spectrum for 4d.

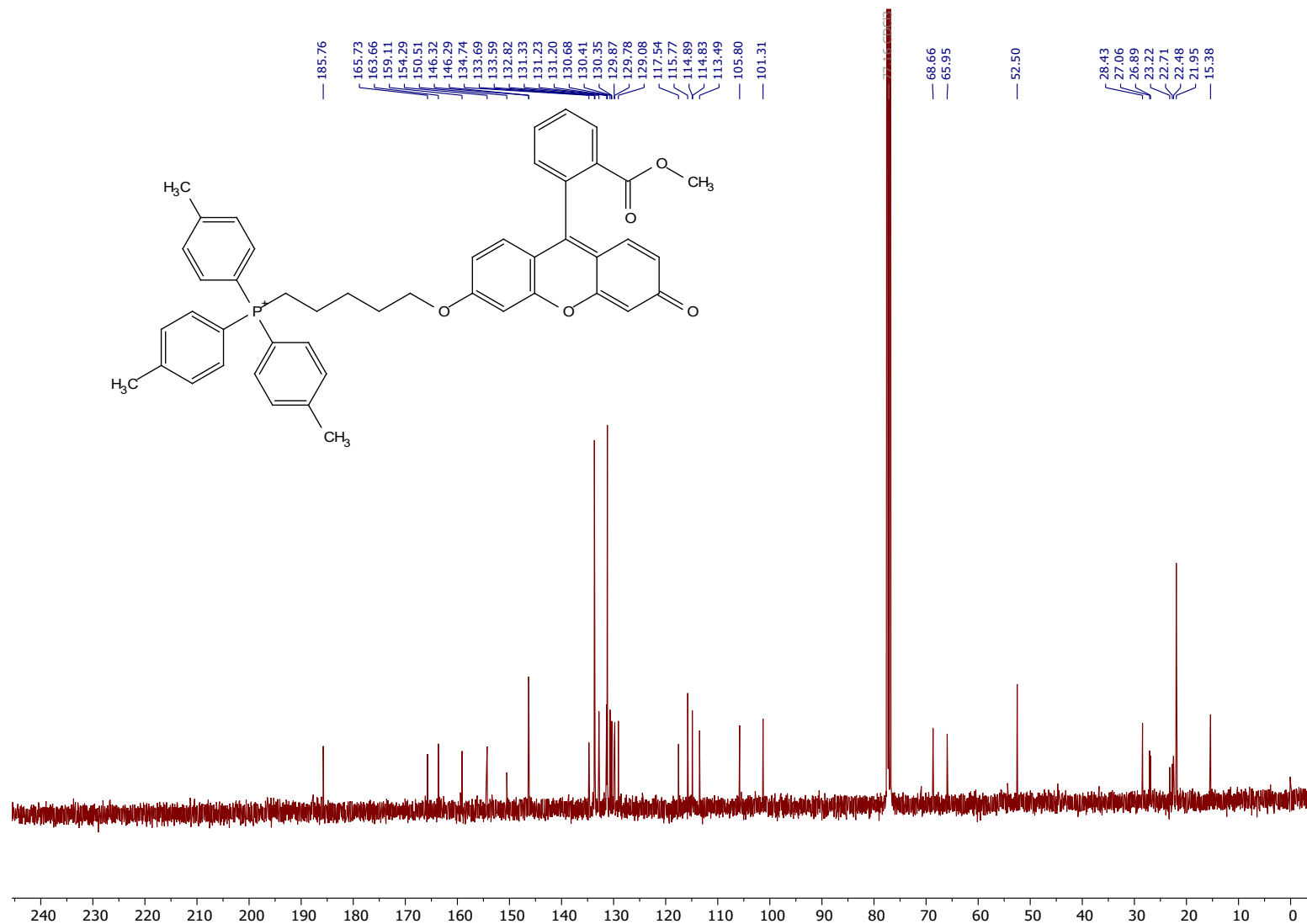
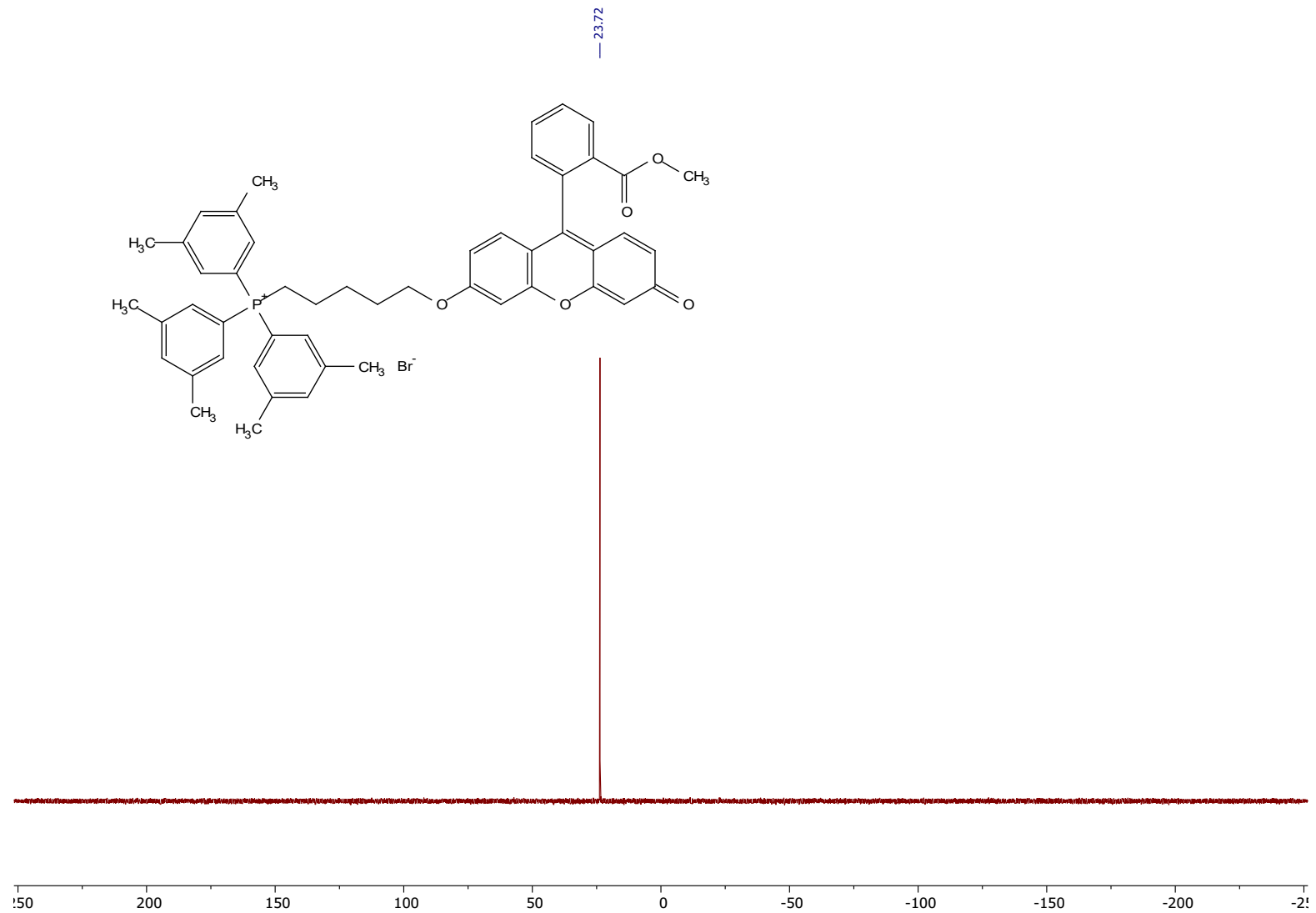


Figure S39. <sup>13</sup>C{<sup>1</sup>H} NMR spectrum for 4d.



**Figure S40.**  $^{31}\text{P}\{^1\text{H}\}$  NMR spectrum for **4e**.

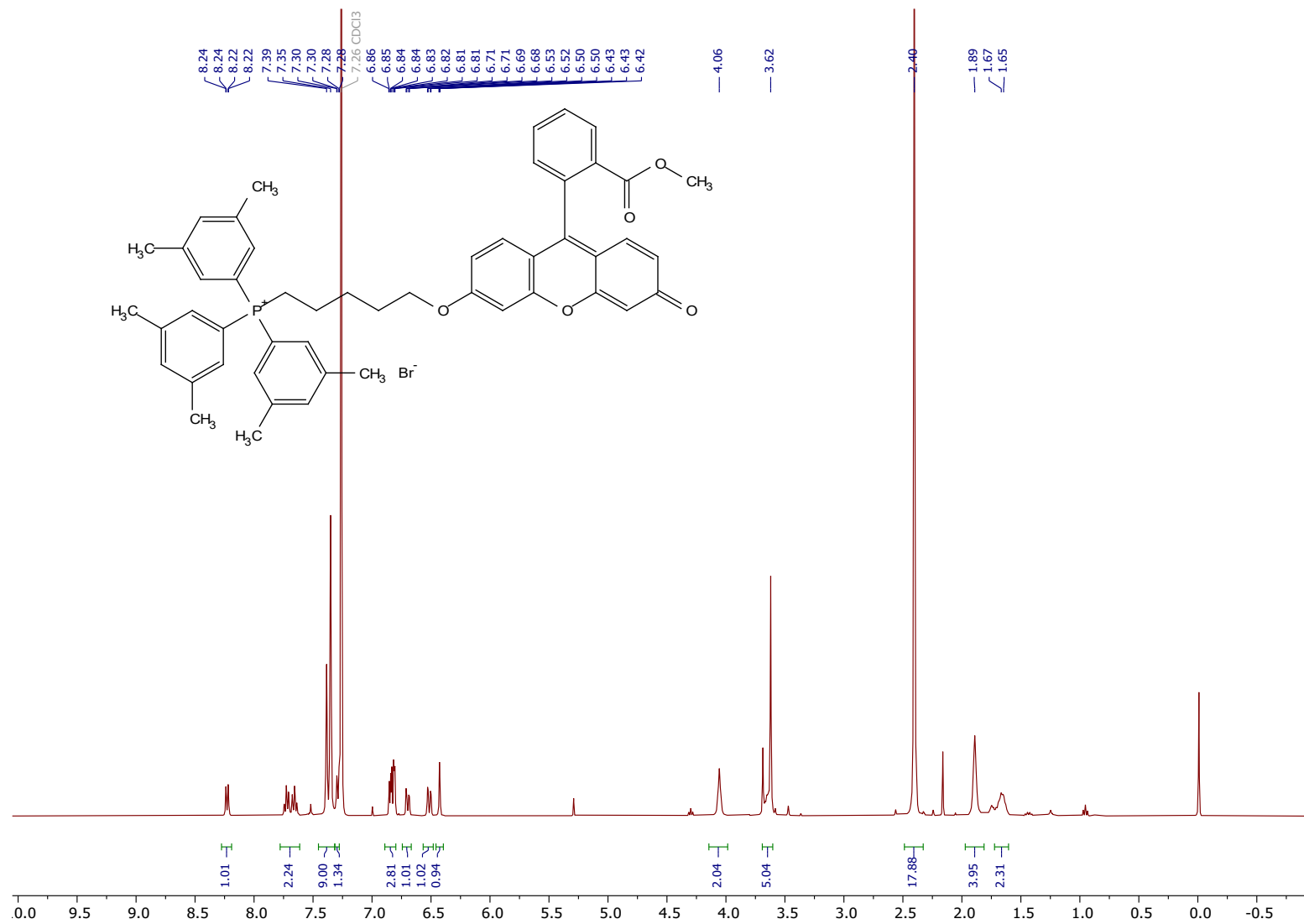


Figure S41.  $^1\text{H}$  NMR spectrum for **4e**.

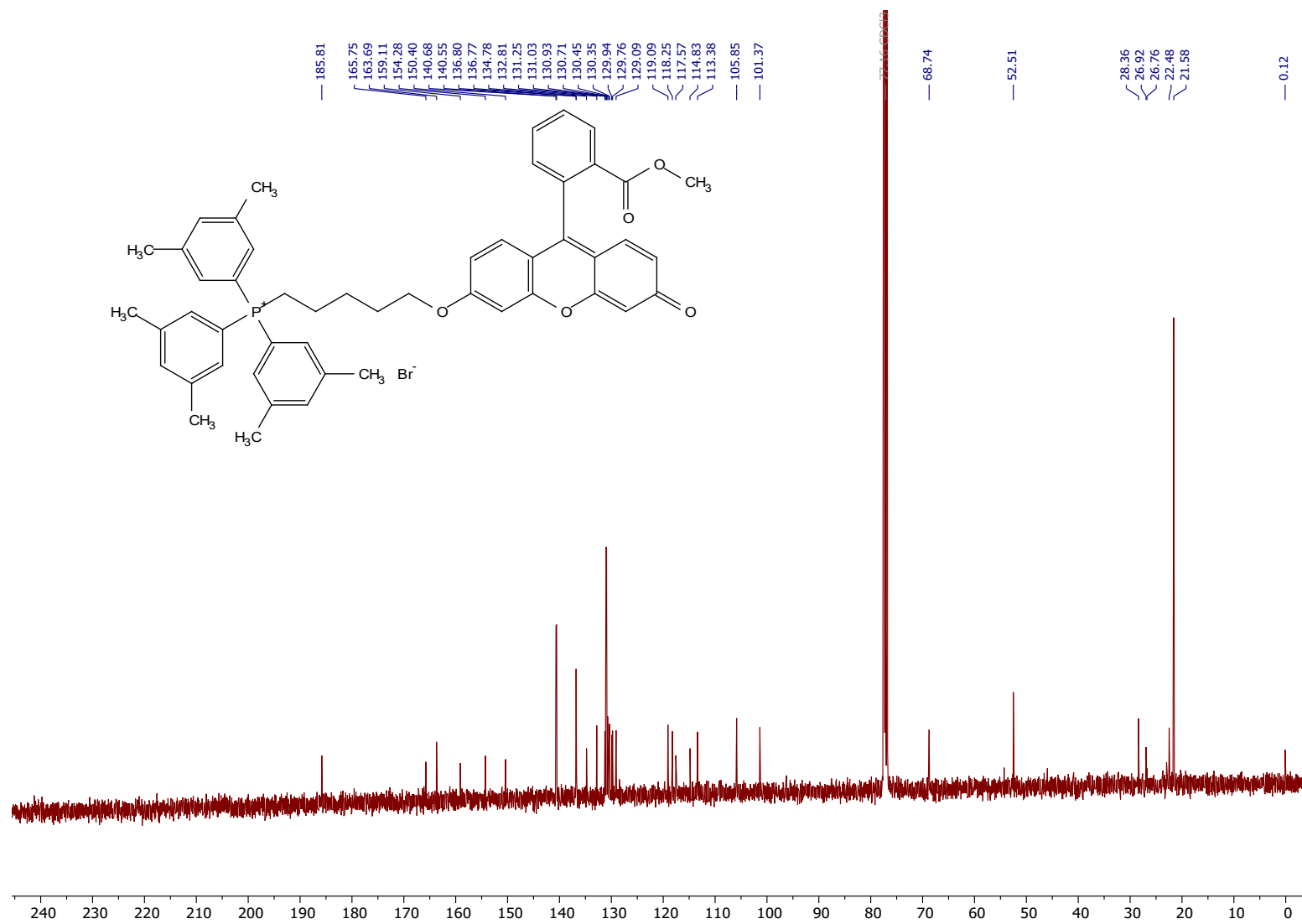


Figure S42.  $^{13}\text{C}\{^1\text{H}\}$  NMR spectrum for **4e**.

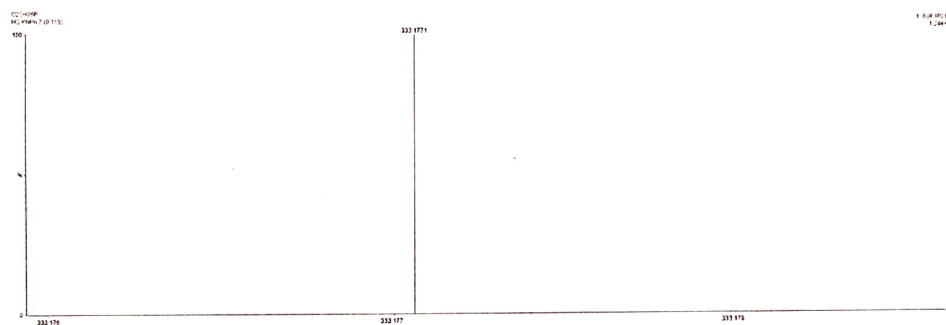
## 11. High Resolution Mass Spectra

### Elemental Composition Report

Tolerance = 10.0 PPM / DBE: min = -1.5, max = 50.0

Element prediction: Off

Number of isotope peaks used for i-FIT = 3



Monoisotopic Mass, Even Electron Ions

4 formula(e) evaluated with 1 results within limits (all results (up to 1000) for each mass)

Elements Used:

C: 0-26 H: 0-32 P: 0-1

Minimum: 80.00 -1.5

Maximum: 100.00 5.0 10.0 50.0

Mass	RA	Calc. Mass	mDa	PPM	DBE	i-FIT	Norm	Conf(%)
------	----	------------	-----	-----	-----	-------	------	---------

Formula

333.1771	100.00	333.1772	-0.1	-0.3	11.5	24.3	n/a	n/a	C23 H26 P
----------	--------	----------	------	------	------	------	-----	-----	-----------

**Figure S43.** High resolution mass spectrum for **1b**.

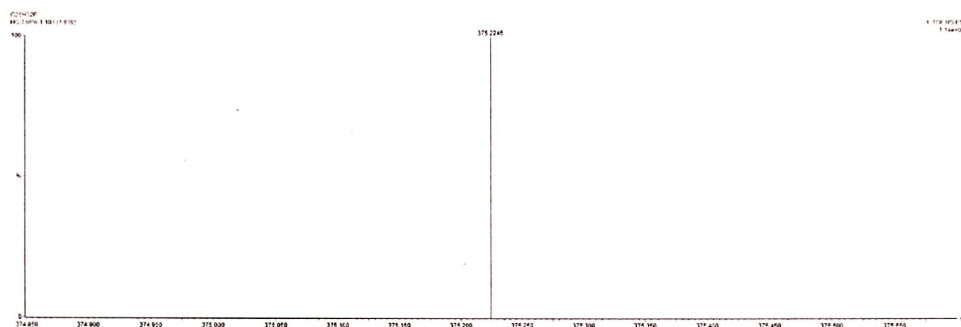


## Elemental Composition Report

Tolerance = 10.0 PPM / DBE: min = -1.5, max = 50.0

Element prediction: Off

Number of isotope peaks used for i-FIT = 3



Monoisotopic Mass, Even Electron Ions

1 formula(e) evaluated with 1 results within limits (all results (up to 1000) for each mass)

Elements Used:

C: 0-26 H: 0-32 P: 0-1

Minimum: -1.5

Maximum: 5.0 10.0 50.0

Mass	Calc. Mass	mDa	PPM	DBE	i-FIT	Norm	Conf(%)	Formula
375.2245	375.2242	0.3	0.8	11.5	35.9	n/a	n/a	C26 H32 P

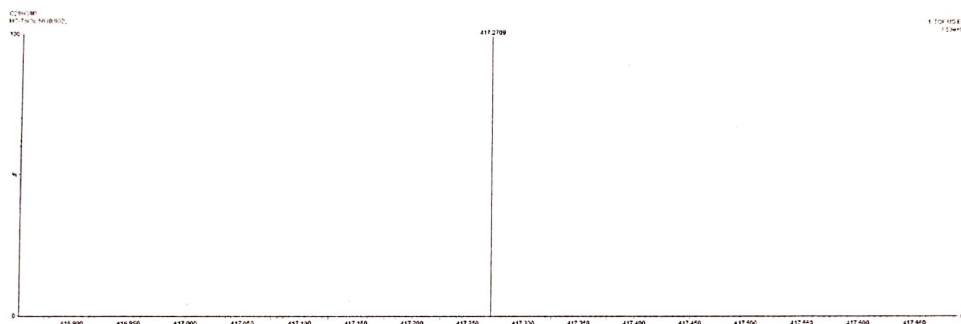
**Figure S45.** High resolution mass spectrum for **2b**.

## Elemental Composition Report

Tolerance = 10.0 PPM / DBE: min = -1.5, max = 50.0

Element prediction: Off

Number of isotope peaks used for i-FIT = 3



Monoisotopic Mass, Even Electron Ions

5 formula(e) evaluated with 1 results within limits (all results (up to 1000) for each mass)

Elements Used:

C: 0-32 H: 0-44 P: 0-1

Minimum: -1.5

Maximum: 5.0 10.0 50.0

Mass	Calc. Mass	mDa	PPM	DBE	i-FIT	Norm	Conf(%)	Formula
417.2709	417.2711	-0.2	-0.5	11.5	17.6	n/a	n/a	C29 H38 P

**Figure S46.** High resolution mass spectrum for **2c**.

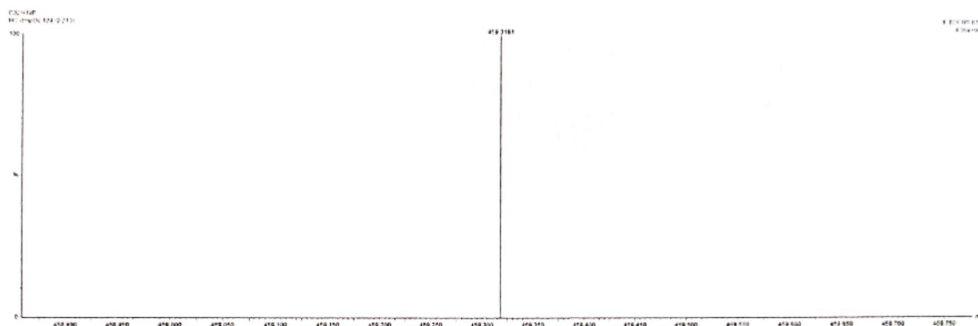


## Elemental Composition Report

Tolerance = 10.0 PPM / DBE: min = -1.5, max = 50.0

Element prediction: Off

Number of isotope peaks used for i-FIT = 3



Monoisotopic Mass, Even Electron Ions

1 formula(e) evaluated with 1 results within limits (all results (up to 1000) for each mass)

Elements Used:

C: 0-32 H: 0-44 P: 0-1

Minimum: -1.5

Maximum: 5.0 10.0 50.0

Mass	Calc. Mass	mDa	PPM	DBE	i-FIT	Norm	Conf(%)	Formula
459.3181	459.3181	0.0	0.0	11.5	33.6	n/a	n/a	C32 H44 P

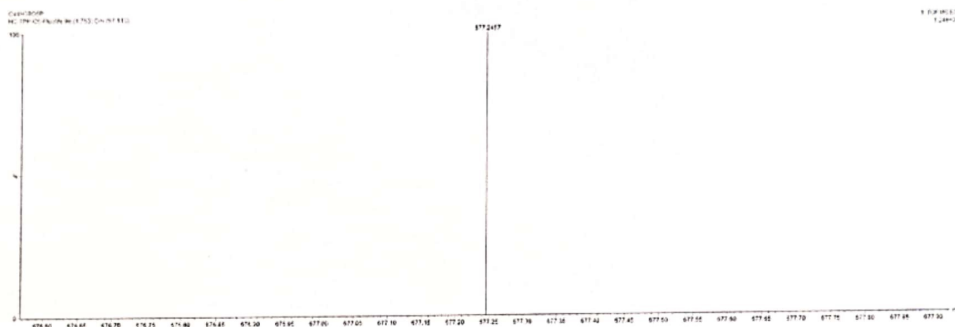
**Figure S48.** High resolution mass spectrum for **3c**.

## Elemental Composition Report

Tolerance = 10.0 PPM / DBE: min = -1.5, max = 50.0

Element prediction: Off

Number of isotope peaks used for i-FIT = 3



Monoisotopic Mass, Even Electron Ions

31 formula(e) evaluated with 1 results within limits (all results (up to 1000) for each mass)

Elements Used:

C: 0-50 H: 0-50 O: 0-5 P: 0-1

Minimum: -1.5

Maximum: 5.0 10.0 50.0

Mass	Calc. Mass	mDa	PPM	DBE	i-FIT	Norm	Conf(%)	Formula
677.2457	677.2457	0.0	0.0	26.5	31.2	n/a	n/a	C44 H38 O5 P

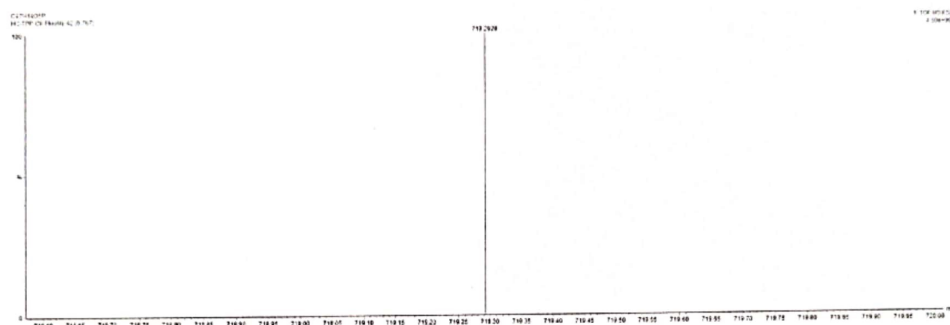
**Figure S49.** High resolution mass spectrum for **4a**.

Elemental Composition Report

Tolerance = 10.0 PPM / DBE: min = -1.5, max = 50.0

Element prediction: Off

Number of isotope peaks used for i-FIT = 3



Monoisotopic Mass, Even Electron Ions

10 formula(e) evaluated with 1 results within limits (all results (up to 1000) for each mass)

Elements Used:

C: 0-50 H: 0-50 O: 0-5 P: 0-1

Minimum: -1.5

Maximum: 5.0 10.0 50.0

Mass	Calc. Mass	mDa	PPM	DBE	i-FIT	Norm	Conf(%)	Formula
719.2928	719.2926	0.2	0.3	26.5	17.4	n/a	n/a	C47 H44 O5 P

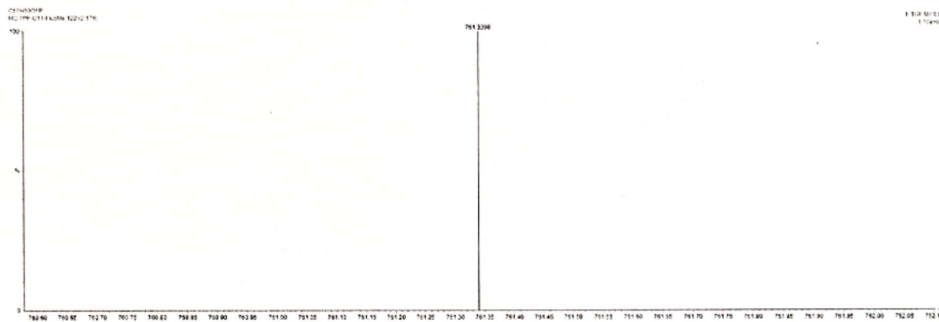
**Figure S50.** High resolution mass spectrum for **4b**.

Elemental Composition Report

Tolerance = 10.0 PPM / DBE: min = -1.5, max = 50.0

Element prediction: Off

Number of isotope peaks used for i-FIT = 3



Monoisotopic Mass, Even Electron Ions

7 formula(e) evaluated with 1 results within limits (all results (up to 1000) for each mass)

Elements Used:

C: 0-50 H: 0-50 O: 0-5 P: 0-1

Minimum: -1.5

Maximum: 5.0 10.0 50.0

Mass	Calc. Mass	mDa	PPM	DBE	i-FIT	Norm	Conf(%)	Formula
761.3398	761.3396	0.2	0.3	26.5	25.4	n/a	n/a	C50 H50 O5 P

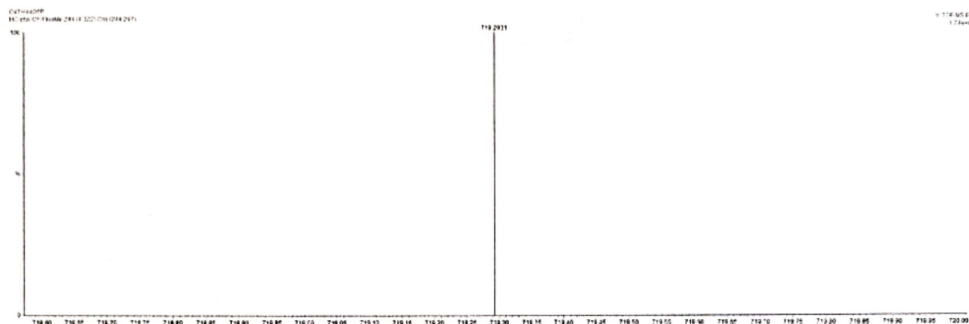
**Figure S51.** High resolution mass spectrum for **4c**.

## Elemental Composition Report

Tolerance = 10.0 PPM / DBE: min = -1.5, max = 50.0

Element prediction: Off

Number of isotope peaks used for i-FIT = 3



Monoisotopic Mass, Even Electron Ions

10 formula(e) evaluated with 1 results within limits (all results (up to 1000) for each mass)

Elements Used:

C: 0-50 H: 0-50 O: 0-5 P: 0-1

Minimum: -1.5

Maximum: 5.0 10.0 50.0

Mass	Calc. Mass	mDa	PPM	DBE	i-FIT	Norm	Conf(%)	Formula
719.2931	719.2926	0.5	0.7	26.5	26.4	n/a	n/a	C47 H44 O5 P

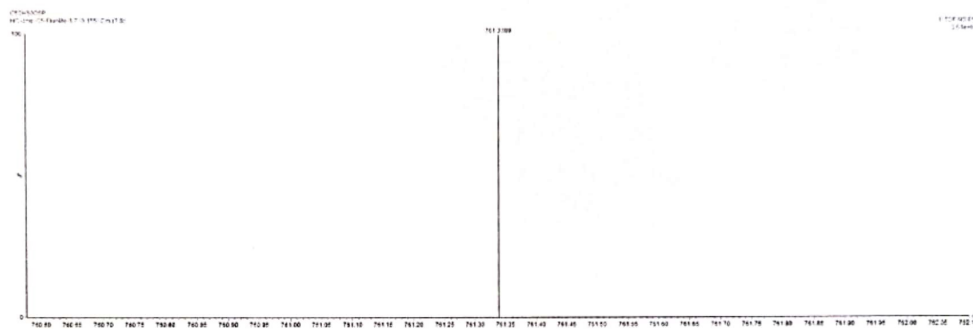
**Figure S52.** High resolution mass spectrum for **4d**.

## Elemental Composition Report

Tolerance = 10.0 PPM / DBE: min = -1.5, max = 50.0

Element prediction: Off

Number of isotope peaks used for i-FIT = 3



Monoisotopic Mass, Even Electron Ions

7 formula(e) evaluated with 1 results within limits (all results (up to 1000) for each mass)

Elements Used:

C: 0-50 H: 0-50 O: 0-5 P: 0-1

Minimum: -1.5

Maximum: 5.0 10.0 50.0

Mass	Calc. Mass	mDa	PPM	DBE	i-FIT	Norm	Conf(%)	Formula
761.3389	761.3396	-0.7	-0.9	26.5	28.3	n/a	n/a	C50 H50 O5 P

**Figure S53.** High resolution mass spectrum for **4e**.

## 12. Single crystal X-ray data

**Table S4.** X-ray data of compounds **2b** and **3b**.

	<b>2b</b>	<b>3b</b>
Empirical formula	C <sub>26</sub> H <sub>32</sub> BrP	C <sub>29</sub> H <sub>38</sub> BrP
Formula weight	455.39 g/mol	497.47 g/mol
Crystal system	monoclinic	monoclinic
Space group	P2 <sub>1</sub> /c	C2/c
a/ Å	10.9878(3)	17.4833(10)
b /Å	12.2294(3)	14.5439(9)
c/ Å	17.2004(5)	20.9956(13)
α/°	90	90
β/°	90.035(2)°	100.798(2)
γ/°	90	90
Volume/ Å <sup>3</sup>	2311.29(11)	5244.1(5)
Z	4	8
ρ (Calc)/Mg.m <sup>-3</sup>	1.309	1.260
Absorp. Coeff./ mm <sup>-1</sup>	1.857	1.643
F(000)	952	2096
Crystal Size/ mm <sup>3</sup>	0.06 x 0.10 x 0.12	0.10 x 0.10 x 0.40
Θ range/ °	2.49 to 30.49	1.83 to 25.02
	-15<=h<=15	-19<=h<=20
Index range	-17<=k<=17	-17<=k<=17
	-24<=l<=24	-24<=l<=20
Refl. collected	27688	32456
Indep. Refns. (R <sub>int</sub> )	3557 (0.061)	4644 (0.0649)
Completeness to Θ =	99.3%	100.0%
Absorp. Corr.	Multi-Scan	Multi-Scan
Max., min., transmission	0.8970, 0.8080	0.8530 and 0.5590
Refinement Method	Full-matrix least-squares on F <sup>2</sup>	Full-matrix least-squares on F <sup>2</sup>
Data/ restraint/parameters	7004 / 0 / 257	4644 / 0 / 288
Goodness-of-fit on F <sup>2</sup>	1.031	1.037
Final R indices [I>2σ(I)]	R1 = 0.0527 wR2 = 0.0911	R1 = 0.0351 wR2 = 0.0721
R indices (all data)	R1 = 0.1161 wR2 = 0.1110	R1 = 0.0661 wR2 = 0.0835
Largest diff. peak and hole/ e. Å <sup>-3</sup>	0.815, -0.625	0.369, -0.522
Temperature/ K	100(2)	100(2)

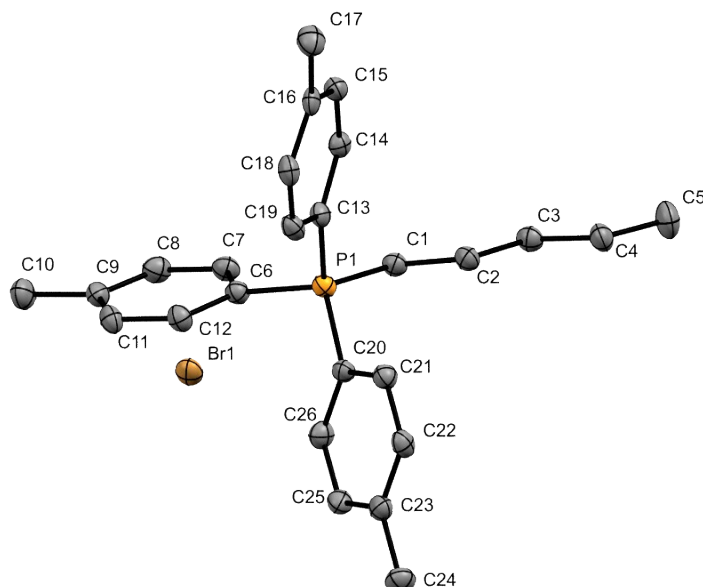


**Figure S54.** Structure of compound **2b**. Hydrogen atoms are removed for clarity. The atoms were refined without using any restraints or constraints. Selected bond lengths [Å] and Angles [deg]: P1-C1 1.793(3), P1-C6 1.799(3), P1-C13 1.797(3), P1-C20 1.788(3), C1-P1-C6 112.15(14), C1-P1-C13 107.82(14), C1-P1-C20 109.20(14), C6-P1-C13 08.22(13), C6-P1-C20 108.31(14), C13-P1-C20 111.16(14).

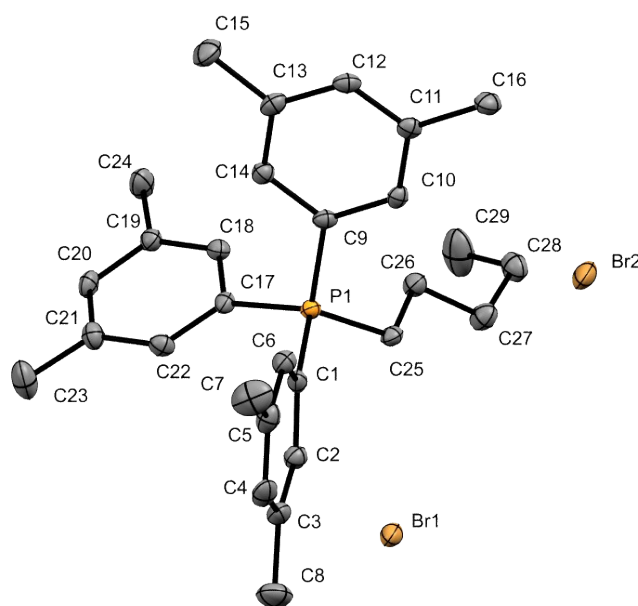


**Figure S55.** Structure of compound **3b**. Hydrogen atoms are removed for clarity. The bromide ion was disordered over 2 positions with an occupancy of 1:1. The atoms were refined without using any restraints or constraints. Selected bond lengths [Å] and Angles [deg]: P1-C1 1.802(3), P1-C9 1.792(3), P1-C17 1.804(3), P1-C25 1.798(3), C1-P1-C9 110.04(13), C1-P1-C17 107.86(13), C1-P1-C25 107.23(12), C9-P1-C17 107.19(13), C9-P1-C25 110.85(13), C17-P1-C25 113.61(13).

---

## References

1. SMART version 5.628; Bruker AXS Inc., Madison, WI, USA, 2001.
2. Sheldrick, G. M. SADABS V2014/4 (Bruker AXS Inc.) University of Göttingen, Göttingen, Germany, 2014.
3. SHELXL-2014/6 (Sheldrick, 2014); Bruker AXS Inc., Madison, WI, USA, 2014.
4. Hu, Z.; Sim, Y.; Kon, O. L.; Ng, W. H.; Ribeiro, A. J. M.; Ramos, M. J.; Fernandes, P. A.; Ganguly, R.; Xing, B. G.; Garcia, F.; Yeow, E. K. L., Unique Triphenylphosphonium Derivatives for Enhanced Mitochondrial Uptake and Photodynamic Therapy. *Bioconjugate Chem* 2017, 28 (2), 590-599.
5. Rezazgui, O.; Trouillas, P.; Qiu, S.-h.; Siegler, B.; Gierschner, J.; Leroy-Lhez, S., Synthesis and conformation of a novel fluorescein-Zn-porphyrin dyad and intramolecular energy transfer. *New Journal of Chemistry* 2016, 40 (4), 3843-3856.
6. Andres, A.; Roses, M.; Rafols, C.; Bosch, E.; Espinosa, S.; Segarra, V.; Huerta, J. M., Setup and validation of shake-flask procedures for the determination of partition coefficients (logD) from low drug amounts. *Eur J Pharm Sci* 2015, 76, 181-91.
7. Abraham, M. J.; Murtola, T.; Schulz, R.; Páll, S.; Smith, J. C.; Hess, B.; Lindahl, E., GROMACS: High performance molecular simulations through multi-level parallelism from laptops to supercomputers. *SoftwareX* 2015, 1-2, 19-25.
8. Berendsen, H. J. C.; Vandespoel, D.; Vandrunen, R., Gromacs - a Message-Passing Parallel Molecular-Dynamics Implementation. *Comput Phys Commun* 1995, 91 (1-3), 43-56.
9. Van der Spoel, D.; Lindahl, E.; Hess, B.; Groenhof, G.; Mark, A. E.; Berendsen, H. J. C., GROMACS: Fast, flexible, and free. *Journal of Computational Chemistry* 2005, 26 (16), 1701-1718.
10. Wang, J. M.; Wang, W.; Kollman, P. A.; Case, D. A., Automatic atom type and bond type perception in molecular mechanical calculations. *J Mol Graph Model* 2006, 25 (2), 247-260.
11. Bayly, C. I.; Cieplak, P.; Cornell, W. D.; Kollman, P. A., A Well-Behaved Electrostatic Potential Based Method Using Charge Restraints for Deriving Atomic Charges - the Resp Model. *J Phys Chem-Us* 1993, 97 (40), 10269-10280.
12. Case D. A., B.-S. I. Y., Brozell S. R., Cerutti D. S., Cheatham, III T. E., Cruzeiro V. W. D., Darden T. A., Duke R. E., Ghoreishi D., Gilson M. K., Gohlke H., Goetz A. W., Greene D., Harris R., Homeyer N., Huang Y., Izadi S., Kovalenko A., Kurtzman T., Lee T. S., LeGrand S., Li P., Lin C., Liu J., Luchko T., Luo R., Mermelstein D. J., Merz K. M., Miao Y., Monard G., Nguyen C., Nguyen H., Omelyan I., Onufriev A., Pan F., Qi R., Roe D. R., Roitberg A., Sagui C., Schott-Verdugo S., Shen J., Simmerling C. L., Smith J., Salomon-Ferrer R., Swails J., Walker R. C., Wang J., Wei H., Wolf R. M., Wu X., Xiao L., York D. M., Kollman P. A., AMBER 2018. University of California, San Francisco 2018.
13. M. J. Frisch, G. W. T., H. B. Schlegel, G. E. Scuseria, M. A. Robb, J. R. Cheeseman, G. Scalmani, V. Barone, G. A. Petersson, H. Nakatsuji, X. Li, M. Caricato, A. Marenich, J. Bloino, B. G. Janesko, R. Gomperts, B. Mennucci, H. P. Hratchian, J. V. Ortiz, A. F. Izmaylov, J. L. Sonnenberg, D. Williams-Young, F. Ding, F. Lipparini, F. Egidi, J. Goings, B. Peng, A. Petrone, T. Henderson, D. Ranasinghe, V. G. Zakrzewski, J. Gao, N. Rega, G. Zheng, W. Liang, M. Hada, M. Ehara, K. Toyota, R. Fukuda, J. Hasegawa, M. Ishida, T. Nakajima, Y. Honda, O. Kitao, H. Nakai, T. Vreven, K. Throssell, J. A. Montgomery, Jr., J. E. Peralta, F. Ogliaro, M. Bearpark, J. J. Heyd, E. Brothers, K. N. Kudin, V. N. Staroverov, T. Keith, R. Kobayashi, J. Normand, K. Raghavachari, A. Rendell, J. C. Burant, S. S. Iyengar, J. Tomasi, M. Cossi, J. M. Millam, M. Klene, C. Adamo, R. Cammi, J. W. Ochterski, R. L. Martin, K. Morokuma, O. Farkas, J. B. Foresman, and D. J. Fox Gaussian 09, Revision D.01, Gaussian, Inc., Wallingford CT: 2016.
14. Jorgensen, W. L.; Chandrasekhar, J.; Madura, J. D.; Impey, R. W.; Klein, M. L., Comparison of Simple Potential Functions for Simulating Liquid Water. *J Chem Phys* 1983, 79 (2), 926-935.
15. Sorin, E. J.; Pande, V. S., Exploring the helix-coil transition via all-atom equilibrium ensemble simulations. *Biophys J* 2005, 88 (4), 2472-2493.
16. Schott-Verdugo, S.; Gohlke, H., PACKMOL-Memgen: A Simple-To-Use, Generalized Workflow for Membrane-Protein-Lipid-Bilayer System Building. *J Chem Inf Model* 2019, 59 (6), 2522-2528.

- 
17. Darden, T.; York, D.; Pedersen, L., Particle Mesh Ewald - an N.Log(N) Method for Ewald Sums in Large Systems. *J Chem Phys* 1993, 98 (12), 10089-10092.
  18. Hess, B.; Bekker, H.; Berendsen, H. J. C.; Fraaije, J. G. E. M., LINCS: A linear constraint solver for molecular simulations. *Journal of Computational Chemistry* 1997, 18 (12), 1463-1472.
  19. Berendsen, H. J. C.; Postma, J. P. M.; Vangunsteren, W. F.; Dinola, A.; Haak, J. R., Molecular-Dynamics with Coupling to an External Bath. *J Chem Phys* 1984, 81 (8), 3684-3690.
  20. Nose, S.; Klein, M. L., Constant Pressure Molecular-Dynamics for Molecular-Systems. *Mol Phys* 1983, 50 (5), 1055-1076.
  21. Parrinello, M.; Rahman, A., Polymorphic Transitions in Single-Crystals - a New Molecular-Dynamics Method. *J Appl Phys* 1981, 52 (12), 7182-7190.
  22. Hansen, N.; van Gunsteren, W. F., Practical Aspects of Free-Energy Calculations: A Review. *J Chem Theory Comput* 2014, 10 (7), 2632-2647.
  23. Bannan, C. C.; Calabro, G.; Kyu, D. Y.; Mobley, D. L., Calculating Partition Coefficients of Small Molecules in Octanol/Water and Cyclohexane/Water. *J Chem Theory Comput* 2016, 12 (8), 4015-4024.
  24. Shirts, M. R.; Chodera, J. D., Statistically optimal analysis of samples from multiple equilibrium states. *J Chem Phys* 2008, 129 (12).
  25. Klimovich, P. V.; Shirts, M. R.; Mobley, D. L., Guidelines for the analysis of free energy calculations. *J Comput Aid Mol Des* 2015, 29 (5), 397-411.
  26. Jo, S.; Kim, T.; Iyer, V. G.; Im, W., CHARMM-GUI: a web-based graphical user interface for CHARMM. *J Comput Chem* 2008, 29 (11), 1859-65.
  27. Qi, Y. F.; Ingolfsson, H. I.; Cheng, X.; Lee, J.; Marrink, S. J.; Im, W., CHARMM-GUI Martini Maker for Coarse-Grained Simulations with the Martini Force Field. *J Chem Theory Comput* 2015, 11 (9), 4486-4494.
  28. Wu, E. L.; Cheng, X.; Jo, S.; Rui, H.; Song, K. C.; Davila-Contreras, E. M.; Qi, Y. F.; Lee, J. M.; Monje-Galvan, V.; Venable, R. M.; Klauda, J. B.; Im, W., CHARMM-GUI Membrane Builder Toward Realistic Biological Membrane Simulations. *Journal of Computational Chemistry* 2014, 35 (27), 1997-2004.
  29. Lee, J.; Hitzenberger, M.; Rieger, M.; Kern, N. R.; Zacharias, M.; Im, W., CHARMM-GUI supports the Amber force fields. *J Chem Phys* 2020, 153 (3).
  30. Hopkins, C. W.; Le Grand, S.; Walker, R. C.; Roitberg, A. E., Long-Time-Step Molecular Dynamics through Hydrogen Mass Repartitioning. *J Chem Theory Comput* 2015, 11 (4), 1864-1874.
  31. Bussi, G.; Donadio, D.; Parrinello, M., Canonical sampling through velocity rescaling. *J Chem Phys* 2007, 126 (1).
  32. MacCallum, J. L.; Bennett, W. F. D.; Tieleman, D. P., Distribution of amino acids in a lipid bilayer from computer simulations. *Biophys J* 2008, 94 (9), 3393-3404.
  33. Marrink, S. J.; de Vries, A. H.; Mark, A. E., Coarse grained model for semiquantitative lipid simulations. *J Phys Chem B* 2004, 108 (2), 750-760.
  34. Coimbra, J. T. S.; Feghali, R.; Ribeiro, R. P.; Ramos, M. J.; Fernandes, P. A., The importance of intramolecular hydrogen bonds on the translocation of the small drug piracetam through a lipid bilayer. *Rsc Adv* 2021, 11 (2), 899-908.
  35. MacCallum, J. L.; Tieleman, D. P., Computer simulation of the distribution of hexane in a lipid bilayer: Spatially resolved free energy, entropy, and enthalpy profiles. *J Am Chem Soc* 2006, 128 (1), 125-130.
  36. Neale, C.; Bennett, W. F. D.; Tieleman, D. P.; Pomes, R., Statistical Convergence of Equilibrium Properties in Simulations of Molecular Solutes Embedded in Lipid Bilayers. *J Chem Theory Comput* 2011, 7 (12), 4175-4188.
  37. Jambeck, J. P. M.; Lyubartsev, A. P., Implicit inclusion of atomic polarization in modeling of partitioning between water and lipid bilayers. *Phys Chem Chem Phys* 2013, 15 (13), 4677-4686.

- 
38. Hub, J. S.; de Groot, B. L.; van der Spoel, D., g\_wham-A Free Weighted Histogram Analysis Implementation Including Robust Error and Autocorrelation Estimates. *J Chem Theory Comput* 2010, 6 (12), 3713-3720.
39. Kumar, S.; Bouzida, D.; Swendsen, R. H.; Kollman, P. A.; Rosenberg, J. M., The Weighted Histogram Analysis Method for Free-Energy Calculations on Biomolecules .1. The Method. *Journal of Computational Chemistry* 1992, 13 (8), 1011-1021.
40. Humphrey, W.; Dalke, A.; Schulten, K., VMD: Visual molecular dynamics. *J Mol Graph Model* 1996, 14 (1), 33-38.